# Chapter 10
# Gravitational Waves from Merging Binary Neutron-Star Systems


**Tanja Hinderer, Luciano Rezzolla, and Luca Baiotti**

**Abstract** The merger of binary neutron-star systems is among the scientifically richest events in the universe: it involves extremes of matter and gravity, copious emission of gravitational waves, complex microphysics, and electromagnetic processes that can lead to astrophysical signatures observable at the largest redshifts. We review here the recent progress in understanding the gravitational-wave signal emitted in this process, focussing in particular on its properties during the inspiral and then after the merger.

## 10.1 Introduction

Neutron stars are believed to be born in supernova explosions triggered by the collapse of the iron core in massive stars. Many astronomical observations have revealed that binary neutron stars (BNSs) indeed exist (Kramer et al. 2004; Abbott et al. 2017). Despite this observational evidence of existence, the formation mechanisms of BNS systems are not known in detail. The general picture is that in a binary system made of two massive main-sequence stars of masses between approximately 8 and 25 $M_\odot$, the more massive one undergoes a supernova explosion and becomes a neutron star. This is followed by a very uncertain phase in which the neutron star and the main-sequence star evolve in a "common envelope", that is, with the neutron star orbiting in the extended outer layers of the secondary star

T. Hinderer
Department of Astrophysics/IMAPP, Radboud University, Nijmegen, The Netherlands

L. Rezzolla (✉)
Institute for Theoretical Physics, Frankfurt, Germany

Frankfurt Institute for Advanced Studies, Frankfurt, Germany
e-mail: rezzolla@itp.uni-frankfurt.de

L. Baiotti
Graduate School of Science, Osaka University, Toyonaka, Japan



L. Rezzolla et al. (eds.), *The Physics and Astrophysics of Neutron Stars*,
Astrophysics and Space Science Library 457,
https://doi.org/10.1007/978-3-319-97616-7_10

(Kiziltan et al. 2013; Ivanova et al. 2013; Özel and Freire 2016). At the end of this stage, also the second main-sequence star undergoes a supernova explosion and, if the stars are still bound after the explosions, a BNS system is formed. The common-envelope phase, though brief, is crucial because in that phase the distance between the stars becomes much smaller as a result of drag, and this allows the birth of BNS systems that are compact enough to merge within a Hubble time, following the dissipation of their angular momentum through the emission of gravitational radiation. It is also possible that during the common-envelope phase the neutron star collapses to a black hole, thus preventing the formation of a BNS. Another possible channel for the formation of BNS systems may be the interaction of two isolated neutron stars in dense stellar regions, such as globular clusters, in a process called "dynamical capture" (O'Leary et al. 2009; Lee et al. 2010; Thompson 2011). Dynamically formed binary systems are different from the others because they have higher ellipticities. It is presently not known what fraction of BNS systems would originate from dynamical capture, but it is expected that these binaries are only a small part of the whole population.

This is undoubtedly an exciting and dynamical time for research on BNS mergers, when many accomplishments have been achieved (especially since 2008), while many more need to be achieved in order to describe such fascinating objects and the related physical phenomena. The first direct detection through the advanced interferometric LIGO detectors (Harry et al. 2010) of the gravitational-wave (GW) signal from what has been interpreted as the inspiral, merger and ringdown of a binary system of black holes (The LIGO Scientific Collaboration and the Virgo Collaboration 2016) marks, in many respects, the beginning of GW astronomy and other detections of these systems have been made over the last few months (Abbott et al. 2016).

More importantly, however, a long-awaited event has taken place on August 17, 2017: the Advanced LIGO and Virgo (Accadia et al. 2011) network of GW detectors have recorded the signal from the inspiral and merger of a binary neutron-star (BNS) system: GW170817 (Abbott et al. 2017). The correlated electromagnetic signals that have been recorded by $\sim$70 astronomical observatories and satellites have provided the striking confirmation that such mergers can be associated directly with the observation of short gamma-ray bursts (SGRBs). Although the detection rate of these events is still very uncertain and spans three orders of magnitude, it is expected to be of several events per year (Abadie et al. 2010), so that the operation of additional advanced detectors, such as KAGRA (Aso et al. 2013) and LIGO India (see e.g., Fairhurst 2014), are likely to increase the number of detections in the near future.

This Chapter aims at providing a quick overview of the efforts made to date to model the GW signal produced by the (late) inspiral, merger and post-merger of BNS systems (see also Baiotti and Rezzolla (2017), Paschalidis (2017) for some recent reviews). Because the merger represents a natural divide—both in terms of the physics involved and of the methods employed to describe this signal—the report is organised in a first part dedicated to the inspiral and merger dynamics

(Sect. 10.3) and to a second part devoted instead to the post-merger dynamics (Sect. 10.4). Both of these parts are prefaced by a general broadbrush description of the whole process (Sect. 10.2).[1]

## 10.2 The Broadbrush Picture

General-relativistic hydrodynamical simulations of BNSs started being performed in Japan almost 20 years ago (Nakamura and Oohara 1998; Oohara and Nakamura 1999; Shibata 1999). Even if nowadays many state-of-the-art codes are able to solve more complex sets of equations (e.g., for the evolution of magnetic fields, neutrino emission, etc.), simulations involving only general-relativistic hydrodynamics are still the benchmark for any new code and the necessary testbed for more advanced codes. Furthermore, in many cases, results obtained with pure hydrodynamics, most notably, gravitational waveforms, provide already a wealth of information on BNS systems, especially during the inspiral. In many respects, the inspiral may be considered the *easiest* part of the problem, in which the stars spiral towards each other as a result of gravitational-radiation losses, being scarcely or not at all affected by magnetic fields or neutrinos. Its simplicity notwithstanding, this problem is still the object of continuous efforts and improvements, which are often carried out through the synergy of numerical simulations and analytical calculations based on post-Newtonian expansions or other approximation schemes. We describe progress on this topic in Sect. 10.3. The inspiral has also recently attracted renewed attention with the first simulations of arbitrarily spinning BNS systems (see Sect. 10.3).

In what follows, we give a general description of the BNS dynamics using the figures of Baiotti et al. (2008), which was one of the first to provide complete and accurate evolutions. Our description is here intentionally qualitative, as we focus on those aspects that are robust and independent of the EOS. As an aid to the discussion we show in Fig. 10.1 the various stages in the evolution of an equal-mass binary system of neutron stars as a function of the initial mass of the binary. More specifically, the diagram shows on the horizontal axis the progress of time during the evolution of the system (the intervals in square brackets indicate the expected duration range of each stage), while on the vertical axis it displays the ratio of the total (gravitational) mass of the binary (i.e., the sum of the gravitational masses of the stars composing the system), $M$, to the maximum mass of an isolated nonrotating star,[2] $M_{\rm TOV}$. Because the EOS describing neutron stars is still unknown, the precise

[1] Much of the material presented in the second part relative to the post-merger dynamics has been presented elsewhere either in the form of original journal articles, as a Chapter in a textbook (Rezzolla and Zanotti 2013), or as a part of a Review of Progress in Physics (Baiotti and Rezzolla 2017).

[2] An isolated nonrotating neutron star is the solution of the Tolman-Oppenheimer-Volkoff (TOV) equation (Tolman 1939; Oppenheimer and Volkoff 1939) and so it is often called a "TOV" star.

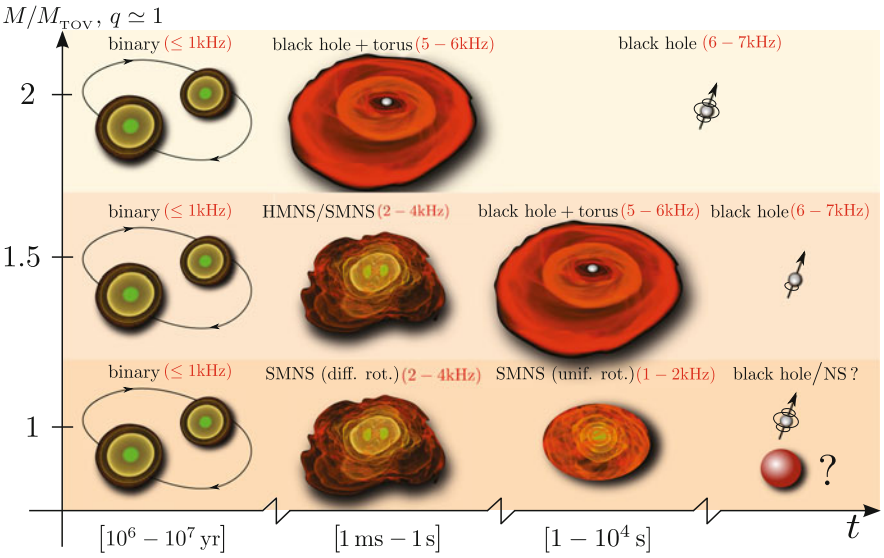


**Fig. 10.1** Schematic diagram illustrating the various stages in the evolution of an equal-mass binary system of neutron stars as a function of the initial mass of the binary. Depending on the initial total mass of the binary $M$, and on how it relates to the maximum mass of a nonrotating neutron star $M_{\rm TOV}$, the binary can either collapse promptly to a black hole surrounded by a torus (top row), or give rise to an hypermassive (HMNS) (or to a supramassive neutron star (SMNS) that ultimately collapses to a black hole and torus (middle row), or even lead to a SMNS (first differentially and subsequently uniformly rotating) neutron star that eventually yields a black hole or a nonrotating neutron star (bottom row). Also indicated in red are the typical frequencies at which gravitational waves are expected to be emitted [Adapted from Rezzolla and Zanotti (2013) by permission of Oxford University Press www.oup.com]

value of $M_{\rm TOV}$ cannot be determined, although a number of different studies have now converged on a possible upper limit of $M_{\rm TOV}/M_\odot \lesssim 2.16^{+0.17}_{-0.15}$ (Margalit and Metzger 2017; Rezzolla et al. 2018; Ruiz et al. 2018; Shibata et al. 2017). Furthermore, astronomical observations indicate that it should be larger than about two solar masses, since there are two different systems that have been measured to have masses in this range: PSR J0348+0432 with $M = 2.01 \pm 0.04\,M_\odot$ (Antoniadis et al. 2013), and PSR J1614–2230 with $M = 1.97 \pm 0.04\,M_\odot$ (Demorest et al. 2010).

For millions of years a comparatively slow inspiral progressively speeds up until the two neutron stars become so close that tidal waves produced by the (tidal) interaction start appearing on the stellar surface (these are clearly visible in the second and third panels of Fig. 10.2). Such waves are accompanied by emission of matter stripped from the surface and by shocks that represent the evolution of small sound waves that propagate from the central regions of the stars, steepening as they move outwards in regions of smaller rest-mass density (Stergioulas et al. 2004; Nagakura et al. 2014).

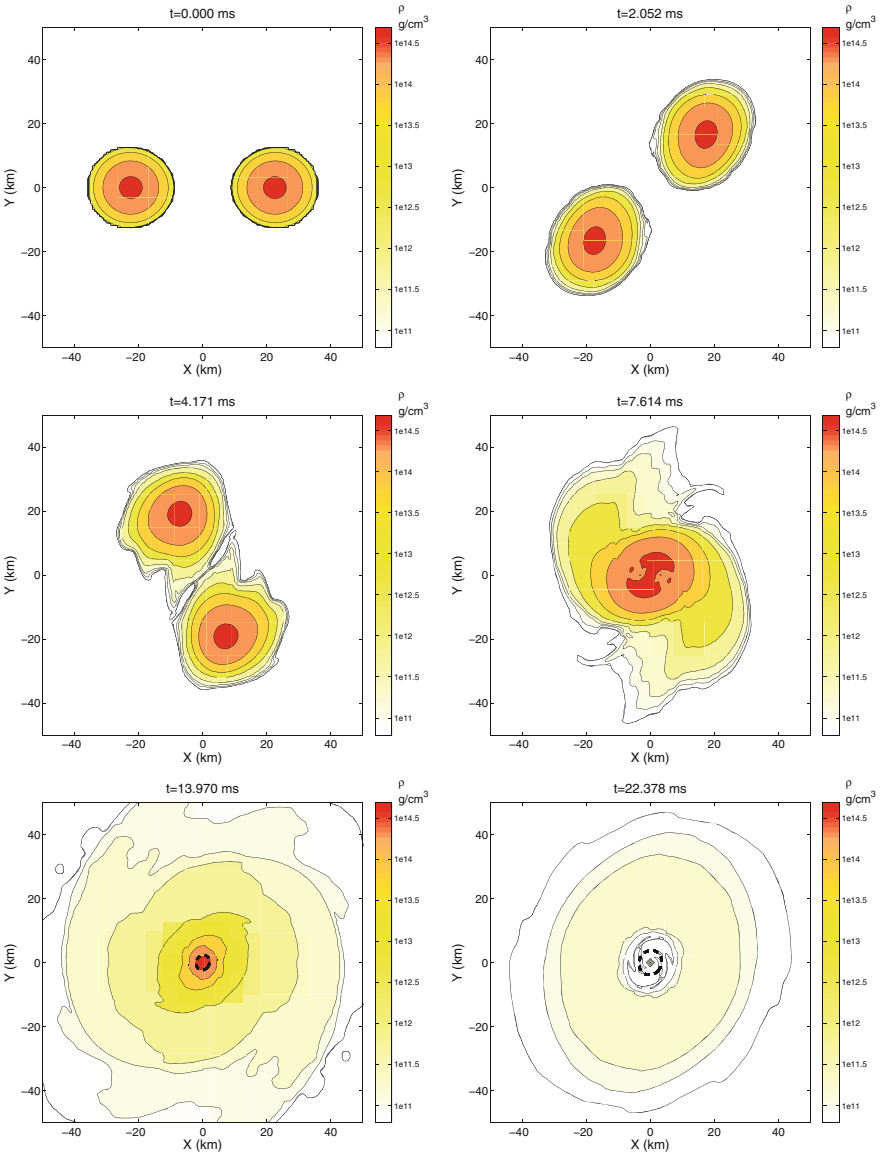


**Fig. 10.2** Isodensity contours in the $(x, y)$ plane for the evolution of a high-mass (individual stellar rest mass $1.625 M_{\odot}$) binary with an ideal-fluid EOS. The thick dashed lines in the lower panels show the location of the apparent horizon [Reprinted with permission from Baiotti et al. (2008). © (2008) by the American Physical Society]

At the merger, the two stars collide with a rather large impact parameter. A *vortex sheet* (or *shear interface*) develops, where the tangential component of the velocity exhibits a discontinuity. This condition is known to be unstable to very small perturbations and it can develop Kelvin-Helmholtz instability (KHI), which curls the interface forming a series of vortices at all wavelengths (Chandrasekhar 1981; Bodo et al. 1994). Even if this instability is purely hydrodynamical and it is likely to be important only for binaries with very similar masses, it can have strong consequences if the stars possess magnetic fields. It has in fact been shown that, in the presence of an initially poloidal magnetic field, this instability may lead to an exponential growth of the toroidal component (Price and Rosswog 2006; Giacomazzo et al. 2011; Rezzolla et al. 2011; Neilsen et al. 2014; Kiuchi et al. 2014, 2017). Such a growth is the result of the exponentially rapid formation of vortices that curl magnetic-field lines that were initially purely poloidal. The exponential growth caused by the KHI leads to an overall amplification of the magnetic field of about three orders of magnitude (Kiuchi et al. 2014). At the same time, high-resolution simulations in core-collapse supernovae find that parasitic instabilities quench the MRI, with a magnetic-field amplification factor of 100 at most, independently of the initial magnetic field strength (Rembiasz et al. 2016). Of course, KHI and MRI are two different instabilities, but the lesson these simulations provide is that parasitic instabilities may also appear during the development of the KHI and limit the overall magnetic-field amplification; such parasitic instabilities are at present not yet apparent because of the comparatively small resolutions employed when modelling BNS mergers.

The hypermassive neutron star (HMNS) produced from the merger may not collapse promptly to a black hole, but rather undergo large oscillations with variations such that the maximum of the rest-mass density may grow to be twice as large (or more) as the value in the original stars (see the right panel of Fig. 10.3). These oscillations have a dominant $m = 2$ non-axisymmetric character (Stergioulas et al. 2011) and will be discussed in detail in Sect. 10.4. As mentioned earlier, the formation and duration of the HMNS depends on the stellar masses, the EOS, the effects of radiative cooling, magnetic fields (Ravi and Lasky 2014; Rezzolla and Kumar 2015; Ciolfi and Siegel 2015), and the development of GW driven instabilities (Doneva et al. 2015). Furthermore, the equilibrium of the HMNS can also be modified by the losses of rest mass via winds that can be driven by shock heating (Sekiguchi et al. 2015; Bovard et al. 2017), by magnetic fields (Shibata et al. 2011; Kiuchi et al. 2012a; Siegel et al. 2014; Rezzolla and Kumar 2015; Ciolfi and Siegel 2015; Murguia-Berthier et al. 2017), or by viscosity and neutrino emission (Dessart et al. 2009; Perego et al. 2014; Just et al. 2015; Martin et al. 2015; Murguia-Berthier et al. 2014, 2017; Fujibayashi et al. 2017).

In essentially all cases when a black hole is formed, some amount of matter remains outside of it, having sufficient angular momentum to stay orbiting around the black hole on stable orbits. In turn, this leads to the formation of an accretion torus that may be rather dense ($\rho \sim 10^{12}$–$10^{13}\,\mathrm{g\,cm^{-3}}$) and extended horizontally for tens of kilometres and vertically for a few tens of kilometres. Also this point will be discussed in more detail in Sect. 10.4.

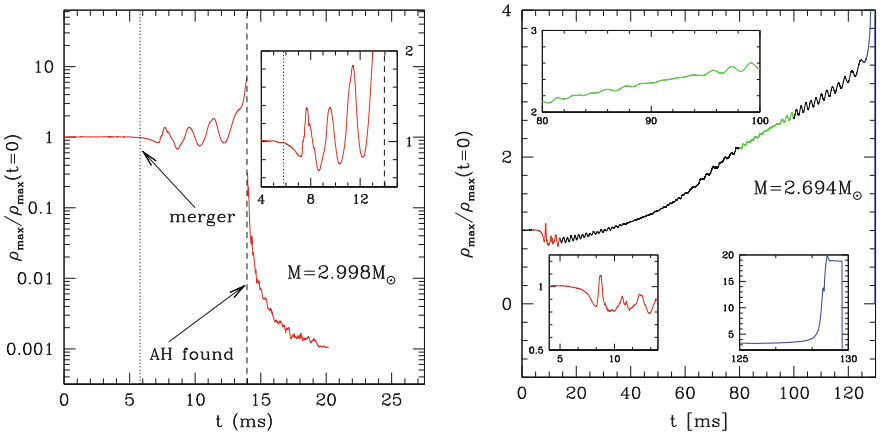


**Fig. 10.3** *Left panel:* Evolution of the maximum rest-mass density normalized to its initial value for a high-mass (individual stellar rest mass $1.625M_\odot$; gravitational mass of the system $2.998M_\odot$) binary using an ideal-fluid EOS. Indicated with a dotted vertical line is the time at which the binary merges, while a vertical dashed line shows the time at which an apparent horizon is found. After this time, the maximum rest-mass density is computed in a region outside the apparent horizon [from Baiotti et al. (2008). © (2008) by the American Physical Society]. *Right panel:* The same as in the left panel but for a low-mass binary (individual stellar rest mass $1.456M_\odot$; gravitational mass of the system $2.694M_\odot$). Note that the evolution is much longer in this case and that different colours are used to denote the different parts of the evolution (see insets) [Adapted from Rezzolla et al. (2010). © IOP Publishing. Reproduced with permission. All rights reserved]

The dynamics of the inspiral and merger of a reference equal-mass binary system is summarised in Fig. 10.3, whose panels show the evolution of the maximum rest-mass density normalized to its initial value (after the formation of the apparent horizon, the curve shows the maximum rest-mass density in the region outside the apparent horizon). Note that together with the large oscillations, the rest-mass density also experiences a secular growth and the increased compactness eventually leads to the collapse to a rotating black hole. The differences in the two panels are essentially related to the initial mass of the system (i.e., $M = 2.998\,M_\odot$ in the left panel and $M = 2.694\,M_\odot$ in the right panel) and it can be seen that, for a given EOS (even a very simple one like the ideal-fluid EOS used in this case) smaller masses will yield systematically longer-lived HMNSs.

The matter dynamics described so far in the various stages of the evolution of a BNS system are imprinted in the GW signal, which then can be used to extract important information on the properties of the neutron stars. Different parts of the evolution will provide distinct pieces of information and with different overall signal-to-noise (SNR) ratios. For example, the post-merger signal would provide rather clear signatures but at such high frequencies that it may be difficult to measure them with present detectors. On the other hand, as we will discuss in detail in the following section, the inspiral signal does depend on the EOS much more weakly, but in a way that is still measurable because it comes at frequencies where the detectors are more sensitive.

## 10.3 Matter Effects During a Binary Inspiral

For inspiraling compact-object binary systems, GW measurements of the source parameters are based on matched filtering, where the datastream is cross-correlated with theoretically predicted template waveforms for different possible parameters within the wide physically plausible range. A detailed understanding and modelling of the effect of neutron-star matter on the binary dynamics and GWs is therefore essential to enhance the science gains from GW observations. For nonspinning compact objects the main imprint of their internal structure on the GW signal from the *inspiral* is due to tidal effects. The energy cost of the tidal deformation together with the contribution from the moving tidal bulges to gravitational radiation accelerate the inspiral inspiral and change the GWs compared to the signal from a black-hole binary. The main characteristic equation-of-state parameter imprinted in the GWs is the star's tidal deformability, as recently measured for GW170817 (Abbott et al. 2017) the ratio of the induced quadrupole moment to the perturbing tidal field.

Tidal effects in binary neutron-star systems are well-known in Newtonian gravity (Bildsten and Cutler 1992; Reisenegger and Goldreich 1994; Lai 1994; Kochanek 1992; Kokkotas and Schaefer 1995), and in post-Newtonian (PN) theory (Damour et al. 1992; Lombardi et al. 1997; Mora and Will 2004). A formal description of the coupling of the neutron-star's internal structure, described by full General Relativity (GR), to the orbital dynamics of a binary at large separation was developed in Flanagan (1998) and expounded upon in Racine and Flanagan (2005). This provided a rigorous proof that there are no new relativistic "star crushing" forces (Wilson and Mathews 1995) and that tidal interactions are the leading-order finite-size effects for nonspinning objects with arbitrarily strong self-gravity at large separation. The dominant tidal effects in the GWs and the associated relativistic tidal parameter were derived in Flanagan and Hinderer (2008), Hinderer (2008). Recent work computed the tidal parameters for higher multipole moments (Damour and Nagar 2009; Binnington and Poisson 2009), for a wide range of equations of state models (Hinderer et al. 2010; Postnikov et al. 2010), examined their physics content (Fattoyev et al. 2013, 2014; Steiner et al. 2015; Lattimer and Lim 2013; Van Oeveren and Friedman 2017) and the effect of stratification and elasticity (Penner et al. 2011), considered various other quantities characterising tidal deformations (Damour and Nagar 2009; Landry and Poisson 2014), the tidal parameters of black holes (Damour and Lecian 2009; Kol and Smolkin 2012; Porto 2016; Gurlebeck 2015) and of exotic objects (Cardoso et al. 2017; Sennett et al. 2017; Mendes and Yang 2017; Uchikata and Yoshida 2016; Pani 2015), and new tidal parameters that appear for slowly rotating neutron stars (Pani et al. 2015a; Landry and Poisson 2015a). Substantial recent interest has also focused on I-Love-Q relations (Yagi and Yunes 2013a,b) that link dimensionless parameters characterising various global properties of the neutron star in an approximately EOS-independent way (Lattimer and Lim 2013; Pappas and Apostolatos 2014; Yagi et al. 2014a; Pappas 2017, 2015; Haskell et al. 2014; Chakrabarti et al. 2014; Maselli

et al. 2013a; AlGendy and Morsink 2014; Chirenti et al. 2015; Pannarale et al. 2015; Steiner et al. 2016; Breu and Rezzolla 2016; Silva et al. 2016; Yagi 2014; Reina et al. 2017; Chan et al. 2015, 2016); see also Chap. 13 of this book.

Significant progress has also been made on describing the tidal effects on the orbital dynamics and gravitational radiation, within post-Newtonian theory (Vines et al. 2011a,b; Bini et al. 2012; Steinhoff et al. 2016), a post-Newtonian affine approach (Ferrari et al. 2012; Maselli et al. 2012), the gravitational self-force formalism (Dolan et al. 2015; Bini and Damour 2014; Nolan et al. 2015; Shah and Pound 2015), effective field theory (Goldberger and Rothstein 2006), and the effective-one-body model (Damour and Nagar 2010; Vines et al. 2011a; Bini et al. 2012; Bini and Damour 2014; Damour et al. 2012; Bernuzzi et al. 2015a; Hinderer et al. 2016; Steinhoff et al. 2016). Comparisons and tests of these descriptions against numerical relativity simulations will be reported in Sect. 10.4 of this chapter. Based on the above models, several measurability studies of the tidal signature in the GW signal have been performed using Bayesian data analysis methods, both for double neutron-star binaries (Del Pozzo et al. 2013; Agathos et al. 2015; Lackey and Wade 2015; Wade et al. 2014; Chatziioannou et al. 2015; Markakis et al. 2009) and for neutron-star–black-hole systems (Lackey et al. 2012, 2014; Kumar et al. 2017), and a first result from LIGO and Virgo observations has recently been reported (Abbott et al. 2017).

This section will focus on theoretical models of matter effects during the inspiral epoch of a neutron-star binary system. We will focus on the main imprints from tidal effects, but in Sect. 10.3.5 will also point out references containing discussions of other effects including rotational deformations, the tidal excitation of a neutron star's various oscillation modes beyond the fundamental mode, nonlinear tidal effects, and other tidal interactions in general relativity that are not present in Newtonian gravity. To introduce the theoretical approaches for describing the inspiral, we will start by recalling tidal effects in Newtonian gravity in Sect. 10.3.1. The Newtonian discussion will be formulated in way that can be promoted to general relativity with appropriate modifications, as will be delineated in Sect. 10.3.2, where we will also review the information needed to compute the tidal parameters for a given equation of state model, and briefly outline approximate universal relations between these parameters and similar parameters characterising the rotational deformation and moment of inertia in Sect. 10.3.3. The effect on the GW signal from a binary inspiral will be considered in Sect. 10.3.4.

*Conventions* We will use units in which $G = c = 1$ unless otherwise indicated. Indices on tensors consisting of Greek letters $\alpha, \beta, \ldots$ denote four-dimensional spacetime quantities, while Latin indices $i, j, k, \ldots$ denote spatial, three-dimensional quantities. We will use overdots on quantities to denote derivatives with respect to coordinate time, e.g., $\dot{x} = dx/dt$.

### *10.3.1 Tidal Interactions in Newtonian Compact Binaries*

In this section we will review Newtonian tidal interactions in a binary system, discuss the characteristic tidal parameters, and derive an effective action that compactly summarizes the dynamics. This formalism, with appropriate modifications, will carry over to the relativistic case discussed in Sect. 10.3.2. We will first review the multipole expansion of the self-field of a body and the gravitational potential of a binary system, then consider the equations of motion and a corresponding action principle. The discussion is based on Vines et al. (2011a) and Steinhoff et al. (2016); some of the introductory material can also be found in the book Gravity by Poisson and Will (2014).

#### 10.3.1.1 Multipole Expansion of the Self-gravitational Potential

We consider two bodies labeled by $A, B$. In Newtonian gravity the gravitational potential generated by a mass distribution with density $\rho_A$ at a field point $\boldsymbol{x}$ is a solution to Poisson's equation $\nabla^2 U_A = -4\pi\rho_A$ or

$$U_A(t,\boldsymbol{x}) = \int d^3x' \rho_A(t,\boldsymbol{x}') \frac{1}{|\boldsymbol{x}-\boldsymbol{x}'|} \tag{10.1}$$

Outside the body's mass distribution, for points $\boldsymbol{x} > \boldsymbol{x}'$, the potential can be written as a Taylor series expansion around a moving reference point $\boldsymbol{z}_A(t)$ as

$$U_A = \int d^3x' \rho_A(t,\boldsymbol{x}') \sum_{\ell=0}^{\infty} \frac{1}{\ell!}(x'-z_A)^L \left(\frac{\partial}{\partial x'^L}\frac{1}{|\boldsymbol{x}-\boldsymbol{x}'|}\right)|_{\boldsymbol{x}'=\boldsymbol{z}_A} \tag{10.2a}$$

$$= \int d^3x' \rho_A(t,\boldsymbol{x}') \sum_{\ell=0}^{\infty} \frac{(-1)^\ell}{\ell!}(x'-z_A)^L \partial_L \frac{1}{|\boldsymbol{x}-\boldsymbol{z}_A|}. \tag{10.2b}$$

Here, the notation is that $L = a_1 a_2 \cdots a_\ell$ denotes a string of $\ell$ indices and

$$x^L = x^{a_1}x^{a_2}\cdots x^{a_\ell}, \qquad \partial_L = \frac{\partial}{\partial x^L} = \frac{\partial}{\partial x^{a_1}}\cdots\frac{\partial}{\partial x^{a_\ell}}, \tag{10.3}$$

Throughout this review, the summation over repeated indices is implied.

Similar to the definitions in electromagnetism, we define the body's Newtonian mass multipole moments by the following integrals

$$M_A = \int_A d^3x\ \rho_A(t,\boldsymbol{x}), \qquad Q_A^L = \int_A d^3x\ \rho_A(t,\boldsymbol{x})(x-z_A)^{<L>}, \tag{10.4}$$

where $M_A$ is the mass of the body and the integration is over a sphere surrounding the matter distribution. The angular brackets around the indices denote the symmet-

ric and trace-free projection of the tensor, e.g., $x^{<ij>} = x^i x^j - \delta^{ij}|\boldsymbol{x}|^2$; see Thorne (1980), Hartmann et al. (1994) for a pedagogical introduction to symmetric and trace-free tensors. The reason that the mass multipole moments defined in Eq. (10.4) are only the trace-free parts of the integrals that would be read off from (10.2b) is that the derivative $\partial_L|\boldsymbol{x} - \boldsymbol{x}'|^{-1}$ is a symmetric and trace-free tensor that projects out only trace-free piece $Q^L$ in the contribution to the potential (10.2a). Finally, the mass dipole term ($\ell = 1$) has been omitted from the expansion (10.4) since it can always be made to vanish by choosing the reference point $z^i_A(t)$ for the multipole expansion to be the body's center of mass. With the definitions from Eq. (10.4), the potential outside the body becomes

$$U_A(t, \boldsymbol{x}) = \frac{M_A}{|\boldsymbol{x} - \boldsymbol{z}_A|} + \sum_{\ell=2}^{\infty} \frac{(-1)^\ell}{\ell!} Q^L \partial_L \frac{1}{|\boldsymbol{x} - \boldsymbol{z}_A|}. \tag{10.5}$$

This form of the potential is convenient for computing the dynamics of a binary system. When considering the deformation of a single object, it is useful to work with spherical coordinates $(x - z_A)^i/|\boldsymbol{x} - \boldsymbol{z}_A| = (\sin\theta\cos\phi, \sin\theta\sin\phi, \cos\theta)$ and express (10.5) as a spherical-harmonic expansion

$$U_A(t, \boldsymbol{x}) = \frac{M_A}{|\boldsymbol{x} - \boldsymbol{z}_A|} + \sum_{\ell=2}^{\infty} \sum_{m=-\ell}^{\ell} Q_{\ell m} \frac{Y_{\ell m}(\theta, \phi)}{|\boldsymbol{x} - \boldsymbol{z}_A|^{\ell+1}}. \tag{10.6}$$

The spherical-harmonic components of the multipole moments are related to the Cartesian multipole moments by (Thorne 1980)

$$Q^A_{\ell m} = \frac{4\pi}{2\ell + 1} \mathcal{Y}^{*\,\ell m}_L Q_L \qquad Q_L = \frac{\ell!}{(2\ell - 1)!!} \sum_{m=-\ell}^{\ell} Q_{\ell m} \mathcal{Y}^{\ell m}_L. \tag{10.7}$$

Here, the quantities $\mathcal{Y}^{\ell m}_L$ are symmetric-trace-free tensors consisting of complex coefficients that appear in the conversion between unit vectors $\boldsymbol{n}$ and spherical harmonics (Thorne 1980)

$$Y_{\ell m} = \mathcal{Y}^{\ell m}_L n^{<L>} \qquad n^{<L>} = \frac{4\pi\,\ell!}{(2\ell + 1)!!} \sum_{m=-\ell}^{\ell} \mathcal{Y}^{\ell m}_L Y^*_{\ell m}. \tag{10.8}$$

#### 10.3.1.2 Expansion of the Companion's Potential and Tidal Moments

Throughout the subsequent discussion, we will consider a binary system in the regime where the separation between the bodies is large compared to the characteristic size of the bodies. The potential due to external sources such as a companion in the binary that is felt by body $A$ is denoted by $U^{\rm ext}_A$ and can be written as a Taylor

expansion around $A$'s center of mass in the form

$$U_A^{\rm ext}(t,\boldsymbol{x}) = U_A^{\rm ext}(t,\boldsymbol{z}_A) + (x-z_A)^j \left[\partial_j U_A^{\rm ext}(t,\boldsymbol{x})\right]_{\boldsymbol{x}=\boldsymbol{z}_A} - \sum_{l=2}^{\infty} \frac{1}{\ell!}(x-z_A)^L \mathcal{E}_A^L, \tag{10.9a}$$

where "ext" denotes that the source of this part of the potential is external to the body. The coefficients $\mathcal{E}_A^L$ in the second line of (10.9) are the body $A$'s tidal moments (Thorne and Hartle 1984). Assuming that the source of the external potential is the potential of body $B$ in a binary system, denoted by $U_B$, the tidal moments are

$$\mathcal{E}_A^L = -\left(\frac{\partial}{\partial x^L} U_B(t,\boldsymbol{x})\right)_{\boldsymbol{x}=\boldsymbol{z}_A(t)}. \tag{10.9b}$$

Similar to the self-field, the decomposition of the external potential in Eq. (10.9) can also be written as a spherical-harmonic expansion using the same conversion and thus not given explicitly here.

### 10.3.1.3 Equations of Motion and Action Principle

The total potential for the binary is $U = U_A + U_B$ and the equations of motion for the center-of-mass positions of either the bodies ($C = A$ or $C = B$) can be derived from Newton's second law:

$$M_C \ddot{z}_C^j = \int d^3x\, \rho_C \frac{\partial}{\partial x^j} U(t,\boldsymbol{x}) = M \frac{\partial}{\partial x^j} U_C^{\rm ext}(t,\boldsymbol{x})\,|_{\boldsymbol{x}=\boldsymbol{z}_C} - \sum_{\ell=2}^{\infty} \frac{1}{\ell!} Q_C^L \mathcal{E}_{jL}, \tag{10.10}$$

where in the second equality we have used the multipole expansions described above and the fact that only the potential sourced by the companion contributes to the body's motion, as can be verified by direct calculation.

The dynamics can be conveniently summarised by an action principle constructed from the Lagrangian $\mathcal{L} = T - V$, where $T = T_A + T_B$ is the total kinetic energy and $V = V_A + V_B$ the potential energy for the binary system. As reviewed in detail in Vines et al. (2011a), each of these contributions can be split into a the center-of-mass motion of the body and an internal contribution:

$$T_A = \frac{1}{2}\int_A d^3x \rho_A \dot{z}_A^2 + T_A^{\rm int}, \qquad V_A = \frac{1}{2}\int_A d^3x \rho_A U_B + V_{\rm int}. \tag{10.11}$$

For simplicity, we will specialise the subsequent discussion to the case where only $A$ is an extended body while $B$ is a point mass. To linear order in the finite-size effects, the case of two extended objects can be recovered by adding the same contribution with $A$ and $B$ interchanged. Performing the expansions around $A$'s center of mass,

using the definitions of the multipole and tidal moments, adding the contributions $T_B$ and $V_B$ from the companion, and transforming to the barycentric frame of the binary system leads to

$$T = \frac{1}{2}\mu v^2 + T_{\rm int}, \qquad V = -\frac{\mu M}{r} + \sum_{\ell\geq 2}\frac{1}{\ell!}Q_L\mathcal{E}_L + V_{\rm int}. \tag{10.12}$$

Here, we have defined the total mass $M = M_A + M_B$, the reduced mass $\mu = M_A M_B/M$, and the relative separation $\boldsymbol{r} = \boldsymbol{z}_A - \boldsymbol{z}_B$ whose magnitude we denote by $r = |\boldsymbol{r}|$, as well as the relative velocity $v^2 = \dot{\boldsymbol{r}}\cdot\dot{\boldsymbol{r}}$. The action is then given by (Flanagan and Hinderer 2008; Rathore et al. 2003; Lai 1994)

$$S = S_{\rm orbit} + \int dt \sum_{\ell\geq 2}\Big[-\frac{1}{\ell!}Q_L\mathcal{E}_L + \mathcal{L}^{\rm int}\Big], \tag{10.13}$$

where $S_{\rm orbit} = \int dt\, L_{\rm orbit}$, with $L_{\rm orbit} = (\mu/2)v^2 + \mu M/r$, describes the orbital motion of point-masses and $\mathcal{L}^{\rm int}$ encapsulates the internal dynamics of the multipole moments mass multipole moment that still remain to be specified. We will discuss the form of $\mathcal{L}^{\rm int}$ for the case where the multipole moments are tidally induced in the next subsection. The advantage of the formulation in Eq. (10.13) is that the information about the binary dynamics in summarised in a simple, single scalar function.

#### 10.3.1.4 Tidally Induced Multipole Moments

We will now further specialise to the case of a body that would be spherically symmetric in isolation and whose multipole moments result only from the response to the companion's tidal field (Bildsten and Cutler 1992; Reisenegger and Goldreich 1994; Lai et al. 1993; Lai 1994; Zahn 1977, 1970; Kopal 1978; Kochanek 1992; Hansen 2006; Mora and Will 2004; Kokkotas and Schaefer 1995; Flanagan and Hinderer 2008; Ferrari et al. 2012; Damour et al. 1992; Shibata 1994). For a neutron star, the main dynamics of the tidally induced multipole moments can be described by its fundamental oscillation modes ($f$-modes) with an internal Lagrangian having the form of a harmonic oscillator (Flanagan and Hinderer 2008; Rathore et al. 2003; Lai 1994; Kokkotas and Schaefer 1995)

$$\mathcal{L}^{\rm int} = \frac{1}{2\ell!\lambda_\ell\omega_{0\ell}^2}\Big[\dot{Q}_L\dot{Q}^L - \omega_{0\ell}^2 Q_L Q^L\Big]. \tag{10.14}$$

An explicit derivation of this Lagrangian starting from the mode amplitudes of the fluid displacement and their relation to the multipole moments is exhibited in Chakrabarti et al. (2013). Here, the quantities $\omega_{0\ell}$ denote the $f$-mode frequencies, and only the contribution from the modes with no radial nodes have been included

since higher modes contribute very little to the effect (McDermott et al. 1985). The parameters $\lambda_\ell$ are the tidal deformability coefficients that are defined by considering the *adiabatic* limit, where the body's internal time scales $\tau^{\rm int} \sim \omega_{0\ell}^{-1} \sim \sqrt{R^3/M_A}$ are fast compared to the time scale of variations in the tidal field $\tau_{\rm orb} \sim \sqrt{r^3/(M_A+M_B)}$. They characterize the equation-of-state-dependent ratio between the induced multipoles and the tidal field

$$Q_L^{\rm adiab} = -\lambda_\ell \, \mathcal{E}_L, \tag{10.15}$$

and are sometimes also referred to as the tidal polarizability. The tidal parameters $\lambda_\ell$ are related to the body's tidal Love numbers $k_\ell$ (or apsidal constants) that were introduced by the British scientist A.E.H. Love in (1909) and its radius $R$ by

$$\lambda_\ell = \frac{2}{(2\ell-1)!!} k_\ell R^{2\ell+1}. \tag{10.16}$$

In many contexts it is useful to work with the dimensionless tidal deformabilities

$$\Lambda_\ell = \frac{\lambda_\ell}{M^{2\ell+1}} = \frac{2}{(2\ell-1)!!} k_\ell C^{-(2\ell+1)}, \tag{10.17}$$

where $C = M/R$ is the star's compactness.

For adiabatically induced multipoles, $dQ_L/dt = 0$ and the internal Lagrangian is only the elastic potential energy associated with the deformation

$$\mathcal{L}^{\rm int}_{\rm adiab} = -\frac{1}{2\ell!\lambda_\ell} Q_L Q^L. \tag{10.18}$$

Using the relation (10.15), the finite size effects can be written entirely in terms of the orbital variables and $\lambda_\ell$:

$$S_{\rm adiab} = S_{\rm orbit} + \int dt \left[ \frac{\lambda_\ell}{2\ell!} \mathcal{E}_L \mathcal{E}^L \right], \tag{10.19}$$

where in this Newtonian context $\mathcal{E}_L = -M_B \partial_L r^{-1}$. The quantities $\lambda_\ell$ or $k_\ell$ depend on the details of the body's internal structure, and their computation therefore requires an explicit description of the perturbed interior.

For the Newtonian calculations of $\lambda_\ell$ we work in the rest frame of the body, in a region surrounding it that excludes the companion. The first step is to obtain an equilibrium configuration for the body in isolation, by solving to the Poisson equation for the gravitational potential together with the continuity and Euler's equations that express the conservation of mass and momentum:

$$\nabla^2 U = -4\pi\rho, \qquad \frac{\partial \rho}{\partial t} + \nabla\cdot(\rho \boldsymbol{v}) = 0, \qquad \frac{\partial v^i}{\partial t} + (\boldsymbol{v}\cdot\nabla) v^i = -\frac{\partial^i p}{\rho} + \partial_i U + a^i_{\rm ext}, \tag{10.20}$$

where $a^i_{\rm ext}$ is the acceleration due to external forces. Next, we suppose that the star is disturbed by an external static tidal gravitational field, e.g., due to a distant companion. The tidal disturbance is characterized by the set of moments $\mathcal{E}_L$, that each cause the star to deform in response and settle down to a new static configuration which has a nonzero set of mass multipole moments $Q_L$. The gravitational potential outside the perturbed star is

$$U_{\rm total} = U_{\rm self} + U_{\rm tidal} = \frac{M}{r} + \sum_{\ell=2}^{\infty} \sum_{m=-\ell}^{\ell} Y_{\ell m} \left[ \frac{Q_{\ell m}}{r^{\ell+1}} - \frac{1}{(2\ell-1)!!} \mathcal{E}_{\ell m} r^{\ell} \right] \tag{10.21}$$

The multipole moments $Q_{\ell m}$ characterising the body's response are associated with the piece of the exterior potential that falls off as $1/r^{\ell+1}$, while the external tidal field is related to the terms that grow as $r^{\ell}$. To linear order in the external tidal perturbation and in the adiabatic limit, the induced distortion will be linearly proportional to the tidal perturbation as in Eq. (10.15). Using the properties from (10.8) and an analogous decomposition as in (10.7) for $\mathcal{E}_L$ the relation (10.15) can be written as

$$Q_{\ell m} = -\lambda_{\ell} \mathcal{E}_{\ell m} \tag{10.22}$$

for each $\ell$th multipole. To compute $\lambda_{\ell}$ it is sufficient to consider a single value of $m$. The parameters are computed by matching the interior solution and the exterior description (10.21) at the surface of the star, as we briefly recall here. First, we compute the interior solution by noting that the perturbed neutron star is still described by (10.20) but with perturbed pressure $p = p_0 + \delta p$, density $\rho = \rho_0 + \delta\rho$, gravitational potential $U = U_0 + \delta U$, and an external acceleration $\boldsymbol{a}_{\rm ext} = \boldsymbol{\nabla} U_{\rm tidal}$. The fluid perturbation can be represented by a Lagrangian displacement $\xi(x,t)$ which is defined so that the fluid element at position $x$ in the unperturbed star is at position $x + \xi(x,t)$ in the perturbed star. Expanding Euler's equation about the background star to linear order in the perturbations yields

$$\frac{d^2\xi^i}{dt^2} = -\frac{\partial_i \delta p}{\rho_0} + \frac{\partial_i p_0}{\rho_0^2}\delta\rho + \partial_i \delta U + a^i_{\rm ext}. \tag{10.23}$$

For a barotropic equation-of-state relation of the form $p = p(\rho)$ we can eliminate $\delta p$ from (10.23) in terms of $\delta\rho$. After further specialising (10.23) to static perturbations ($\dot{\xi} = 0$), combining all terms that involve $\delta\rho$ into a total derivative, and integrating we obtain

$$\frac{1}{\rho_0}\frac{dp_0}{d\rho_0}\delta\rho - \delta U_{\rm tot} = \text{const}, \tag{10.24}$$

where $\delta U_{\rm tot} = \delta U + U_{\rm tidal}$. Using the expansions

$$\delta\rho = f(r)Y_{\ell m}(\theta,\phi), \qquad \delta U_{\rm tot} = H(r)Y_{\ell m}(\theta,\phi), \tag{10.25}$$

and substituting this decomposition into the linearized Poisson's equation leads to

$$-4\pi f(r)Y_{\ell m} = Y_{\ell m}\frac{1}{r^2}\frac{d}{dr}r^2\frac{dH(r)}{dr} + H(r)\left[\frac{1}{r^2\sin\theta}\partial_\theta\sin\theta\partial_\theta + \frac{1}{r^2\sin^2\theta}\partial_\phi^2\right]Y_{\ell m} \tag{10.26}$$

$$= Y_{\ell m}\left[H'' + \frac{2}{r}H'\right] - H(r)\frac{\ell(\ell+1)}{r^2}Y_{\ell m}. \tag{10.27}$$

Next, using (10.25) in Eq. (10.24) shows that the integration constant must vanish since the rest of the equation is purely $\ell \geq 2$, and we obtain the relation between the radial functions

$$\frac{1}{\rho_0}\frac{dp_0}{d\rho_0}f - H = 0. \tag{10.28}$$

Combining Eqs. (10.27) and (10.28) leads to a single master equation for $H(r)$ in the region $r \leq R$:

$$H'' + \frac{2}{r}H' - \frac{\ell(\ell+1)}{r^2}H = -4\pi\left(\frac{1}{\rho_0}\frac{dp_0}{d\rho_0}\right)^{-1}H. \tag{10.29}$$

Except for special choices of the equation of state (EOS), this ODE has to be integrated numerically in the interior of the object, with the boundary condition that ensures regularity at the center of the star, $H \propto r^\ell$ for $r \to 0$. For $r > R$ the exterior solution is

$$H^{\rm ext} = \frac{Q_{\ell m}}{r^{\ell+1}} - \frac{1}{(2\ell-1)!!}\mathcal{E}_{\ell m}r^\ell = -\mathcal{E}_{\ell m}\left[\frac{\lambda_\ell}{r^{\ell+1}} + \frac{1}{(2\ell-1)!!}r^\ell\right]. \tag{10.30}$$

To extract the Love numbers we eliminate $\mathcal{E}_{\ell m}$ by considering the logarithmic derivative

$$y(r) = \frac{rH'(r)}{H(r)}. \tag{10.31}$$

We solve for $k_\ell$ by using (10.30) in (10.31) and matching the results for $y(R)$ obtained from the interior and exterior solutions at the stellar surface:

$$k_\ell = \frac{\ell - y(R)}{2\left[\ell + 1 + y(R)\right]}. \tag{10.32}$$

The strategy for practical computations of the Love number is thus the following: (1) obtain a solution for the background configuration, (2) compute the perturbed

interior described by (10.29) and evaluate from it $y(R)$ at the surface, and (3) use this result in Eq. (10.32) to obtain the Love number. Exact solutions can be obtained for simple EOSs, for example for an incompressible $n = 0$ polytrope $k_\ell = 3/(4\ell - 4)$. The same general method applies in the relativistic case, where, however, one has to use Einstein's equations and a more general definition of the multipole moments and hence the solutions become more complex.

### *10.3.2 Tidal Effects in General Relativity*

The Newtonian results for the binary dynamics of extended nonspinning objects (10.14) and computation of the characteristic tidal deformability coefficients can be turned into a relativistic result in the following way (Flanagan and Hinderer 2008; Hinderer 2008; Steinhoff et al. 2016), see also Bini et al. (2012) for the action in the adiabatic limit and Goldberger and Rothstein (2006) for an effective field theory approach. We still consider the regime where the separation between the bodies is large compared to their size, so that the description of the binary can be divided into several zones, each amenable to a different approximation method (Flanagan 1998; Racine and Flanagan 2005): (1) The "body-zone" extending over the neighbourhood of each body, where the presence of the companion produces small perturbations to its equilibrium structure but a fully relativistic description is required. (2) The "orbital zone" far from the bodies where the dynamics can be computed from post-Newtonian (PN) theory and is dominated by their point-mass contributions, with small corrections due to their finite size encoded in their multipole moments. (3) The "buffer zone", at distances large compared to the size of the body but small compared to the orbital separation, where both descriptions are connected by matching; this is also the region where the body's multipole and tidal moments are defined.

#### 10.3.2.1 Definition of the Body's Tidal Moments

The generalisation of expanding the gravitational potential around the body's center of mass is the so-called worldline-skeleton description (Dixon 1970), where one considers a reference center-of-mass worldline $z^\mu(\sigma)$ with $\sigma$ being a parameter along the worldline, together with a set of multipole moments of the body. The body's gravitoelectric tidal moments $\mathcal{E}_{\mu\nu}$ are given by projecting the "electric part" of the spacetime curvature due to the companion that is characterized by the Weyl tensor $C_{\mu\alpha\nu\beta}$ as (Thorne and Hartle 1984)

$$\mathcal{E}_{\mu\nu} = C_{\mu\alpha\nu\beta}\frac{u^\alpha u^\beta}{z^2} \tag{10.33}$$

where $u^\mu = dz^\mu/d\sigma$ is the tangent to the worldline and

$$z = \sqrt{-u^\gamma u_\gamma} \tag{10.34}$$

Since we are considering a region of spacetime that excludes the source of the curvature, the Weyl tensor is the same as the Riemann tensor and $R_{\mu\alpha\nu\beta}$ could equivalently be used in (10.33). The tensor $\mathcal{E}_{\mu\nu}$ has the properties that it is symmetric and trace free and is purely spatial in the body's rest frame, $\mathcal{E}_{\mu\nu}u^\nu = 0$. In the rest frame, $u^\mu = (-1, 0, 0, 0)$ and $\mathcal{E}_{ij} = C_{0i0j}$ replaces (10.33). Higher multipole tidal moments are defined in an analogous way from covariant derivatives of the Weyl tensor projection

$$\mathcal{E}_L = \frac{1}{(\ell-2)!} C_{\langle 0a_1 0a_2; a_3 \cdots a_\ell \rangle}, \tag{10.35}$$

where a semicolon denotes a covariant derivative.

#### 10.3.2.2 Definition of the Body's Multipole Moments

To define the body's multipole moments we consider a region of spacetime at distances outside the body that are large compared to the size of the object but small compared to the radius of curvature of the source of the tidal perturbations. In this zone, the body's multipole moments can be read off from the asymptotic metric expressed in a local asymptotic frame (Thorne 1980, 1998). For example, the time-time component of the metric can be written in terms of an effective potential $U_{\rm eff}$ that is analogous to the Newtonian gravitational potential:

$$g_{tt} = -\left(1 - 2U_{\rm eff}\right), \tag{10.36}$$

where for a spherical body described by the Schwarzschild exterior spacetime $U_{\rm eff} = M/r$ with $r$ denoting the distance from the body. For a nonspherical body, the asymptotic form of this metric function is

$$\lim_{r\to\infty} U_{\rm eff} = \frac{M}{r} + \frac{3n^{<ij>}Q_{ij}}{2r^3} + \mathcal{O}(r^{-4}) - \frac{1}{2}n^{<ij>}\mathcal{E}_{ij}r^2 + \mathcal{O}(r^3). \tag{10.37}$$

In this setting, the $\ell$th mass multipole moment is associated with the piece in the asymptotic expansion that falls off as $r^{-(\ell+1)}$. This method to define the multipole moments of a body is equivalent to the Geroch-Hansen multipole moments for stationary spacetimes (Guersel 1983). However, for tidally induced moments in a binary system a small ambiguity remains in the above definitions (Thorne and Hartle 1984).

Finally, the definition of $\lambda_\ell$ from Eq. (10.15) still applies for the relativistic definitions of $\mathcal{E}_L$ and $Q_L$.

Another new feature of General Relativity that is absent in Newtonian gravity is that there are also gravitomagnetic tidal fields that induce current multipoles. In the local frame of the star, the gravitomagnetic part of the curvature is given by

$$\mathcal{B}_L = \frac{3}{2(\ell+1)(\ell-2)!}\epsilon_{<a_1 jk} C^{jk}{}_{a_2 0; a_3 \cdots a_\ell >}, \tag{10.38}$$

where $\epsilon_{ijk}$ is the completely antisymmetric permutation tensor. The induced current moments $\mathcal{S}_L$ appear in the time-space part of the asymptotic metric in a local asymptotic frame

$$g_{tj} = -\frac{8}{r^3}\epsilon_{jki}\mathcal{S}_{ki} n^{<ki>} + \mathcal{O}(r^{-4}) + \frac{2}{3}\epsilon_{jpq}\mathcal{B}^q_{\ k} r^2 n^{<pk>} + \mathcal{O}(r^3), \tag{10.39}$$

where $S_{ij}$ is the body's current quadrupole moment and $\mathcal{B}_{ij}$ the quadrupolar gravitomagnetic tidal moment. Similar to the tidal deformability tidal deformability coefficients $\lambda_\ell$, the relation between $\mathcal{S}_L$ and $\mathcal{B}_L$ is characterized by a set of gravitomagnetic Love numbers $\sigma_\ell$

$$\mathcal{S}_L = -\sigma_\ell \mathcal{B}_L \,. \tag{10.40}$$

These have no Newtonian analogue but can also be written in terms of dimensionless Love numbers $j_\ell$ as $\sigma_\ell = (\ell-1)/[4(\ell+2)(2\ell-1)!!]R^{2\ell+1} j_\ell$ . See e.g. Damour and Nagar (2009) and Landry and Poisson (2015b) for further details.

#### 10.3.2.3 Computation of Tidal Love Numbers in General Relativity

Before discussing tidally perturbed bodies we briefly review the construction of a spherically symmetric, isolated nonspinning neutron-star solution. The metric can be expressed as (Hartle 1967)

$$ds_0^2 = -e^{\nu(r)}dt^2 + e^{\gamma(r)}dr^2 + r^2(d\theta^2 + \sin^2\theta d\varphi^2)\,, \tag{10.41}$$

and neutron-star matter is modeled by a perfect-fluid stress-energy tensor

$$T_{\mu\nu} = (\rho + p)u_\mu u_\nu + p g_{\mu\nu}\,, \tag{10.42}$$

where $p$ and $\rho$ are the neutron-star's pressure and energy density and $u^\mu$ is the fluid's four-velocity. In the body's rest frame, the normalization condition $u_\mu u^\mu = -1$ implies that $u^\mu = (e^{-\nu/2}, 0, 0, 0)$. Substituting these expressions into the field equations $G_{\mu\nu} = 8\pi T_{\mu\nu}$ yields the Oppenheimer-Volkoff equations:

$$\frac{dm}{dr} = 4\pi r^2 \rho\,, \qquad \frac{d\nu}{dr} = 2\frac{4\pi r^3 p + m}{r(r-2m)}\,, \qquad \frac{dp}{dr} = -\frac{(4\pi r^3 p + m)(\rho + p)}{r(r-2m)}\,, \tag{10.43}$$

where $m(r)$ is defined by

$$m(r) \equiv \frac{\left[1 - e^{-\gamma(r)}\right] r}{2} \,. \tag{10.44}$$

Outside the star, $m(r)$ becomes the body's constant gravitational mass $M$. To solve Eq. (10.43) requires specifying an EOS, $p = p(\rho)$. The interior solution is obtained by imposing regularity at the neutron-star center with a choice of central density $\rho_c$. The initial conditions close to the center $r \to 0$ are $\rho = \rho_c + \mathcal{O}(r^2)$, $p = p_c + \mathcal{O}(r^2)$, and $m = (4\pi/3)\rho_c r^3 + \mathcal{O}(r^5)$ where $p_c$ is the central pressure. The neutron-star's surface $r = R$ corresponds to a vanishing pressure $p(R) = 0$.

We next consider linear, static perturbations to the equilibrium configuration described by the metric

$$ds^2 = ds_0^2 + h_{\mu\nu} dx^\mu dx^\nu . \tag{10.45}$$

We will work in the Regge-Wheeler gauge where $h_{\mu\nu}$ can be analysed into tensorial spherical harmonics (Regge and Wheeler 1957; Thorne and Campolattaro 1967; Ipser and Price 1991; Detweiler and Lindblom 1985). These are characterized by the mode integers $(\ell, m)$ and by a parity $\pi$ which can be either $(-1)^\ell$ or $(-1)^{\ell+1}$. For small perturbations the $(\ell, m, \pi)$ modes are decoupled and the electric-type or even-parity $\pi = (-1)^\ell$ perturbations to the metric take the form

$$h^{\rm e}_{\mu\nu} dx^\mu dx^\nu = \sum_{\ell,m} \left[ - e^\nu H_0^{\ell m} dt^2 + 2 H_1^{\ell m} dt dr + e^\gamma H_2^{\ell m} dr^2 + r^2 K^{\ell m} d\Omega^2 \right] Y^{\ell m} \tag{10.46}$$

Here, the functions $H_0$, $H_2$ and $K$ generically depend on $(t, r)$. However, for our purposes it is sufficient to consider static perturbations, where these functions depend only on $r$. The perturbations to the stress-energy tensor are given by (Thorne and Campolattaro 1967)

$$\delta T^0_0 = -\delta\rho_\ell Y_{\ell m}(\theta, \varphi) = -\frac{d\rho}{dp} \delta p_\ell Y_{\ell m}(\theta, \varphi) \,, \qquad \delta T^i_i = \delta p_\ell Y_{\ell m}(\theta, \varphi) \,. \tag{10.47}$$

We substitute the above decompositions into the Einstein field equations $G^\nu_\mu = 8\pi T^\nu_\mu$ and the stress-energy conservation $\nabla_\mu T^{\mu\nu} = 0$, and extract only the pieces that are linear in the perturbations in all the components. This leads to the relations

$$H_0 = H_2 \equiv H \,, \qquad H_1 = 0 \,, \qquad \frac{\delta p}{\rho + p} = -\frac{1}{2} H \,. \tag{10.48}$$

Further, the $(r, r)$ and $(r, \theta)$-components can be used to algebraically eliminate $K$ and $K'$ in favour of $H$ and its derivatives. Finally, the $(t, t)$ component leads to the

following second-order differential equation

$$0 = \frac{d^2H}{dr^2} + \left\{\frac{2}{r} + e^{\gamma}\left[\frac{2M}{r^2} + 4\pi r(p-\rho)\right]\right\}\frac{dH}{dr} + \left\{e^{\gamma}\left[-\frac{\ell(\ell+1)}{r^2} + 4\pi(\rho+p)\frac{d\rho}{dp} + 4\pi(5\rho+9p)\right] - \left(\frac{dv}{dr}\right)^2\right\}H\,. \quad (10.49)$$

The initial condition at the center, for $r \to 0$, is $H \propto r^{\ell}$ to ensure regularity of the solution. The constant of proportionality is irrelevant in further calculations of the tidal deformabilities and can be chosen arbitrarily.

Outside the star, the metric perturbation reduces to the general form

$$H_\ell = a_\ell^Q Q_{\ell 2}(x) + a_\ell^P P_{\ell 2}(x)\,, \quad (10.50)$$

where $x \equiv r/M - 1$ and $P_{\ell 2}(x)$ and $Q_{\ell 2}(x)$ are the normalized associated Legendre functions of the first and second kinds respectively. The normalization is such that for $x \to \infty$ the asymptotic forms are $P_{\ell 2}(x) \sim x^{\ell}$ and $Q_{\ell 2}(x) \sim x^{-(\ell+1)}$. The constants $a_\ell^P$ and $a_\ell^Q$ are determined by matching the logarithmic derivative of the interior and exterior solutions,

$$y_\ell \equiv \frac{r}{H_\ell}\frac{dH_\ell}{dr}\,, \quad (10.51)$$

at the neutron-star surface. Comparing with the definition of $Q_\ell$ and $\mathcal{E}_\ell$ in the asymptotic metric (10.37) and the definition of the Love numbers enables writing the general expression for $\Lambda_\ell$ in the form given in Damour and Nagar (2009) (see Binnington and Poisson (2009) for an alternative expression):

$$(2\ell-1)!!\Lambda_\ell = -\left.\frac{P'_{\ell 2}(x) - C y_\ell P_{\ell 2}(x)}{Q'_{\ell 2}(x) - C y_\ell Q_{\ell 2}(x)}\right|_{x=1/C-1}\,, \quad (10.52)$$

where $C = M/R$ is the neutron-star's compactness. The computation of $\Lambda_\ell$ thus proceeds by numerically solving for the background and perturbations in the interior, evaluating the results at the neutron-star surface, and using Eq. (10.52). For the dominant quadrupolar effect the explicit expression is

$$\Lambda\,|_{\ell=2} = \frac{16}{15}(1-2C)^2[2+2C(y-1)-y] \times \Big\{2C[6-3y+3C(5y-8)] + 4C^3[13-11y+C(3y-2)+2C^2(1+y)] + 3(1-2C)^2[2-y+2C(y-1)]\ln(1-2C)\Big\}^{-1}\,, \quad (10.53)$$

where $y$ is evaluated at the surface $r = R$. Since $H$ itself does not enter into Eq. (10.53) and only the combination of potentials (10.51) is needed it is more efficient to transform Eq. (10.49) into an equation for $y$. For $\ell = 2$ this becomes (Lindblom and Indik 2014; Landry and Poisson 2014):

$$\frac{dy}{dr} = \frac{4(m+4\pi r^3 p)^2}{r(r-2m)^2} + \frac{6}{r-2m} - \frac{y^2}{r} - \frac{r+4\pi r^3(p-\rho)}{r(r-2m)}y - \frac{4\pi r^2}{r-2m}\left[5\rho + 9p + \frac{\rho+p}{(dp/d\rho)}\right]. \tag{10.54}$$

Recasting the problem into the form (10.54) thus requires only integrating the first order differential equation with the boundary condition $y = 2$ at the center and evaluating the result at $r = R$. See Chakrabarti et al. (2013b) for a more general approach that simultaneously determines the tidal deformability and oscillation mode frequencies.

For an incompressible star with $\rho = \text{const}$ or $p = K\rho^{1+1/n}$ with $n = 0$, the density profile is a step function and the matching of the interior and exterior solutions must be modified in the following way (Damour and Nagar 2009). After obtaining a numerical solution to Eq. (10.54) in the interior the result is evaluated at the surface to determine $y^{\text{in}}(R)$. The step-function density discontinuity has a nonvanishing derivative at the neutron star surface, which must be taken into account and leads to a correction to the value of $y$ just outside the star $y^{\text{out}}$ that is computed from the relation, valid for any $\ell$,

$$y^{\text{out}}_{\text{incompressible}} = y^{\text{in}}_{\text{incompressible}} - 3. \tag{10.55}$$

#### 10.3.2.4 Tidal Love Numbers for Current Multipoles

Gravitomagnetic tidal perturbations are described by the odd-parity sector of the metric. They can be decomposed as (Thorne and Campolattaro 1967)

$$ds^2 = ds_0^2 - 2h_{0,\ell}(r)\frac{\partial_\varphi Y_{\ell m}(\theta,\varphi)}{\sin\theta}dtd\theta + 2h_{0,\ell}(r)\sin\theta\partial_\theta Y_{\ell m}(\theta,\varphi)dtd\varphi\,. \tag{10.56}$$

The perturbations to the stress-energy tensor depend on the assumptions on the fluid such as strict hydrostatic equilibrium as used in Damour and Nagar (2009) or that an irrotational configuration as a more realistic scenario studied in Landry and Poisson (2015b). The differential equations for the perturbed metric components can be derived similar to the procedure in the even-parity case. The master variable in this case is defined by

$$h \equiv r^3\frac{d}{dr}\left(\frac{h_{0,\ell}}{r^2}\right) \tag{10.57}$$

and it satisfies the differential equation (Landry and Poisson 2015b)

$$\frac{d^2h}{dr^2}+\frac{e^\gamma}{r^2}\left[2M+4\pi(p-\rho)r^3\right]\frac{dh}{dr}-e^\gamma\left[\frac{\ell(\ell+1)}{r^2}-\frac{6M}{r^3}+(1-2\varepsilon)4\pi(\rho-p)\right]h=0\,. \tag{10.58}$$

Here, the parameter $\varepsilon$ characterises the assumptions on the fluid: $\varepsilon = 1$ for the irrotational case, and $\varepsilon = 0$ for strict hydrostatic equilibrium.

The gravitomagnetic Love numbers $\sigma_\ell$ are computed similar to the electric-type ones. The differential equation (10.58) is integrated numerically in the neutron-star interior with the initial condition at the center $h \propto r^{\ell+1}$ to ensure regularity, where the constant of proportionality is irrelevant for the final result. For the exterior solution, the asymptotic behavior of the two independent solutions at spatial infinity is $\hat{h}^P_\ell \sim (r/M)^{\ell+1}$ and $\hat{h}^Q_\ell \sim (r/M)^{-\ell}$. Specifically, for $\ell = 2$, the exterior solutions are given by $\hat{h}^P_2 = (r/M)^3$ and $\hat{h}^Q_2 = -(r/M)^3\partial_{(r/M)}[F(1,4;6;2M/r)M^4/r^4]/4$, where $F(a,b;c;z)$ is a hypergeometric function. As in the even-parity case, Love numbers are determined by matching $y^\sigma_\ell \equiv (r/h)(dh/dr)$ at the neutron-star surface, which leads to (Damour and Nagar 2009; Landry and Poisson 2015b)

$$\sigma_\ell = -\frac{(\ell-1)M^{2\ell+1}}{4(\ell+2)(2\ell-1)!!}\frac{\hat{h}^{P\prime}_\ell(C^{-1})-Cy^\sigma_\ell(C^{-1})\hat{h}^P_\ell(C^{-1})}{\hat{h}^{Q\prime}_\ell(C^{-1})-Cy^\sigma_\ell(C^{-1})\hat{h}^Q_\ell(C^{-1})}\,. \tag{10.59}$$

#### 10.3.2.5 Love Numbers for Deformations of Isodensity Surfaces

The Love numbers discussed in the previous sections characterize the spacetime geometry at large distances from the deformed object. In the Newtonian limit, the multipole moments of the gravitational potential are related to the shape or surficial Love numbers $h_\ell$ characterising the deformation of the object's surface by $h_\ell = 1 + 2k_\ell$. In General Relativity, this relation becomes more complex and must be obtained by considering gauge-invariant quantities such as curvature scalars. Consider an initially spherical star of radius $R$ whose surface deforms in response to a tidal disturbance. To linear order in the deformation, the Ricci scalar curvature of the surface is given by (Damour and Nagar 2009; Landry and Poisson 2014)

$$\mathcal{R} = \frac{1}{R^2}(2+\delta\mathcal{R}), \qquad \delta\mathcal{R} = -2\sum_{\ell=2}^{\infty}\frac{\ell+2}{\ell}h_\ell\frac{R^{\ell+1}}{M}\mathcal{E}_L n^L. \tag{10.60}$$

The general-relativistic relation between shape and tidal Love numbers is (Landry and Poisson 2014)

$$h_\ell = \Gamma_1 + 2\Gamma_2\, k_\ell, \tag{10.61}$$

where

$$\Gamma_1 = \frac{\ell+1}{\ell-1}(1-M/R)F(-\ell,-\ell;-2\ell;2M/R) - \frac{2}{\ell-1}F(-\ell,-\ell-1;-2\ell;2M/R), \tag{10.62a}$$

$$\Gamma_2 = \frac{\ell}{\ell+2}(1-M/R)F(\ell+1,\ell+1;2\ell+2;2M/R) + \frac{2}{\ell+2}F(\ell+1,\ell;2\ell+2;2M/R), \tag{10.62b}$$

where $F(a,b;c;z)$ is the hypergeometric function.

The relation of Eq. (10.61) can be applied directly to black holes, for which $M/R = 1/2$ and $k_\ell = 0$, and thus (Damour and Lecian 2009)

$$h_\ell^{\rm BH} = \frac{\ell+1}{2(\ell-1)}\frac{\ell!^2}{(2\ell)!}, \tag{10.63}$$

#### 10.3.2.6 Love Numbers for Tidally Perturbed Spinning Neutron Stars

For spinning neutron stars, new kinds of tidal couplings arise for which there are corresponding new Love numbers (Pani et al. 2015b; Landry 2017). The calculations become more complicated than for nonspinning objects because it leads to a coupling between spherical harmonic modes in the perturbation equations and because the identification of the Love numbers from asymptotic considerations becomes more subtle (Pani et al. 2015a,b; Landry and Poisson 2015a; Landry 2017). These issues have only recently received consideration and work is still ongoing to fully address the calculations of spin-tidal effects in a binary systems.

### *10.3.3 I-Love-Q Relations*

The I-Love-Q relations are inter-relations between dimensionless quantities characterising the stellar moment of inertia $I$, the tidal parameter $\Lambda$, and spin-induced quadrupole moment $Q$ that are insensitive to the equation of state to within a good approximation. These and similar relations in more general contexts beyond the inspiral and post-merger are discussed in Chap. 13. The computation of $I$ and $Q$ is reviewed in Yagi and Yunes (2017a) and will not be discussed in detail here.

The moment of inertia and spin-induced quadrupole moment are computed using a similar approach as for the computation of tidal deformabilities discussed above, by solving Einstein's equations and stress-energy conservation for small perturbations around an equilibrium stellar configuration. In this case the perturbations are due to the star's rotation instead of an external tidal field. At linear order in the spin the perturbation equations give the moment of inertia $I$ relating the magnitude of the spin angular momentum $S$ to the angular frequency $\Omega$ through $S = I\Omega$ and

computed from (Hartle 1967; Kalogera and Psaltis 2000)

$$I = \frac{8\pi}{3}\frac{1}{\Omega}\int_0^R \frac{e^{-(\nu+\gamma)/2} r^5 (\rho + p)\omega_1^{\rm int}}{r - 2m(r)} dr\,, \tag{10.64}$$

where $\omega_1^{\rm int}$ is the solution to the following differential equation in the interior of the star:

$$\frac{d^2\omega_1}{dr^2} + \frac{4 - 4\pi r^2(\rho + p)e^{\lambda}}{r}\frac{d\omega_1}{dr} - 16\pi(\rho + p)e^{\lambda}\omega_1 = 0\,. \tag{10.65}$$

In the Newtonian limit, Eq. (10.64) reduces to (Hartle 1967) $I^{\rm N} = (8\pi/3)\int_0^R r^4 \rho(r) dr$.

The spin-induced quadrupole moment $Q$ determines the magnitude of the quadrupolar deformation of a star due to rotation and is obtained by carrying out the perturbative analysis to quadratic order in the spin. The details are described in Laarakkers and Poisson (1999), Mora and Will (2004), Berti et al. (2008) and will not be discussed here. Similar to the tidal Love numbers, the dimensionless measures of the spin-induced deformations are known as rotational Love numbers. In the Newtonian limit, the rotational and tidal Love numbers quadrupolar are exactly the same, however, relativistic effects break this degeneracy. Nevertheless for current models of neutron star EOSs, there exist mutual relations between the dimensionless parameters $\Lambda$ and

$$\bar{I} = \frac{I}{M^3} \qquad\qquad \bar{Q} = -\frac{QM}{|\vec{S}|^2}, \tag{10.66}$$

that are nearly independent of the EOS, to within percent-level accuracy. These take the empirical form that were tested for a large set of currently available EOSs (Yagi and Yunes 2017a)

$$\begin{aligned}
\ln(\bar{Q}) &= 0.1940 + 0.09163\ln\Lambda + 0.04812(\ln\Lambda)^2 - 4.283\times10^{-3}(\ln\Lambda)^3 \\
&\quad + 1.245\times10^{-4}(\ln\Lambda)^4 \qquad (10.67a)\\
\ln(\bar{I}) &= 1.496 + 0.05951\ln\Lambda + 0.02238(\ln\Lambda)^2 - 6.953\times10^{-4}(\ln\Lambda)^3 \\
&\quad + 8.345\times10^{-6}(\ln\Lambda)^4 \qquad (10.67b)\\
\ln(\bar{I}) &= 1.393 + 0.5471\ln\bar{Q} + 0.03028(\ln\bar{Q})^2 + 0.01926(\ln\bar{Q})^3 \\
&\quad + 4.434\times10^{-4}(\ln\bar{Q})^4. \qquad (10.67c)
\end{aligned}$$

The above relations are only valid in the region where the fit was developed, roughly for the intervals $M \in [0.8, 2.4]M_\odot$, $\bar{I} \in [5, 30]$, $\Lambda \in [2, 4000]$, and $\bar{Q} \in [2, 10]$; see Yagi and Yunes (2013a,b) and Lattimer and Lim (2013).

The $I - Q$ universality encodes a relation between the neutron-star's spin or current dipole moment and its mass quadrupole moment that in some sense is reminiscent of a generalisation of the no-hair relations for black holes. A similar relation was also found for higher multipole moments (Pappas and Apostolatos 2014; Yagi et al. 2014a) that greatly simplify the structure of the exterior spacetime of a neutron star (Pappas 2017, 2015). The universal relations were also found to hold in the presence of weak magnetic fields (Haskell et al. 2014), and rapid rotation (Doneva et al. 2014; Chakrabarti et al. 2014). Universal relations between different neutron-star parameters had been found previously (Lattimer and Prakash 2001, 2004; Lattimer and Yahil 1989; Prakash et al. 1997; Andersson and Kokkotas 1998; Bejger and Haensel 2002; Carriere et al. 2003; Benhar et al. 2004; Tsui and Leung 2005; Lattimer and Schutz 2005; Morsink et al. 2007; Haensel et al. 2009; Lau et al. 2010; Urbanec et al. 2013; Bauböck et al. 2013). The work of Yagi and Yunes (2013a,b) prompted a number of further studies of universal relations (Maselli et al. 2013a; AlGendy and Morsink 2014; Chirenti et al. 2015; Pannarale et al. 2015; Steiner et al. 2016; Breu and Rezzolla 2016; Silva et al. 2016; Yagi 2014; Reina et al. 2017; Chan et al. 2015, 2016). From the studies in Majumder et al. (2015), Doneva et al. (2014), Pappas and Apostolatos (2014), Chakrabarti et al. (2014), Gagnon-Bischoff et al. (2018), from which it has become clear that universality holds only between dimensionless measures of the neutron-star properties, and that the choice of normalization for such appropriate quantities has an impact on the accuracy with which the interrelations hold. Approximate universal relations were recently also found for quantities characterising neutron-star binaries (Kiuchi et al. 2010; Kyutoku et al. 2010; Bauswein and Janka 2012; Takami et al. 2014, 2015; Bernuzzi et al. 2014a, 2015b; Bauswein and Stergioulas 2015; Yagi and Yunes 2016, 2017b; Rezzolla and Takami 2016; Maione et al. 2016); a more comprehensive review of universality in binaries will be discussed in Sect. 10.4. Finally, a list of work on (non-)universality in alternative theories of gravity and for exotic compact objects can be found in the review article (Yagi and Yunes 2017a) and also in Chap. 13 of this review.

Various possible reasons for the existence of universal relations for neutron stars have been considered, see e.g., the discussion in Yagi et al. (2014b). There is evidence that an approximate symmetry, specifically the self-similarity of radial profiles of iso-density surfaces in the interior of stars containing cold degenerate nuclear matter, is linked to the emergence of the universal relations in neutron stars and their absence in ordinary stars (Yagi et al. 2014b). The universal relations have several applications (Yagi and Yunes 2013a,b). For example, they be used to improve measurements by reducing the number of parameters, and for cross-comparisons between interpretations of measurements such as from GW and electromagnetic observations. The fact that the universal relations break down for exotic objects and in some alternative theories of gravity can also be used for tests of General Relativity and the nature of compact objects.

### *10.3.4 Binary Inspiral Dynamics and GWs*

Having discussed the calculation of the relevant parameters we now return to the description of finite-size effects during a binary inspiral, specialising to nonspinning binaries where the models are currently well-developed. We will focus on the dominant mass-quadrupolar tidal effects, and only indicate extensions to other mass multipole moments and to gravitomagnetic interactions. As in the Newtonian context, unless explicitly indicated, we will take the system to be one extended object and a point-mass for simplicity and throughout work only to linear order in the tidal effects.

The action describing tidal interactions in a *relativistic* binary system can be obtained as follows. Recall that in the relativistic context we consider a worldline $z^\mu(\sigma)$ with tangent $u^\mu = dz^\mu/d\sigma$, where $\sigma$ is an evolution parameter. We start by expressing the Newtonian result from Eq. (10.13) in a covariant form and inserting the appropriate redshift factors, defined in Eq. (10.34), to ensure invariance under re-parametrizations (Steinhoff et al. 2016):

$$S = S_{\rm orbit} + \int d\sigma \left[ -\frac{z}{2} \mathcal{E}_{\mu\nu} Q^{\mu\nu} + \mathcal{L}^{\rm int}_{\rm rel} \right], \tag{10.68}$$

Here, $\mathcal{L}^{\rm int}_{\rm rel}$ denotes the relativistic internal Lagrangian. The action (10.68) can also be derived from an effective-field-theoretical approach (Goldberger and Rothstein 2006), by considering all possible terms that respect the symmetries (general covariance, parity, and time reversal) and re-defining variables to eliminate accelerations. For tidally induced quadrupoles due to the $f$-mode we can obtain $\mathcal{L}^{\rm int}_{\rm rel}$ from the Newtonian result given in Eq. (10.14) by replacing all time derivatives by covariant derivatives along the center-of-mass worldline and inserting appropriate factors of the redshift. This leads to (Steinhoff et al. 2016)

$$\mathcal{L}^{\rm int}_{\rm rel} = \frac{z}{4\lambda z^2 \omega_{02}^2} \left[ \frac{DQ_{\mu\nu}}{d\sigma} \frac{DQ^{\mu\nu}}{d\sigma} - z^2 \omega_{02}^2 Q_{\mu\nu} Q^{\mu\nu} \right], \tag{10.69}$$

where

$$\frac{D}{d\sigma} = u^\beta \nabla_\beta \tag{10.70}$$

and $\nabla_\alpha$ is the covariant derivative. This neglects contributions from quadrupolar modes with higher radial nodes, as in the Newtonian case, and also omits other terms due to the incompleteness of the mode spectrum of relativistic compact objects. Contributions from higher multipoles can be described in a similar manner but are not given explicitly here. After decomposing Eq. (10.68) into the time and space components and imposing the constraints to isolate only the physical degrees of

freedom, the action takes the form

$$S = S_{\rm orbit} + \int d\sigma \left[ -\frac{z}{2}\mathcal{E}_{ij}\, Q^{ij} + \frac{z}{4\lambda z^2 \omega_{02}^2}\left( \dot{Q}_{ij}\, \dot{Q}^{ij} - z^2 \omega_{02}^2 Q_{ij}\, Q^{ij} \right) + L_{\rm FD} \right]. \tag{10.71}$$

Here, the term $L_{\rm FD}$ describes relativistic frame-dragging effects that are contained in the kinematical term $(DQ^{\mu\nu}/d\sigma)^2$ when it is expressed with coordinate time as the evolution parameter. Specifically, $L_{\rm FD}$ describes the coupling of the orbital angular momentum to the angular momentum (or spin $\boldsymbol{S}_Q$) associated with the quadrupole

$$S_Q^i = \frac{1}{\lambda \omega_{02}^2} \epsilon_{ijm} \left[ Q^{kj}\, \dot{Q}^m{}_k - Q^{km}\, \dot{Q}^j{}_k \right]. \tag{10.72}$$

To proceed with computing the dynamics and GWs requires explicit expressions for the various quantities such as $\mathcal{E}_{ij}$ and $z$ and the frame-dragging terms appearing in the action. These have been computed in post-Newtonian (PN) theory (Vines et al. 2011a; Bini et al. 2012; Steinhoff et al. 2016), in the test-particle limit (Bini and Geralico 2015) or the gravitational self-force formalism (Dolan et al. 2015; Bini and Damour 2014; Nolan et al. 2015; Shah and Pound 2015). There also exists an alternative approach to the worldline-skeleton method termed the affine model. In the affine approach, the stars are described as triaxial ellipsoids and one solves a set of coupled ODEs for the evolution of the axes and the orbit. The most recent developments that take into account PN effects are derived in Ferrari et al. (2012), Maselli et al. (2012), where we refer the reader for more details about this model. Below, we will continue to work within the worldline-skeleton approach and outline the computation of tidal effects in the GW signal in PN theory before discussing their inclusion in more sophisticated GW models.

In PN theory, the GW signal can be computed by imposing that the power radiated by a binary system is balanced by a change in the energy of the binary. This enables computing the phase evolution of the orbital dynamics where at the leading order, the GW phase is twice the orbital phase. The radiated power is computed in a multipolar approximation that at leading order gives the quadrupole formula involving the total quadrupole moment of the system $Q_{ij}^{\rm T} = \mu r^2 n^{<ij>} + Q_{ij}$. The energy of the binary is $E = E_{\rm pm} + E_{\rm tidal}$, where the subscript "pm" denotes point-masses. The computations starting from the action, are described in detail in Vines et al. (2011b) for the current state-of-the art complete knowledge at 1PN order in the tidal effects, and in Flanagan and Hinderer (2008), Hinderer et al. (2010) in Newtonian but more general contexts that include various other effects and estimate the size of the corrections. Partial information at higher PN orders is also available (Damour et al. 2012). The idea is to start from the action written out explicitly to 1PN order, derive from it the equations of motion, specialise to circular orbits $\ddot{r} = \dot{r} = 0$ and $\dot{\phi} = \Omega$, $\ddot{\phi} = 0$, and perturbatively solve from this for the orbital separation $r$ in terms of the frequency variable $x = (M\Omega)^{2/3}$. The reason for wanting to eliminate $r$ is that it is a gauge-dependent quantity whereas the

frequency is an observable and hence less gauge-dependent. From the potential and kinetic energies contained in the action one can compute the energy of the system $E$ and find the following tidal contribution in the limit of adiabatic tides (Vines et al. 2011a)

$$E_{\rm tidal}(x) = -\frac{1}{2}\mu x\left[-9\frac{M_B}{M_A}\frac{\lambda_A x^5}{M^5} - \frac{11}{2}\left(\frac{3M}{M_A} - \frac{M_B}{M} - 3\frac{M_A^2}{M^2}\right)\frac{\lambda_A x^6}{M^5}\right] + (A \leftrightarrow B). \tag{10.73}$$

The factor outside the brackets is the result for Newtonian point masses. The results when including the finite $f$-mode frequency at Newtonian order can be found in Flanagan and Hinderer (2008), and the 1PN extension can be determined from the Hamiltonian and circular-orbit solutions given in Hinderer et al. (2016), Steinhoff et al. (2016). Next, the mass-quadrupole tidal corrections contribute to the power radiated in GWs as (Vines et al. 2011b)

$$P_{\rm GW}^{\rm tidal} = \frac{32\mu^2}{5M^2}x^{5/2}\left[\left(\frac{18M}{M_A} - 12\right)\frac{\lambda_A x^5}{M^5} + \left(\frac{643M_A}{4M} - \frac{176M}{7M_A} - \frac{1803}{28} - \frac{155M_A^2}{2M^2}\right)\frac{\lambda_A x^6}{M^5}\right]. \tag{10.74}$$

By requiring that $P_{\rm GW}$ be balanced by a change in the energy $E$ of the binary one can derive the evolution equations

$$\frac{d\phi}{dt} = \frac{x^{3/2}}{M} \qquad \frac{dx}{dt} = \frac{-P_{\rm GW}}{dE/dx} \tag{10.75}$$

There are several ways to solve for $\phi$ in a PN approximation. For example, one can numerically solve Eq. (10.75) for $\phi(t)$ and $x(t)$ after first expanding the ratio $P_{\rm GW}/(dE/dx)$ about $x = 0$ to the consistent PN order. These waveforms are known as TaylorT4 approximants as reviewed in Buonanno et al. (2009), where the point-mass terms are also given explicitly. The adiabatic quadrupolar tidal corrections that add linearly to the point-mass contributions are (Vines et al. 2011b):

$$\frac{dx}{dt}\Big|_{\rm tidal} = \frac{32}{5}\frac{M_B}{M^7}\lambda_A x^{10}\left[12\left(1 + 11\frac{M_B}{M}\right) + x\left(\frac{4421}{28} - \frac{12263}{28}\frac{M_A}{M} + \frac{1893}{2}\frac{M_A^2}{M^2} - 661\frac{M_A^3}{M^3}\right)\right] + (A \leftrightarrow B). \tag{10.76}$$

Other possibilities to perturbatively solve (10.75) and obtain the tidal contributions to different approximants for the gravitational waveform are detailed in the Appendix of Wade et al. (2014). The reason why the phase evolution is the most important prediction for GW data analysis is that matched filtering is employed to identify and interpret signals, where the datastream is cross-correlated with theoretical predictions for the GWs (see e.g., Cutler and Flanagan 1994), thus making the process very sensitive to the phasing (Cutler et al. 1992). Besides

the TaylorT4 approximants, another widely utilised class of template waveforms for data analysis are TaylorF2 waveforms. Their advantage is that they provide a fully analytic frequency-domain model and are thus very fast to generate. The derivation is explained e.g., in Cutler and Flanagan (1994) and in the stationary phase approximation leads to a Fourier transform of the signal, denoted by $\tilde{h}$, of the form

$$\tilde{h}(f) = \mathcal{A} f^{-7/6} \exp\left[i\left(\psi_{\rm pm} + \psi_{\rm tidal}\right)\right]. \tag{10.77}$$

Here $f$ is the GW frequency, $\mathcal{A} \propto \mathcal{M}^{5/6}/D$, where $\mathcal{M}$ is the chirp mass $\mathcal{M} = \eta^{3/5} M$, and $D$ is the distance between the GW detector and the binary. Extrinsic parameters of the source such as the location on the sky are also contained in $\mathcal{A}$, where higher PN order (and tidal) corrections to the amplitude also enter. The point-mass phase $\psi_{\rm pm}$ to the current best knowledge for nonspinning binaries is given e.g., in Eq. (3.18) of Buonanno et al. (2009). The mass-quadrupole adiabatic tidal contributions to $\psi_{\rm tidal}$ in the adiabatic limit can be expressed in the following form given explictly in Wade et al. (2014):

$$\delta\psi_{\rm tidal} = \frac{3}{128\eta x^{5/2}}\left[-\frac{39}{2}\tilde{\Lambda} x^5 + \left(-\frac{3115}{64}\tilde{\Lambda} + \frac{6595}{364}\sqrt{1-4\frac{\mu}{M}}\,\delta\tilde{\Lambda}\right) x^6\right], \tag{10.78a}$$

where

$$\tilde{\Lambda} = \frac{16}{13}\left[\left(1+\frac{12M_B}{M_A}\right)\frac{\Lambda_A M_A^5}{M^5} + \left(1+\frac{12M_A}{M_B}\right)\frac{\Lambda_B M_B^5}{M^5}\right] \tag{10.78b}$$

$$\delta\tilde{\Lambda} = \left(1 - \frac{7996M_B}{1319M_A} - \frac{11005M_B^2}{1319M_A^2}\right)\frac{\Lambda_A M_A^6}{M^6} + \left(\frac{11005M_A^2}{1319M_B^2} + \frac{7996M_A}{1319M_B} - 1\right)\frac{\Lambda_B M_B^6}{M^6} \tag{10.78c}$$

In Eq. (10.78c) the assumption is that $M_A > M_B$. The parameter $\tilde{\Lambda}$ plays an analogous role as in GW measurements as the chirp mass $\mathcal{M}_{\rm chirp} = \mu^{3/5} M^{2/5}$ as the most readily measurable combination of parameters. For equal-mass binary neutron stars $\tilde{\Lambda}$ reduces to $\Lambda$ of the individual neutron stars, and the parameter $\delta\tilde{\Lambda}$ vanishes. Other combinations of the two parameters $\Lambda_A$ and $\Lambda_B$ are also in use and have advantages in different contexts, e.g., to characterize the dominant effect in the conservative dynamics (Damour and Nagar 2010), or to improve the measurability (Yagi and Yunes 2016, 2017b). The key point to note is that for a double neutron-star system GW measurements are most sensitive to a weighted average of the deformability parameters of the two objects.

From the discussion above, it is apparent that the fractional corrections to the Newtonian point-mass results due to tidal effects scale as a high power of the frequency, $x^5$ and higher, where $x = (\pi M f)^{2/3}$. This means that in a PN counting that is based on assigning to each power of $x$ an additional PN order, tidal effects first enter effectively as 5PN corrections, although physically, they are Newtonian effects. Point-mass terms are currently only known to 4PN order in the dynamics

(Damour et al. 2016; Marchand et al. 2017) and only to 3.5PN order in the GW phasing (Blanchet 2006). This lack of complete information has raised concerns about systematic errors in GW measurements of tidal effects (Favata 2014; Yagi and Yunes 2014; Wade et al. 2014). However, there are two classes of effective or phenomenological models for black hole binaries that effectively include all PN orders in an approximate way. These are the effective one body (EOB) model (Buonanno and Damour 1999, 2000) and the so-called "Phenom" models (Ajith et al. 2007, 2008), both of which aim to combine the available information on the relativistic two-body problem from different regimes into a single framework to generate waveforms for data analysis.

The EOB approach is a framework to compute the dynamics and GWs from a binary by evolving a description of the coupled system of ODEs for the orbital motion, GW generation, and radiation-backreaction in the time-domain. The purpose of the Phenom models is to provide an efficient description of the dominant effects in the GW signal in the frequency-domain, through a generalisation of (10.77). Both approaches rely not only on analytical results but also include information from numerical relativity simulations for black hole binaries; the current state-of-the art refinements and calibrations of the models are described in Bohe et al. (2017), Babak et al. (2017) and Nagar et al. (2017, 2018) for an alternative version of the EOB model, and Khan et al. (2016), Schmidt et al. (2015) for the Phenom models. By design, these models therefore include high-PN order information, albeit only in an approximate and phenomenological manner. When tidal effects are included in such models one might expect the systematic uncertainties due to missing high-PN-order point-mass terms to be reduced. However, the level of remaining systematic errors must be assessed by testing the models in various ways, such as by comparing to numerical relativity simulations or comparing results from data analysis studies with the two different classes of models.

The Phenom models are frequency-domain models that prescribe an analytical expression for the amplitude and phase of $\tilde{h}$. In the Phenom models, the tidal terms from Eq. (10.78a) can directly be added to the black hole waveforms without further work. Alternative tidal phasing models based on a fit to numerical relativity results have recently also been developed (Dietrich et al. 2017, 2018; Kawaguchi et al. 2018) and can likewise be added on top of the black hole waveforms for the inspiral. There also exist surrogate models for EOB waveforms in the frequency domain (Purrer 2016; Lackey et al. 2017) where the tidal contributions can be directly added to the phasing as described for the Phenom models. The different kinds of frequency-domain models are the most efficient for data analysis and were used in the EOS inferences of GW170817 (Abbott et al. 2018a) as the analysis in Abbott et al. (2018b) indicated that statistical errors dominate over modeling uncertainties.

Time-domain models such as the EOB models are less computationally efficient than frequency-domain models but have other advantages, e.g. they describe both the binary dynamics and GWs and are based on additional theoretical considerations about the relativistic two-body problem. To include tidal effects in the

EOB approach at a fundamental level requires both the tidal corrections to the conservative dynamics and to the gravitational radiation. At present, tidal effects have only been fully included in the EOB model for nonspinning binaries. Spin effects for point masses as well as the spin-induced quadrupole effects are currently incorporated in the EOB models, however, including all spin-tidal interactions to the relevant order is the subject of ongoing work. Below, we will briefly summarise the different EOB tidal models available at present and refer the reader to the overviews of models in Dietrich and Hinderer (2017), Nagar et al. (2018) more specific details. For adiabatic tidal effects, tidal contributions to the conservative EOB dynamics were computed from a PN expansion of tidal effects in Damour and Nagar (2010), Vines et al. (2011a), Bini et al. (2012). These effects were also calculated within the gravitational self-force approximation in Bini and Damour (2014). The PN approximation assumes small corrections to Newtonian dynamics but is valid for any mass ratio, whereas the gravitational self-force formalism assumes linear-in-mass-ratio corrections to the strong-field test-particle limit. To a certain extent, the two approximations therefore provide different kinds of information. Tidal corrections to the GW amplitudes that are used in the EOB model to compute the emitted GWs and the radiation reaction forces on the orbital dynamics were given in Damour et al. (2012). These models, however, tend to underestimate finite-size effects when compared against numerical relativity simulations, see e.g. Bernuzzi et al. (2015a), Hinderer et al. (2016), Dietrich and Hinderer (2017) for recent studies. There are three main reasons to expect an enhancement of tidal effects relative to the information included in the models described above: relativistic corrections that lead to a stronger tidal field, an enhanced response of the neutron-star matter to tidal perturbations, and the fact that the tidal models are used to describe the binary including the nonlinear regimes at merger or tidal disruption. These considerations motivated two classes of improved EOB models. The first, discussed in Bernuzzi et al. (2015a), Nagar et al. (2018) is based on extrapolating the results of Bini and Damour (2014) to second-order in the mass ratio in a particular gauge. The second, discussed (Hinderer et al. 2016; Steinhoff et al. 2016) includes dynamical tidal effects due to the $f$-mode oscillations in the EOB model that can lead to a substantial tidal enhancement even if the mode resonance is not fully excited during the inspiral. Note that while the underlying EOB model for black holes are calibrated to numerical relativity simulations, the tidal part of the model of Hinderer et al. (2016), Steinhoff et al. (2016) is currently purely based on analytical results, without any calibrations.

### *10.3.5 Other Finite-Size Effects*

The finite size of neutron stars in a binary system has a number of additional impacts on the dynamics and GWs, besides the tidal effects discussed above. For rotating neutron stars, the spin-induced quadrupole moment (and the higher moments) leads to a contribution to the GW signal that is quadratic in the neutron-

star's spin (Poisson 1998; Laarakkers and Poisson 1999; Mora and Will 2004; Berti et al. 2008). As mentioned above, these effects from the rotational deformations are already included in the template models described in the previous subsection, both in the PN models (see Krishnendu et al. (2017) for the latest update) as well as in the EOB and Phenom models. The GW imprints from gravitomagnetic tidal effects (Banihashemi and Vines 2018) and spin-tidal interactions (Landry 2018; Jimenez-Forteza et al. 2018) have recently also been examined within PN theory.

Tidal interactions can also lead to the resonant excitation of various oscillation modes during the inspiral (Ho and Lai 1999; Flanagan and Racine 2007; Shibata 1994; Yu and Weinberg 2017; Lai 1994; Kokkotas and Schaefer 1995; Tsang 2013; Tsang et al. 2012), to nonlinear mode coupling effects (Xu and Lai 2017; Essick et al. 2016; Landry and Poisson 2015c), and to the full $f$-mode excitations for eccentric orbits (Gold et al. 2012; Chirenti et al. 2017). In neutron-star–black-hole binaries, depending on the parameters, the neutron star may get tidally disrupted, which leads to a sudden shutoff of the GW signal and contains additional equation-of-state information (Vallisneri 2000; Shibata and Taniguchi 2011; Pannarale et al. 2011; Ferrari et al. 2010; Maselli et al. 2013b; Foucart et al. 2014; Kawaguchi et al. 2017; Lackey et al. 2014). For a review article on GWs from neutron-star–black-hole binaries containing a comprehensive list of references on the topic see Shibata and Taniguchi (2011), and for the characteristics of possible associated electromagnetic counterparts see Fernández et al. (2017), Schnittman et al. (2018), Paschalidis et al. (2015a). An additional distinction between neutron stars and black holes is that the neutron star has a surface while a black hole possesses an event horizon that absorbs all incoming GWs; this effect is also imprinted in the GWs (Maselli et al. 2018).

As discussed above, there are several issues in modelling neutron-star binary inspirals that remain to be fully addressed and are an active area of research. Most of these concern currently unmodeled physics, which is also of great interest for enhancing the potential to extract more details about neutron-star interiors from GW observations. Examples of remaining work for the inspiral are to develop full waveform models that incorporate matter effects in spinning neutron-star binaries, to assess the importance of dynamical tides for various oscillation modes for a more realistic description of the neutron stars (e.g., including the effects of superfluidity (Gualtieri et al. 2014) and the effects of spins), and to analyze the effects of nonlinear couplings in a relativistic setting.

Another issue that could be improved concerns the fact that at present the models constructed for the inspiral of isolated, perturbed neutron stars are used up to merger, defined as the peak in the GW amplitude. The peak approximately coincides with the collision of the high-density neutron star cores, shortly after the neutron outer parts have already come into contact. The theoretical predictions of the very late stage in the evolution, could thus be improved by accounting for the main physical effects of the cores moving through the material of their former outer parts. Similarly, for neutron star – black hole binaries, developing an improved description that accounts for nonlinearities of the tidal disruption process remains an open issues.

Other ongoing efforts are focusing on developing a complete model that combines the information from the inspiral, merger and postmerger epochs, and likewise

for the inspiral and possible tidal disruption in mixed binaries for more generic systems than considered to date. These studies must rely on interfacing the theoretical insights with numerical relativity and data analysis to test and improve the models and select the order of priorities for addressing the issues mentioned above. An important application of such models will not only be for the current network of GW detectors but also to inform the design and science case for future, third-generation detectors. More work is also required on optimising methods to combine information from the GWs with those from the electromagnetic counterparts (Baiotti and Rezzolla 2017; Paschalidis 2017), together with nuclear physics knowledge and other astrophysical measurements of neutron-star properties to maximise the overall scientific payoffs. Lastly, other areas of active research are to consider finite-size effects in alternative theories of gravity, for exotic objects, and for possible bound states of fundamental fields around black holes.

## 10.4 Post-merger Dynamics

Research on the post-merger phase has been undergoing intense development over the last few years because of its importance for linking numerical simulations and astrophysical observations. The (early) post-merger is also the phase in which most of the energy in GWs is emitted, as pointed out in Bernuzzi et al. (2016), even though the GWs emitted in this stage are not those that give the largest signal-to-noise ratio, because their frequency range is not in the best sensitivity zone of current interferometric detectors. The numerical description of this stage is far more challenging than the inspiral one because of the highly nonlinear dynamics and of the development of strong, large-scale shocks that inevitably reduce the convergence order, thus requiring far higher resolutions than the ones normally employed. As a result, the accuracy of some quantities computed after the merger is sometimes only marginal. The most notable example of these quantities is the lifetime of the remnant (be it an HMNS or an SMNS) before its collapse to black hole; since this object is only in metastable equilibrium, even small differences in resolution or even grid setup are sufficient to change its dynamical behaviour, accelerating or slowing down its collapse to a black hole. Fortunately, other quantities, such as the spectral properties of the GW post-merger emission appear far more robust and insensitive to the numerical details; we will discuss them later in this section.

Since the first general-relativistic simulations of BNS mergers, several works have studied the nature (neutron star or black hole) of the objects resulting from the mergers (Shibata and Uryū 2000, 2002; Shibata et al. 2005; Shibata and Taniguchi 2006; Yamamoto et al. 2008; Baiotti et al. 2008; Anderson et al. 2008; Giacomazzo et al. 2011). It is of course important to establish whether a black hole forms promptly after the merger or instead an HMNS forms and lives for long times (more than 0.1 s), because the post-merger GW signal in the two cases is clearly different. Anderson et al. (2008) and Giacomazzo et al. (2011) started investigating the dependence of the lifetime of the HMNS on the magnitude of the

initial magnetic field in the case of magnetised binaries. However, as mentioned above, such investigations are extremely delicate since it is not straightforward to completely remove the influence of numerical artefacts on the lifetime of the remnant even in the absence of magnetic fields, at least with present resolutions.

In an alternative approach, Kaplan et al. (2014) have investigated the role of thermal pressure support in hypermassive merger remnants by computing sequences of axisymmetric uniformly and differentially rotating equilibrium solutions to the general-relativistic stellar structure equations and found that this too is a subtle issue: the role of thermal effects on the stability and lifetime of a given configuration depends sensitively and in a complicated way on its details, like central or mean rest-mass density, temperature distribution, degree of differential rotation and rotation rate (see discussion in Hanauske et al. 2016).

Clearly, the issue of the precise lifetime of the binary-merger product before it reaches its asymptotic state, especially when its equilibrium is mediated by the generation of magnetic fields or radiative losses is far from being solved and will require computational resources and/or methods not yet available.

Recently, Paschalidis, East and collaborators (Paschalidis et al. 2015b; East et al. 2016) pointed out that a one-arm spiral instability (Centrella et al. 2001; Watts et al. 2005; Baiotti et al. 2007; Corvino et al. 2010) can develop in HMNSs formed by dynamical-capture and that the $m = 1$ mode associated with this instability may become the dominant oscillation mode if the HMNS persists for long enough[3]; this instability has been subsequently studied also in quasi-circular BNSs (Radice et al. 2016; Lehner et al. 2016). The instability, is reminiscent of the shear instability that has been studied in detail for isolated stars (Baiotti et al. 2007; Corvino et al. 2010; Camarda et al. 2009; Franci et al. 2013; Muhlberger et al. 2014) and seems to be correlated with the generation of vortices near the surface of the HMNS that form due to shearing at the stellar surface. These vortices then spiral in toward the center of the star, creating an underdense region near the center. The growth of the $m = 1$ mode and so of the instability, could be related to the fact that the maximum density does not reside at the center of mass of the star (Saijo et al. 2003), or to the existence of a corotation band (Balbinski 1985; Luyten 1990; Watts et al. 2005). The instability has an imprint on the GW signal, but the prospects of detection are not encouraging, because of the small emitted power (Radice et al. 2016).

### *10.4.1 Gravitational-Wave Spectroscopy of the Post-merger Signal*

Many researchers have taken up the challenge of studying the properties of the binary-merger product, because this may give indications on the ultra-high density EOS, the origin of SGRBs, and even the correct theory of gravity. In what follows

[3]The $m = 1$ mode had been studied previously together with the other modes, but it had never been found to become dominating (see, e.g., Dietrich et al. 2015a).

we will focus in particular on the determination of the EOS. While detectable differences between simulations that employed different EOSs already appear during the inspiral (see Sect. 10.3), the post-merger phase depends more markedly on the EOS (Bauswein et al. 2014; Takami et al. 2014, 2015; Bernuzzi et al. 2014a, 2015a,b; Rezzolla and Takami 2016; Maione et al. 2016). A note of caution is necessary here to say that post-merger waveforms are at rather high frequencies and thus probably only marginally measurable by detectors like Advanced LIGO. Third-generation detectors, such has ET (Punturo et al. 2010a), may provide the first realistic opportunity to use GWs to decipher the stellar structure and EOS (Andersson et al. 2011).

The first attempts to single out the influence of the EOS on the post-merger dynamics were done in Shibata et al. (2005), Shibata and Taniguchi (2006), Yamamoto et al. (2008), Baiotti et al. (2008). These works focused mostly on the dynamics of equal-mass binaries, as these are thought to be the most common (Osłowski et al. 2011) and are easier and faster to compute, since symmetries of the configuration can be exploited to save computational resources. The study of the effect of realistic EOSs in general-relativistic simulations has been subsequently brought forward by many groups. Kiuchi et al. (2009) made use of the Akmal-Pandharipande-Ravenhall (APR) EOS (Akmal et al. 1998).[4] This nuclear-physics EOS describes matter at zero temperature and so during the simulation it needs to be combined with a "thermal" part that accounts for the energy increase due to shock heating (this is mostly done through the addition of an ideal-fluid part to the EOS; see Rezzolla and Zanotti (2013) for a discussion). The resulting *"hybrid EOS"* appears to be appropriate for studying the inspiral and merger, but may not be satisfactory for studying the remnant formation and the evolution of the accretion disc around the formed black hole, because for such cases, effects associated with the thermal energy (finite temperature), neutrino cooling, and magnetic fields are likely to play an important role. In another work of the same group (Hotokezaka et al. 2011), the dependence of the dynamical behavior of BNS mergers on the EOS of the nuclear-density matter with piecewise-polytropic EOSs (Read et al. 2009) was studied.

One family of EOSs that has received special attention in the past years is that describing strange matter, namely matter containing hyperons, which are nucleons containing strange quarks. The strange-matter hypothesis (Witten 1984) considers the possibility that the absolute ground state of matter might not be formed by iron nuclei but by strange quark matter: a mixture of up, down, and strange quarks. This hypothesis introduced the possibility that compact stars could be stars made also of strange-quark matter, or strange stars (Haensel et al. 1986; Alcock et al. 1986). One of the astrophysical consequences of this is the possibility that collision events of

[4]The APR EOS, and many of the proposed EOSs, were later found to violate the light-speed constraint at very high densities and phenomenological constraints (Taranto et al. 2013), but no strong conclusions can be made to rule out such EOSs on this basis because the constraints themselves are affected by errors.

two strange stars lead to the ejection of strangelets, namely small lumps of strange quark matter.

Although the occurrence of hyperons at very large nuclear densities is rather natural, hyperonic EOSs are generally very soft and currently disfavoured by the observation of a $2M_{\odot}$ star (Antoniadis et al. 2013; Demorest et al. 2010), which they can hardly reproduce, except by fine tuning of the parameters (see, e.g., Alford et al. 2005; Rikovska-Stone et al. 2007; Weissenborn et al. 2011). This basic inconsistency between the expectations of many nuclear physicists and the observational evidence of very massive neutron stars is normally referred to as the "hyperon puzzle"; those supporting the use of hyperonic EOSs also state that the existence of exotic phases in strange stars remains unconstrained and could lead to higher masses (Bhowmick et al. 2014). Additional work is needed to settle this "hyperon puzzle" and we will present results on strange-star simulations setting these doubts aside.

The first investigations of binary strange stars were those of Bauswein et al. (2009, 2010), who employed the MIT bag model (Farhi and Jaffe 1984). Within this model, quarks are considered as a free or weakly interacting Fermi gas and the nonperturbative QCD interaction is simulated by a finite pressure of the vacuum, the *bag constant* $B$. Three-dimensional general-relativistic simulations with conformally flat gravity of the coalescence of strange stars were performed and the possibility to discriminate on the strange matter hypothesis by means of GW measurements was explored. The dynamics of mergers of strange stars, which are usually more compact, is different from those of neutron-star mergers, most notably in the tidal disruption during the merger. Furthermore, instead of forming dilute halo-structures around the binary-merger product, as in the case of neutron-star mergers, the coalescence of strange stars results in a differentially rotating hypermassive object with a sharp surface layer surrounded by a geometrically thin, clumpy high-density strange-quark-matter disc. It was found that in some cases (some types of EOS and stellar properties) the analysis of the GW signals emitted by strange-star mergers showed that it may be possible to discern whether strange-star or neutron-star mergers produced the emission. In particular, it was found that the maximal frequency during the inspiral and the frequency of the oscillations of the post-merger remnant are in general higher for strange-star mergers than for neutron-star mergers. In other cases, however, there remains a degeneracy among different models, and a conclusion about the strange-matter hypothesis could be reached only if other types of observations (e.g., of cosmic rays) were available.

Strange-matter EOSs were later studied with a fully general-relativistic code in a series of articles by Sekiguchi, Kiuchi and collaborators (Sekiguchi et al. 2011a, 2012; Kiuchi et al. 2012b,c), who showed results of simulations performed by incorporating both nucleonic and hyperonic finite-temperature EOSs (and neutrino cooling as well). It was found that also for the hyperonic EOS, an HMNS is first formed after the merger and subsequently collapses to a black hole. The radius of such an HMNS decreases in time because of the increase of the mass fraction of hyperons and the consequent decrease in pressure support. Such a shrinking is noticeably larger than the one simply due to angular-momentum loss through GW

emission that is present also in nucleonic EOSs. These differences in the dynamics are clearly visible in the GW signal, whose characteristic peak frequency has an increase of 20–30% during the HMNS evolution. By contrast, for nucleonic EOSs, the peak GW frequency in the HMNS phase is approximately constant on the timescales considered. It was also stressed that these results raise a warning about using the peak frequency of the GW spectrum to extract information of the neutron-star matter (see below), because it may evolve and so make the relation of the peak frequency with the HMNS structure ambiguous. Finally, it was found that the torus mass for the hyperonic EOS is smaller than that for nucleonic EOSs, thus making hyperonic EOSs less favourable for the description of SGRBs.

More recently, Radice et al. (2017) performed numerical simulations of BNS mergers with one EOS, BHB$\Lambda\phi$ (Banik et al. 2014), that includes $\Lambda$-hyperons but that satisfies all presently known EOS constraints, including the astrophysical ones. They found that the rapid contraction of the merged object due to the appearance of hyperons does affect amplitude modulation and phase evolution of the gravitational waveform, but the peak frequencies in the PSD are very similar to those produced in case of a similar EOSs, DD2 (Hempel and Schaffner-Bielich 2010), that however has no phase transitions. It was also found that Advanced LIGO could distinguish the two EOSs considered in that work with the detection a single merger at a distance of up to about 20 Mpc (Radice et al. 2017).

### *10.4.2 Spectral Properties of the Signal*

In addition to simulating BNS mergers with various EOSs, it is important to find ways to connect future GW observation with the EOS of the neutron stars. Recently there have been several suggestions on how to achieve this, based either on the signature represented by the tidal corrections to the orbital phase or on the power spectral density (PSD) of the post-merger gravitational waveforms or on the frequency evolution of the same. The first approach, described in Sect. 10.3, is reasonably well understood analytically (Flanagan and Hinderer 2008; Baiotti et al. 2010; Bernuzzi et al. 2012, 2015b; Read et al. 2013) and can be tracked accurately with advanced high-order numerical codes (Radice et al. 2014a,b). Here we describe works on the post-merger approach in some detail.

Hotokezaka et al. (2013) used their adaptive mesh-refinement (AMR) code[5] SACRA (Yamamoto et al. 2008) to perform a large number of simulations with a variety of mass ranges and EOSs (as done before, approximate finite-temperature effects were added to the cold EOSs through an additional ideal-fluid term), in order to find universal features of the frequency evolution of GWs emitted by the HMNS formed after the merger. In their analysis they found it convenient to decompose the merger and post-merger GW emission in four different parts: (1) a peak in frequency

[5]In previous works by this group, described above, a different code with a uniform grid had been used.

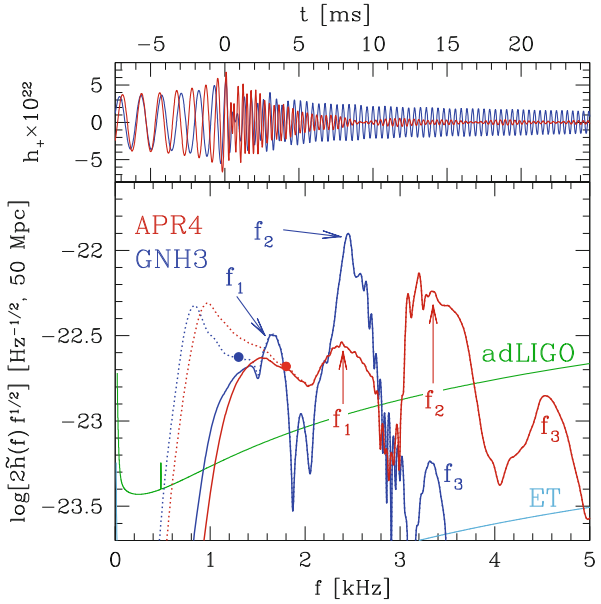


**Fig. 10.4** Top sub-panel: evolution of $h_+$ for binaries with the APR4 and GNH3 EOSs (dark-red and blue lines, respectively) for optimally oriented sources at a distance of 50 Mpc. Bottom sub-panel: spectral density $2\tilde{h}(f)f^{1/2}$ windowed after the merger for the two EOSs and sensitivity curves of Advanced LIGO (green line) and ET (light-blue line); the dotted lines show the power in the inspiral, while the circles mark the contact frequency [Reprinted with permission from Takami et al. (2014). © (2014) by the American Physical Society]

and amplitude soon after the merger starts; (2) a decrease in amplitude during the merger and a new increase when the HMNS forms; (3) a damped oscillation of the frequency during the HMNS phase lasting for several oscillation periods and eventually settling to an approximately constant value (although a long-term secular change associated with the change of the state of the HMNSs is always present); (4) a final decrease in the amplitude during the HMNS phase, either monotonical or with modulations. Based on this, they find an optimal 13-parameters fitting function, using which it may be possible to constrain the neutron star radius with errors of about 1 km (Hotokezaka et al. 2013).

In contrast with this multi-stage, multi-parameter description of Hotokezaka et al. (2013), other groups have concentrated on the analysis of the full PSD of the post-merger signal, isolating those spectral features (i.e., peaks) that could be used to constrain the properties of the nuclear-physics EOSs. As a reference, we show in Fig. 10.4 the PSDs of some representative GWs when compared with the sensitivity curves of current and future GW detectors (Takami et al. 2014). More specifically, two examples are presented in Fig. 10.4, which refers to two equal-mass binaries with APR4 and GNH3 EOSs, and with individual gravitational masses at infinite separation of $\bar{M}/M_\odot = 1.325$, where $\bar{M}$ is the average of the initial gravitational

mass of the two stars. The top sub-panel shows the evolution of the $\ell = m = 2$ plus polarization of the strain ($h_+ \sim h_+^{22}$), aligned at the merger for optimally oriented sources at a distance of 50 Mpc (dark-red and blue lines for the APR4 and GNH3 EOSs, respectively). The bottom panel, on the other hand, shows the spectral densities $2\tilde{h}(f)f^{1/2}$ windowed after the merger for the two EOSs, comparing them with the sensitivity curves of Advanced LIGO (2009) (green line) and of the Einstein Telescope (Punturo et al. 2010b; Sathyaprakash and Schutz 2009) (ET; light-blue line). The dotted lines refer to the whole time series and hence, where visible, indicate the power during the last phase of the inspiral, while the circles mark the "contact frequency" $f_{\rm cont} = \mathcal{C}^{3/2}/(2\pi\bar{M})$ (Damour et al. 2012), where $\mathcal{C} := \bar{M}/\bar{R}$ is the average compactness, $\bar{R} := (R_1 + R_2)/2$, and $R_{1,2}$ are the radii of the nonrotating stars associated with each binary.

Note that besides the peak at low frequencies corresponding to the inspiral (cf., dashed lines), there is one prominent peak and several others of lower amplitudes. These are related to the oscillations of the HMNS and would be absent or much smaller if a black hole forms promptly, in which case the GW signal would terminate abruptly with a cutoff corresponding to the fundamental quasi-normal-mode frequency of the black hole (Kokkotas and Schmidt 1999). The behaviour summarised in Fig. 10.4 is indeed quite robust and has been investigated by a number of authors over the last decade (Oechslin and Janka 2007; Stergioulas et al. 2011; Bauswein and Janka 2012; Bauswein et al. 2012, 2014, 2016; Hotokezaka et al. 2013; Takami et al. 2014, 2015; Clark et al. 2014; Kastaun and Galeazzi 2015; Bernuzzi et al. 2015b; Bauswein and Stergioulas 2015; Dietrich et al. 2015b; Foucart et al. 2016; De Pietri et al. 2016; Rezzolla and Takami 2016; Maione et al. 2016; Bose et al. 2018).

Figure 10.5 provides a summarising view of some of the waveforms (i.e., of $h_+$ for sources at a distance of 50 Mpc) computed in this paper and that are combined with those of Takami et al. (2015) to offer a more comprehensive impression of the GW signal across different masses and EOSs. The figure is composed of 35 panels referring to the 35 equal-mass binaries with nuclear-physics EOSs that were simulated and that have a postmerger signal of at least 20 ms. Different rows refer to models with the same mass, while different columns select the five cold EOSs considered and colour-coded for convenience. It is then rather easy to see how small differences across the various EOSs during the inspiral become marked differences after the merger. In particular, it is straightforward to observe how the GW signal increases considerably in frequency after the merger and how low-mass binaries with stiff EOSs (e.g., top-left panel for the GNH3 EOS) show a qualitatively different behaviour from high-mass binaries with soft EOSs (e.g., bottom-right panel for the APR4 EOS). Also quite apparent is that, independently of the mass considered, the post-merger amplitude depends sensitively on the stiffness of the EOS, with stiff EOSs (e.g., GNH3) yielding systematically larger amplitudes than soft EOSs (e.g., APR4).

The first detailed description of a method for extracting information about the EOS of nuclear matter by carefully investigating the spectral properties of the post-merger signal was provided by Bauswein and Janka (2012), Bauswein et al. (2012).

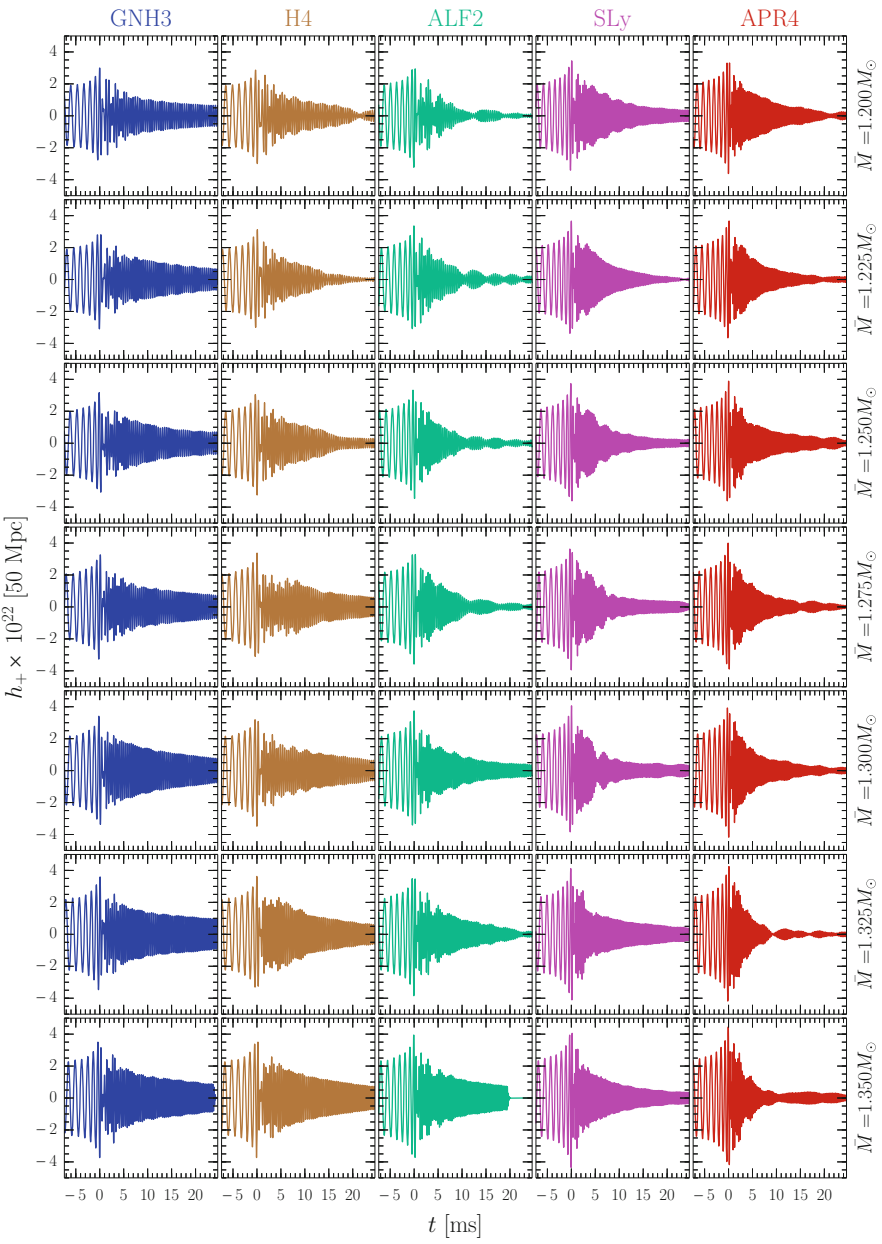


**Fig. 10.5** Gravitational waveforms for some cold-EOS BNSs. The rows correspond to the gravitational masses, $\bar{M} = 1.200, 1.225, 1.250, 1.275, 1.300, 1.325, 1350\, M_\odot$, respectively, while each column refers to a given EOS. All models have formed long-lived HMNSs with $t > 20$ ms [Reprinted with permission from Rezzolla and Takami (2016). © (2016) by the American Physical Society]

After performing a large number of simulations using their conformally-flat SPH code, they pointed out that the largest peak in the PSD (whose frequency is dubbed there $f_{\rm peak}$) correlates with the properties of the EOS, e.g., with the radius of the maximum-mass nonrotating star for the given EOS. The correlation found was rather tight, but this was partly due to the fact that their sample was restricted to binaries having all the same total mass (i.e., $2.7\,M_\odot$ in the specific case). It was shown that such a correlation can be used to gain information on the high-density EOS through GW measurements, if the masses of the neutron stars forming the binaries are known. Additionally, it was recognized that $f_{\rm peak}$ corresponds to a fundamental fluid mode of the HMNS with $\ell = 2 = m$ (Bauswein and Janka 2012; Stergioulas et al. 2011) and that the value of this frequency could also be used to set constraints on the maximum mass of the system and hence on the EOS (Bauswein et al. 2013, 2014). Subsequent analyses were performed by a number of groups with general-relativistic codes (Hotokezaka et al. 2013; Takami et al. 2014, 2015; Dietrich et al. 2015b; Foucart et al. 2016; De Pietri et al. 2016; Rezzolla and Takami 2016; Maione et al. 2016; Radice et al. 2017), which confirmed that the conformally flat approximation employed by Bauswein and collaborators provided a rather accurate estimate of the largest peak frequencies in the PSDs.

Takami et al. (2014, 2015) presented a more advanced method to use detected GWs for determining the EOS of matter in neutron stars. They used the results of a large number of accurate numerical-relativity simulations of binaries with different EOSs and different masses and identified two distinct and robust main spectral features in the post-merger phase. The first one is the largest peak in the PSD (whose frequency was called there $f_2$ and essentially coincides with the $f_{\rm peak}$ of Bauswein and Janka 2012; Bauswein et al. 2012). The functions describing the correlations of $f_2$ with the stellar properties (e.g., with the quantity $(\bar{M}/R^3_{\rm max})^{1/2}$, where $R_{\rm max}$ is the radius of the maximum-mass nonrotating star), which were first proposed by Bauswein and Janka (2012), are not universal, in the sense that different (linear) fits are necessary for describing the $f_2$-correlations for binaries with different total masses. This conclusion can be evinced by looking at Figs. 22–24 of Bauswein et al. (2012), but the different linear correlations were first explicitly computed by Takami et al. (2014, 2015) (see also Hotokezaka et al. 2013).

The second feature identified in all PSDs analysed by Takami et al. (2014, 2015) is the second-largest peak, which appears at lower frequencies and was called $f_1$ there. Clear indications were given about this low-frequency peak being related to the merger process (i.e., the first $\approx$3 ms after the merger). This was done by showing that the power in the peak is greatly diminished if the first few ms after the merger were removed from the waveform. Furthermore, a simple mechanical toy model was devised that can explain rather intuitively the main spectral features of the post-merger signal and therefore shed light on the physical interpretation of the origin of the various peaks. Despite its crudeness, the toy model was even able to reproduce the complex waveforms emitted right after the merger, hence possibly opening the way to an analytical modelling of a part of the signal (Takami et al. 2015).

More importantly, it was shown that the potential measurement of the $f_1$ frequency could reveal the EOS of the merging objects, since a correlation was

found between the $f_1$-frequency and the average compactness of the two stars in the binary. Interestingly, this relation appears to be universal, that is, essentially valid for all EOSs and masses, and could therefore provide a powerful tool to set tight constraints on the EOS (Takami et al. 2014, 2015). Indeed, an analytic expression was suggested in Takami et al. (2015) to express the $f_1$ frequency via a third-order polynomial of the (average) stellar compactness, which reproduces reasonably well the numerical results. In addition to the correlations described above, Takami et al. (2014, 2015) also discussed additional correlations (24 in all), some of which had been already presented in the literature, e.g., in Read et al. (2013), Bernuzzi et al. (2014a), and some of which are presented there for the first time. Examples of these correlations are reported in Fig. 10.6, where different colours refer to different EOSs (see Fig. 1 of Takami et al. (2015) for a legend). The correlations refer to the $f_{\max}$, $f_1$ and $f_2$ frequencies and the physical quantities of the binary system, e.g., the average compactness $\bar{M}/\bar{R}$, the average density $(\bar{M}/\bar{R}^3)^{1/2}$, the pseudo-average rest-mass density $(\bar{M}/R^3_{\max})^{1/2}$, or the dimensionless tidal deformability tidal deformability $(\lambda/\bar{M}^5)^{1/5}$ (cf., also Fig. 15 of Takami et al. 2015). In confirmation of the accuracy of the computed frequencies, very similar values for the $f_1$ frequencies were also found by Dietrich et al. (2015b) in a distinct work aimed at determining the impact

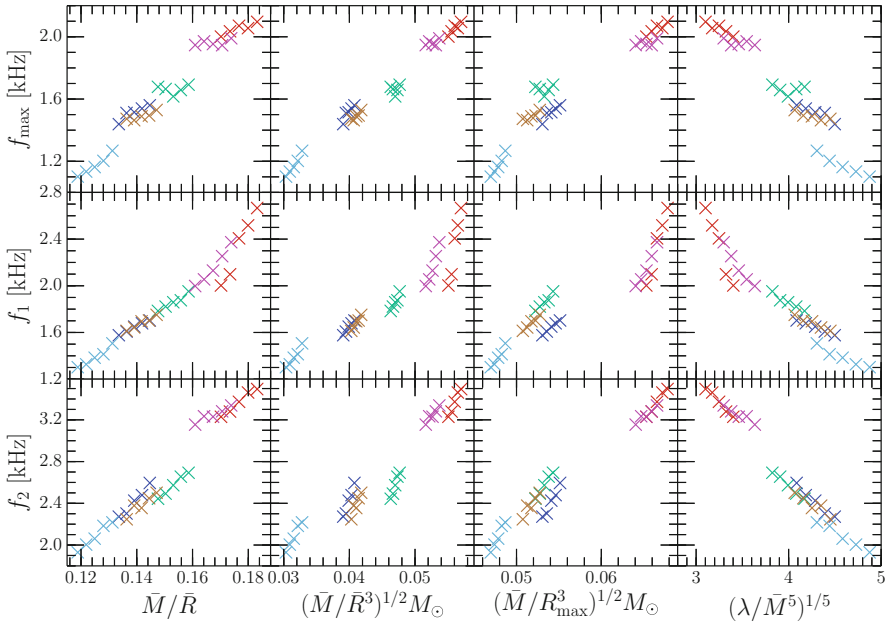


**Fig. 10.6** Empirical correlations between the $f_{\max}$, $f_1$ and $f_2$ frequencies and the physical quantities of the binary system, where different colours refer to different EOSs (see Fig. 1 of Takami et al. (2015) for a legend) [Reprinted with permission from Takami et al. (2015). © (2015) by the American Physical Society]

that conservative mesh-refinement techniques have on the accuracy of the post-merger dynamics.

Even though the toy model proposed by Takami et al. (2015) provides a simple and convincing explanation of the power associated to the $f_1$ frequency peak, alternative interpretations of the low-frequency part of the PSD have also been suggested. More specifically, Bauswein and Stergioulas (2015) claimed that the lower-frequency peak (i.e., the $f_1$ peak in Takami et al. 2014, 2015; Kastaun and Galeazzi 2015) is actually made of two separate peaks originating from different processes. One of these peaks is said to be produced by a nonlinear combination between the dominant quadrupolar oscillation ($f_{\rm peak}$ or $f_2$ in different notations) and the quasi-radial oscillation of the remnant and is named $f_{2\text{-}0}$ (Stergioulas et al. 2011), while the other is said to be caused by a strong deformation initiated at the time of the merger, the pattern of which then rotates (in the inertial frame) more slowly than the inner cores of the remnant and lasts for a few rotational periods, while diminishing in amplitude. The GW emission associated with this motion then powers a peak that was named $f_{\rm spiral}$ in Bauswein and Stergioulas (2015). The connection between the $f_{\rm spiral}$ peak and the deformation was supported by showing that only PSDs computed from time intervals of the gravitational waveform that contain the deformation have the $f_{\rm spiral}$ peak. It was also claimed that the $f_{\rm spiral}$ peak can be roughly reproduced in a toy model, where two bulges orbit as point particles around the central double-core structure for a duration of few milliseconds, but no details were given in Bauswein and Stergioulas (2015).

In their analysis, Bauswein and Stergioulas (2015) also proposed an explanation for the low-frequency modulations seen in quantities like the lapse function at the stellar center, the maximum rest-mass density, and the separation between the two cores of the remnant. Such quantities are modulated according to the orientation of the antipodal bulges of the deformation with respect to the double central cores: the compactness is smaller, the central lapse function larger, and the GW amplitude maximal when the bulges and the cores are aligned, and viceversa.

Making use of a large set of simulations, Bauswein and Stergioulas (2015) were able to obtain empirical relations for both types of low-frequency peaks in terms of the compactness of nonrotating individual neutron stars. Different relations, however, were found for different sequences of constant total mass of the binary, in contrast with what found in Takami et al. (2014, 2015), where a different definition for the low-frequency peak was used. As discussed by Bauswein and Stergioulas (2015), the different behaviour could be due to the fact that the results of Takami et al. (2014, 2015) were based on a limited set of five EOSs of soft or moderate stiffness (with corresponding maximum masses of nonrotating neutron stars only up to $2.2\,M_\odot$), as well as on different chosen mass ranges for each EOS with a spread of only $0.2\,M_\odot$ in the total mass of the binary. In Bauswein and Stergioulas (2015), on the other hand, ten EOSs (including stiff EOSs with maximum masses reaching up to $2.8\,M_\odot$) and a larger mass range of 2.4–3.0 $M_\odot$ were used. Overall, the differences between the results of the two groups are significant only for very low-mass neutron stars (i.e., $M = 1.2\,M_\odot$), which Takami et al. (2014, 2015) had

not included in their sample because of the low statistical incidence they are thought to have (see also below).

One important consideration to bear in mind is that measuring the $f_{\rm spiral}$ frequencies through the motion of matter asymmetries via gauge-dependent quantities such as the rest-mass density is essentially impossible in genuine numerical-relativity calculations. This is because the spatial gauge conditions can easily distort the coordinate appearance of mass distributions and even the trajectories of the two stars during the inspiral (see Appendix A 2 of Baiotti et al. (2008) for some dramatic examples). In an attempt to clarify the different interpretations suggested in Takami et al. (2014, 2015), Bauswein and Stergioulas (2015) and to bring under a unified framework the spectral properties of the post-merger GW signal, Rezzolla and Takami (2016) have recently presented a comprehensive analysis of the GW signal emitted during the inspiral, merger and post-merger of 56 neutron-star binaries (Rezzolla and Takami 2016) (waveforms from this work are shown in Fig. 10.5). This sample of binaries, arguably the largest studied to date with realistic EOSs, spans across five different nuclear-physics EOSs and seven mass values, including the very low-mass binaries (e.g., with individual neutron-star masses of $1.2\,M_\odot$) that were suggested by Bauswein and Stergioulas (2015) to be lacking in the previous analysis of Takami et al. (2015). After a systematic analysis of the complete sample, it was possible to sharpen a number of arguments on the spectral properties of the post-merger GW signal. Overall it was found that: (1) for binaries with individual stellar masses differing no more than 20%, the frequency at the maximum of the GW amplitude is related quasi-universally with the tidal deformability of the two stars; (2) the spectral properties vary during the post-merger phase, with a transient phase lasting a few milliseconds after the merger and followed by a quasi-stationary phase; (3) when distinguishing the spectral peaks between these two phases, a number of ambiguities in the identification of the peaks disappear, leaving a simple and robust picture; (4) using properly identified frequencies, quasi-universal relations are found between the spectral features and the properties of the neutron stars; (5) for the most salient peaks analytic fitting functions can be obtained in terms of the stellar tidal deformability or compactness. Overall, the analysis of Rezzolla and Takami (2016) supports the idea that the EOS of nuclear matter can be constrained tightly when a signal in GWs from BNSs is detected.

An interesting extension of the work of Takami et al. (2014, 2015) was suggested by Bernuzzi et al. (2015b), who expressed the correlation between the peak frequencies $f_2$ with the tidal coupling constant $\kappa_2^T$ instead of the tidal deformability parameter $\Lambda$, as done in Takami et al. (2014, 2015). As found in previous works by Bernuzzi et al. (2014a, 2015a) (see Sect. 10.3), the dimensionless GW frequency depends on the stellar EOS, binary mass, and mass ratio only through the tidal coupling constants $\kappa_2^T$ and thus this is a better choice of parameter, also because it can be extended more straightforwardly to the case of unequal-mass binaries. The relation $f_2(\kappa_2^T)$ was found in Bernuzzi et al. (2015b) to be very weakly dependent on the binary total mass, mass ratio, EOS, and thermal effects (through the ideal-fluid index $\Gamma_{\rm th}$). Relevant dependence on the stellar spins was instead found. This is shown in Fig. 10.7, which reports the dimensionless frequency $Mf_2$ as a function

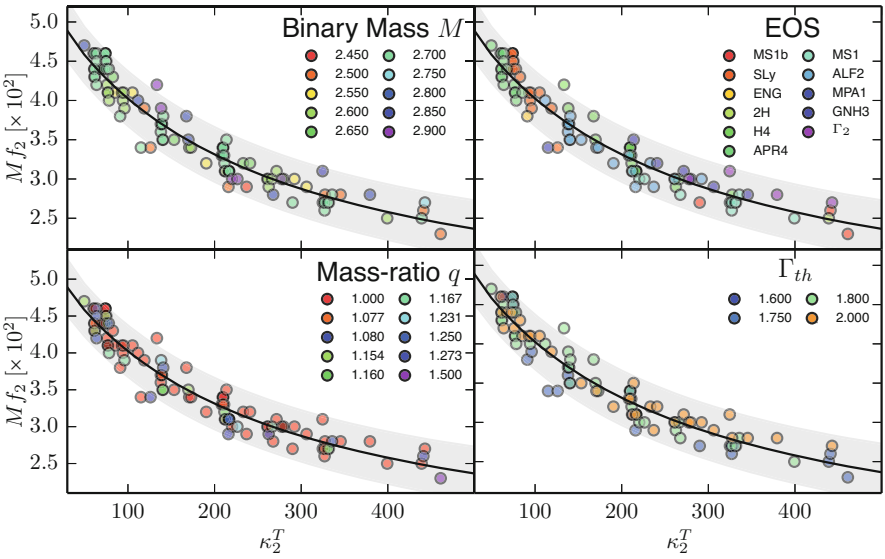


**Fig. 10.7** Dimensionless frequency ($Mf_2$) as a function of the tidal coupling constant $\kappa_2^T$. Each panel shows the same data set; the colour code in each panel indicates the different values of binary mass (top left), EOS (top right), mass-ratio (bottom left), and $\Gamma_{\rm th}$ (bottom right). The black solid line is the fit, while the grey area marks the 95% confidence interval [Reprinted with permission from Bernuzzi et al. (2015b). © (2015) by the American Physical Society]

of the tidal coupling constant $\kappa_2^T$. Each panel shows the same data set; the colour code in each panel indicates the different values of binary mass (top left), EOS (top right), mass-ratio (bottom left), and $\Gamma_{\rm th}$ (bottom right). The black solid line is the fit obtained by Bernuzzi et al. (2015b), while the grey area marks the 95% confidence range.

Although not explicitly stated, all of the considerations made so far about the spectral properties of the post-merger signal refer to binaries that are initially irrotational. It is therefore natural to ask what changes, both qualitatively and quantitatively, when spinning binaries are considered. This was done in part by Bernuzzi et al. (2014b) and by Kastaun et al. (2013) and Kastaun and Galeazzi (2015). The first work considered in particular whether the main-peak frequency $f_2$ is influenced by the initial state of rotation and found that this is indeed the case at least for very rapidly rotating neutron stars, suggesting that spin effects may be more important than those found in Bauswein and Janka (2012). Kastaun and Galeazzi (2015), on the other hand, analysed the spectral changes induced by the initial spin on high-mass binaries and showed that the direct influence of the spin on the frequency $f_2$ is weak and comparable to the width of the corresponding peak. They also studied in detail the Fourier decomposition of the rest-mass density of the binary-merger product and its rotational profile, which is important for determining its lifetime, especially in view of the amplification of the magnetic field. A problem

that needed to be tackled in their analysis is that of potential gauge artefacts. We recall, in fact, that rest-mass density distributions are gauge-dependent quantities and even when the system approaches an axisymmetric state after the merger, the spatial coordinates may not reflect this, because the gauge conditions employed in the evolution introduce local and global deformations. In order to exclude such systematic gauge effects, Kastaun and Galeazzi (2015) introduced a different coordinate system, used just for post-processing. In this new coordinate system, they found that, the Fourier decomposition is far more regular than in the coordinate system normally used in the evolution. Furthermore, they showed that, contrary to common assumptions, the law of differential rotation of the binary-merger product consists of a slowly rotating core with an extended and massive envelope rotating close to Keplerian velocity (see discussion in Hanauske et al. 2016). The latter result has been confirmed recently also for the binary-merger product produced by the merger of unequal-mass magnetised binaries (Endrizzi et al. 2016).

A rather different approach to analysing post-merger waveforms has been taken by Chatziioannou et al. (2017). In order to obtain results that rely less on numerical-relativity simulations, they use a morphology-independent Bayesian data analysis algorithm, BAYESWAVE (Cornish and Littenberg 2015; Littenberg and Cornish 2015), to reconstruct as a sum of wavelets injected post-merger GW signals that are assumed to have been measured (in the absence of observational data, data based on simulations were used). It was found that BAYESWAVE is capable of reconstructing the dominant features of the injected signal, in particular the dominant post-merger frequency, with an overlap between injected and reconstructed signals of above 90% for post-merger SNRs above 5. This allows $f_2$ to be measured at the 90% credible level with an error of about 36 (27) [45] Hz for a stiff (moderate) [soft] EOSs and so to set bounds on the NS radius obtained by the post-merger signal of order 100 m for a signal emitted at 20 Mpc. This accuracy is similar to that predicted by the other methods discussed above, which are completely based on numerical simulations. Actually also Chatziioannou et al. (2017) had to use empirical formulas from numerical simulations (Bauswein and Janka 2012; Bauswein et al. 2012, 2016) to relate $f_2$ to the radius and they indeed found that their error on the radius is dominated by the systematic uncertainty (scatter) in such a formula, rather than the statistical error of the reconstruction.

Before concluding this discussion on the post-merger GW signal we shall also make some additional important remarks.

- First, GW measurements at the expected frequencies and amplitudes are very difficult, namely limited to sources within $\sim$20 Mpc. This number can be easily estimated with back-of-the-envelope calculations, but it was confirmed through detailed analysis of the detectability of the dominant oscillation frequency in Clark et al. (2014), Bose et al. (2018), Yang et al. (2018) via large-scale Monte Carlo studies in which simulated post-merger GW signals are injected into realistic detector data that matches the design goals of Advanced LIGO and Advanced Virgo.

- Second, the post-merger frequencies evolve in time, albeit only slightly. Hence, the spectral properties of the GW signal can be asserted reliably only when the signal-to-noise ratio is sufficiently strong so that even these changes in time can be measured in the evolution of the PSDs (Kiuchi et al. 2012b; Hotokezaka et al. 2013; Takami et al. 2014; Shibata et al. 2014). In light of these considerations, the prospects for high-frequency searches for the post-merger signal are limited to rare nearby events. Yet, if such detections happen, the error in the estimate of the neutron star radius will be of the order of a few hundred metres (Clark et al. 2014, 2016; Bose et al. 2018; Yang et al. 2018).
- Third, viscous dissipation and energy transport in the post-merger phase may considerably affect gravitational waveforms. It has been recently pointed out that shear viscosity and thermal conductivity are not likely to play a major role in post-merger dynamics unless neutrino trapping occurs, which requires temperatures $T \gtrsim 10\,\mathrm{MeV}$, or flows that experience shear over short distances of the order of 0.01 km (Alford et al. 2018). By using the most likely values of the parameters describing shear viscosity other works had already estimated that the post-merger GW amplitude is affected, but its frequency peaks are not (Radice 2017; Shibata and Kiuchi 2017). On the other hand, bulk viscous dissipation could provide significant damping of the high-amplitude density oscillations observed right after merger, if modified-Urca processes (and not direct-Urca processes; see e.g. Lattimer et al. 1991) are those that establish flavor equilibrium (Alford et al. 2018). Hence, viscous dissipative processes deserve more careful investigation since they may well affect the spectral properties of the post-merger gravitational-wave signal, especially the $f_1$ and $f_3$ peaks that are produced right after the merger and that are dissipated rapidly (Takami et al. 2015). In addition, if viscous dissipation is active after the merger, it will also heat the merger product, possibly stabilising it on longer timescales via the extra thermal pressure (Baiotti et al. 2008; Sekiguchi et al. 2011b; Paschalidis et al. 2012; Kaplan et al. 2014). Finally, future gravitational-wave observations may also give indications about the fraction of merger material in which direct or modified Urca processes are dominant.

At the end of this long Section, we summarise the main finding on the spectral properties of the post-merger signal as follows:

- The most powerful methods to connect observations of the post-merger GW with the EOS of those neutron stars is based on analyses of the GW PSD.
- In general, there are three main peaks in the PSDs of the post-merger phase of binary mergers that do not result in a prompt collapse to a black hole. The frequencies of these peaks are named $f_1$, $f_2$, $f_3$ in Takami et al. (2014, 2015), Rezzolla and Takami (2016), while other works use different symbols, in particular the frequency of the highest peak, $f_2$, is referred to as $f_{\mathrm{peak}}$ in e.g., Bauswein and Janka (2012), Bauswein and Stergioulas (2015), Bauswein et al. (2016). The frequencies were found to roughly follow the relation $f_2 \simeq (f_1 + f_3)/2$.

- The $f_2$ frequencies correspond to the $\ell = 2 = m$ fundamental mode of the HMNS and hence are equal to twice the rotation frequency of the bar deformation of the HMNS. Their values change slightly in time (by $\sim$5%). The $f_1$ and $f_3$ frequencies are produced only in the first few milliseconds after the merger. A simple toy model was proposed in Takami et al. (2015) to explain their origin. See also Bauswein and Stergioulas (2015) for another model.
- The frequencies $f_2$ and $f_1$ were found to correlate well with properties of the stars in the BNS system. In particular, $f_2$ correlates well with the quantity $(\bar{M}/R^3_{\rm max})^{1/2}$ for a given total mass of the BNS (Bauswein and Janka 2012), while $f_1$ correlates well with the average compactness of the two stars in the binary and such a relation seems valid for any total mass of the BNS, prompting Takami et al. (2014, 2015) to call the relation *universal*.
- Such correlations between post-merger frequencies and stellar properties can be used to estimate rather accurately the radius of the neutron stars and so to infer information on their EOS. There are, however, caveats against a simplistic use of post-merger frequencies, since they may vary in time, be affected by bulk viscosity (Alford et al. 2018) and by the spins of the stars in the binary (if very high) (Bernuzzi et al. 2014b), and since the post-merger GW signals have a small SNR in current detectors and therefore the chances of a detection are very small.

### *10.4.3 Spectral Properties and the Mass-Redshift Degeneracy*

Besides providing information on the EOS, the spectral properties of the gravitational-wave post-merger signal can also be used in a completely different manner, namely, to remove the degeneracy in the determination of redshift and mass for cosmological investigations. Indeed, a well-known problem of the detection of gravitational waves from compact-object binaries at cosmological distances is the so-called "mass-redshift degeneracy". More precisely, given a source of (gravitational) mass $M$ at a cosmological redshift $z$, a direct gravitational-wave observation provides information only on the combined quantity $M(1 + z)$, so that it is not possible to have an independent measurement of $M$ and of $z$. The standard solution to this problem is to detect an electromagnetic counterpart to the gravitational-wave signal, so as to measure $z$ and hence the mass $M$. However, this may be not easy in some cases.

In a recent investigation, Messenger et al. (2014) described how this degeneracy can be broken when exploiting information on the spectral properties of the post-merger gravitational-wave signal. More specifically, making use of numerically generated BNS waveforms, it was shown that it is possible to construct frequency-domain power-spectrum reference templates that capture the evolution of two of the primary spectral features in the post-merger stage of the waveforms as a function of the total gravitational mass.

This is summarised via a cartoon in Fig. 10.8, which shows how the information on the redshifted mass as a function of the redshift (blue stripe) can be correlated

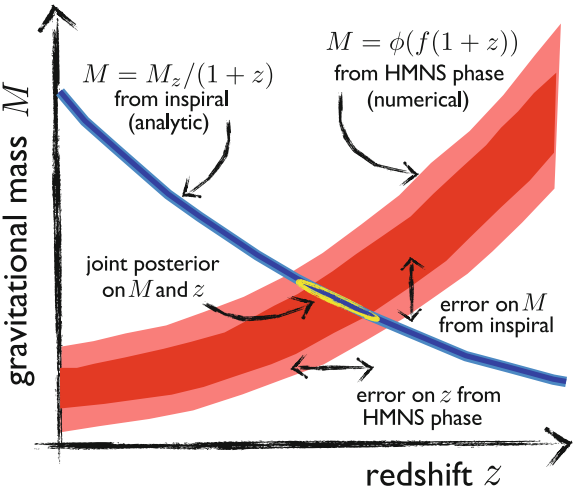


**Fig. 10.8** A cartoon illustrating how the mass-redshift degeneracy is broken through the use of information from the inspiral and HMNS stages of a BNS merger event. Cross-correlating the information on the redshifted mass as a function of the redshift (blue stripe) with the information from the spectral properties of the HMNS phase (red stripe) will provide a localised range in mass and redshift, breaking the degeneracy [Reprinted with permission from Messenger et al. (2014). © (2014) by the American Physical Society]

with complementary information from the spectral properties of the HMNS phase. The overlap will provide a localised range in mass and redshift, breaking the degeneracy. A Bayesian inference method was then used to test the ability of the Einstein Telescope (Punturo et al. 2010b) to measure the characteristic frequencies in the post-merger stage of the signal, finding that redshift and gravitational mass can be determined separately, with uncertainties in the redshift of sources at $z = 0.01$–$0.04$ of 10–20% and in the gravitational mass of $<1\%$ in all cases.

## 10.5 Conclusions

As anticipated in the Introduction, there is little doubt that this is a particularly exciting and highly dynamical time for research on neutron stars, in general, and on BNS mergers, in particular. In about 10 years, i.e., starting approximately from 2008, a considerable effort by several groups across the world has obtained numerous important results about the dynamics of binary systems of neutron stars, employing a large variety of numerical (in most cases) and analytical (in a few cases) techniques and exploring this process with different degrees of approximation and realism.

Altogether, these works have revealed that the merger of a binary system of neutron stars is a marvellous physical laboratory. Indeed, BNS mergers are expected

to be behind several fascinating physical processes, which we recall here: (1) they are significant sources of gravitational radiation; (2) they act as possible progenitors for short-gamma-ray bursts (SGRBs); (3) they have the potential to produce electromagnetic and neutrino emission that is visible from enormous distances; (4) they are likely responsible for the production of a good portion of the very heavy elements in the Universe. When viewed across this lens, it is quite natural to consider BNS mergers as Einstein's richest laboratory, binding in the same environment highly nonlinear gravitational dynamics with complex microphysical processes and astonishing astrophysical phenomena.

The huge progress accomplished over the last 10 years has helped trace a broadbrush picture of BNS mergers that has several sound aspects, among which the most robust in our opinion are the following ones[6]:

- Independently of the fine details of the EOS, of the mass ratio or of the presence of magnetic fields, the merger of a binary system of neutron stars eventually leads to a rapidly rotating black hole with dimensionless spin $J/M^2 \simeq 0.7$–$0.8$ surrounded by a hot accretion torus with mass in the range $M_{\rm torus} \sim 0.001$–$0.1\, M_\odot$. Only very low-mass progenitors whose total mass is below the maximum mass of a (nonrotating) neutron star would not produce a black hole. It is unclear whether such progenitors are statistically important.
- The complete GW signal from inspiralling and merging BNSs can be computed numerically with precision that is smaller but overall comparable with that available for black holes.
- When considering the inspiral-only part of the GW signal, semi-analytical approximations either in the post-Newtonian or EOB approximation, can reproduce the results of numerical-relativity calculations essentially up to the merger.
- The GW spectrum is marked by precise frequencies, either during the inspiral or after the merger that exhibit a "quasi-universal" behaviour. In other words, while the position of the peaks depends on the EOS, it can be easily factored out to obtain EOS-independent relations between the frequencies of the peaks and the properties of the progenitor stars.
- The result of the merger, i.e., the binary-merger product, is a highly massive and differentially rotating neutron star. The lifetime of the binary-merger product depends on a number of factors, including the mass of the progenitors, their mass ratio and EOS, as well as the role played by magnetic fields and neutrino losses. While sufficiently large initial masses can yield a prompt collapse at the merger, for smaller masses the object resulting from the merger can be a neutron star for at least some milliseconds or maybe forever.

Note that many of the aspects listed above are robust but have been addressed mostly at a rather qualitative level, with precisions that range from "a-factor-of-a-few" up to "order-of-magnitude" estimates. Furthermore, these results can be

[6]In this Section we will intentionally omit references to avoid cluttering the text; all the relevant references can be found in the various Sections covering the topics discussed here.

seen as the low-hanging fruits of a tree that still has a number of results to offer, although these will require an equal, if not larger, investment of effort, microphysical and numerical developments, and, of course, of computer time. In conclusion, if GW170817 and the first direct detection of the GW signals from binary systems of neutron stars has officially given birth to the era of multimessenger astronomy, the huge advances that are expected to come in the next few years on the physics and astrophysics of BNSs will help lift many of the veils that still cover Einstein's richest laboratory.

**Acknowledgements** It is a pleasure to thank Kentaro Takami and the relativistic-astrophysics group in Frankfurt for their help and input in preparing this Chapter.

Partial support has come from "NewCompStar", COST Action MP1304, from the LOEWE-Program in HIC for FAIR, the European Union's Horizon 2020 Research and Innovation Programme under grant agreement No. 671698 (call FETHPC-1–2014, project ExaHyPE), from the ERC Synergy Grant "BlackHoleCam - Imaging the Event Horizon of Black Holes" (Grant 610058), from JSPS Grant-in-Aid for Scientific Research(C) No. 18K036220, from the International Centre for Theoretical Sciences Code: ICTS/Prog-GWS/2017/07, and from the Excellence Initiative at Radboud University Nijmegen.

## References

Abadie, J., et al.: Class. Quantum Grav. **27**, 173001 (2010). arXiv:1003.2480 [astro-ph.HE]

Abbott, B.P., Abbott, R., Abbott, T.D., Abernathy, M.R., Acernese, F., Ackley, K., Adams, C., Adams, T., Addesso, P., Adhikari, R.X., et al.: Phys. Rev. Lett. **116**, 241103 (2016). arXiv:1606.04855 [gr-qc]

Abbott, B.P., et al. (Virgo, LIGO Scientific): Phys. Rev. Lett. **119**, 161101 (2017). arXiv:1710.05832 [gr-qc]

Abbott, B.P., et al. (Virgo, LIGO Scientific): (2018a). arXiv:1805.11581

Abbott, B.P., et al. (Virgo, LIGO Scientific): (2018b). arXiv:1805.11579

Accadia, T., et al.: Class. Quantum Grav. **28**, 114002 (2011)

Advanced LIGO Anticipated Sensitivity Curves, LIGO Document No. T0900288-v3 (2009)

Agathos, M., Meidam, J., Del Pozzo, W., Li, T.G.F., Tompitak, M., Veitch, J., Vitale, S., Van Den Broeck, C.: Phys. Rev. D **92**, 023012 (2015). arXiv:1503.05405 [gr-qc]

Ajith, P., et al.: Class. Quantum Grav. **24**, S689 (2007). arXiv:0704.3764

Ajith, P., et al.: Phys. Re. D **77**, 104017 (2008). arXiv:0710.2335

Akmal, A., Pandharipande, V.R., Ravenhall, D.G.: Phys. Rev. C **58**, 1804 (1998). arXiv:hep-ph/9804388

Alcock, C., Farhi, E., Olinto, A.: Astrophys. J. **310**, 261 (1986)

Alford, M., Braby, M., Paris, M., Reddy, S.: Astrophys. J. **629**, 969 (2005). nucl-th/0411016

Alford, M.G., Bovard, L., Hanauske, M., Rezzolla, L., Schwenzer, K.: Phys. Rev. Lett. **120**, 041101 (2018). arXiv:1707.09475 [gr-qc]

AlGendy, M., Morsink, S.M.: Astrophys. J. **791**, 78 (2014). arXiv:1404.0609 [astro-ph.HE]

Anderson, M., Hirschmann, E.W., Lehner, L., Liebling, S.L., Motl, P.M., Neilsen, D., Palenzuela, C., Tohline, J.E.: Phys. Rev. Lett. **100**, 191101 (2008). arXiv:0801.4387 [gr-qc]

Andersson, N., Kokkotas, K.D.: Mon. Not. R. Astron. Soc. **299**, 1059 (1998). arXiv:gr-qc/9711088

Andersson, N., Ferrari, V., Jones, D.I., Kokkotas, K.D., Krishnan, B., Read, J.S., Rezzolla, L., Zink, B.: Gen. Relativ. Gravit. **43**, 409 (2011). arXiv:0912.0384 [astro-ph.SR]

Antoniadis, J., Freire, P.C.C., Wex, N., Tauris, T.M., Lynch, R.S., van Kerkwijk, M.H., Kramer, M., Bassa, C., Dhillon, V.S., Driebe, T., Hessels, J.W.T., Kaspi, V.M., Kondratiev, V.I., Langer,

N., Marsh, T.R., McLaughlin, M.A., Pennucci, T.T., Ransom, S.M., Stairs, I.H., van Leeuwen, J., Verbiest, J.P.W., Whelan, D.G.: Science **340**, 448 (2013). arXiv:1304.6875 [astro-ph.HE]
Aso, Y., Michimura, Y., Somiya, K., Ando, M., Miyakawa, O., Sekiguchi, T., Tatsumi, D., Yamamoto, H.: Phys. Rev. D **88**, 043007 (2013). arXiv:1306.6747 [gr-qc]
Babak, S., Taracchini, A., Buonanno, A.: Phys. Rev. **D95**, 024010 (2017). arXiv:1607.05661 [gr-qc]
Baiotti, L., Rezzolla, L.: Rep. Prog. Phys. **80**, 096901 (2017). arXiv:1607.03540 [gr-qc]
Baiotti, L., de Pietri, R., Manca, G.M., Rezzolla, L.: Phys. Rev. D **75**, 044023 (2007). astro-ph/0609473
Baiotti, L., Giacomazzo, B., Rezzolla, L.: Phys. Rev. D **78**, 084033 (2008). arXiv:0804.0594 [gr-qc]
Baiotti, L., Damour, T., Giacomazzo, B., Nagar, A., Rezzolla, L.: Phys. Rev. Lett. **105**, 261101 (2010). arXiv:1009.0521 [gr-qc]
Balbinski, E.: Mon. Not. R. Astron. Soc. **216**, 897 (1985)
Banihashemi, B., Vines, J. (2018). arXiv:1805.07266
Banik, S., Hempel, M., Bandyopadhyay, D.: Astrohys. J. Suppl. **214**, 22 (2014). arXiv:1404.6173 [astro-ph.HE]
Bauböck, M., Berti, E., Psaltis, D., Özel, F.: Astrophys. J. **777**, 68 (2013). arXiv:1306.0569 [astro-ph.HE]
Bauswein, A., Janka, H.-T.: Phys. Rev. Lett. **108**, 011101 (2012). arXiv:1106.1616 [astro-ph.SR]
Bauswein, A., Stergioulas, N.: Phys. Rev. D **91**, 124056 (2015). arXiv:1502.03176 [astro-ph.SR]
Bauswein, A., Janka, H.-T., Oechslin, R., Pagliara, G., Sagert, I., Schaffner-Bielich, J., Hohle, M.M., Neuhäuser, R.: Phys. Rev. Lett. **103**, 011101 (2009). arXiv:0812.4248
Bauswein, A., Oechslin, R., Janka, H.-T.: Phys. Rev. D **81**, 024012 (2010). arXiv:0910.5169 [astro-ph.SR]
Bauswein, A., Janka, H.-T., Hebeler, K., Schwenk, A.: Phys. Rev. D **86**, 063001 (2012). arXiv:1204.1888 [astro-ph.SR]
Bauswein, A., Baumgarte, T.W., Janka, H.-T.: Phys. Rev. Lett. **111**, 131101 (2013). arXiv:1307.5191 [astro-ph.SR]
Bauswein, A., Stergioulas, N., Janka, H.-T.: Phys. Rev. D **90**, 023002 (2014). arXiv:1403.5301 [astro-ph.SR]
Bauswein, A., Stergioulas, N., Janka, H.-T.: Eur. Phys. J. A **52**, 56 (2016). arXiv:1508.05493 [astro-ph.HE]
Bejger, M., Haensel, P.: Astron. Astrophys. **396**, 917 (2002). arXiv:astro-ph/0209151
Benhar, O., Ferrari, V., Gualtieri, L.: Phys. Rev. D **70**, 124015 (2004). arXiv:astro-ph/0407529
Bernuzzi, S., Nagar, A., Thierfelder, M., Brügmann, B.: Phys. Rev. D **86**, 044030 (2012). arXiv:1205.3403 [gr-qc]
Bernuzzi, S., Nagar, A., Balmelli, S., Dietrich, T., Ujevic, M.: Phys. Rev. Lett. **112**, 201101 (2014a). arXiv:1402.6244 [gr-qc]
Bernuzzi, S., Dietrich, T., Tichy, W., Brügmann, B.: Phys. Rev. D **89**, 104021 (2014b). arXiv:1311.4443 [gr-qc]
Bernuzzi, S., Nagar, A., Dietrich, T., Damour, T.: Phys. Rev. Lett. **114**, 161103 (2015a). arXiv:1412.4553 [gr-qc]
Bernuzzi, S., Dietrich, T., Nagar, A.: Phys. Rev. Lett. **115**, 091101 (2015b). arXiv:1504.01764 [gr-qc]
Bernuzzi, S., Radice, D., Ott, C.D., Roberts, L.F., Moesta, P., Galeazzi, F.: Phys. Rev. D **94**, 024023 (2016). arXiv:1512.06397 [gr-qc]
Berti, E., Iyer, S., Will, C.M.: Phys. Rev. D **77**, 024019 (2008). arXiv:0709.2589
Bhowmick, B., Bhattacharya, M., Bhattacharyya, A., Gangopadhyay, G.: Phys. Rev. **C89**, 065806 (2014). arXiv:1403.0341 [nucl-th]
Bildsten, L., Cutler, C.: Astrophys. J. **400**, 175 (1992)
Bini, D., Damour, T.: Phys. Rev. D **90**, 124037 (2014). arXiv:1409.6933 [gr-qc]
Bini, D., Geralico, A.: Phys. Rev. **D91**, 084012 (2015)
Bini, D., Damour, T., Faye, G.: Phys. Rev. **D85**, 124034 (2012). arXiv:1202.3565 [gr-qc]

Binnington, T., Poisson, E.: Phys. Rev. D **80**, 084018 (2009). arXiv:0906.1366 [gr-qc]
Blanchet, L.: Living Rev. Relativ. **9**, 4 (2006)
Bodo, G., Massaglia, S., Ferrari, A., Trussoni, E.: Astron. Astrophys. **283**, 655 (1994)
Bohe, A., et al.: Phys. Rev. **D95**, 044028 (2017). arXiv:1611.03703 [gr-qc]
Bose, S., Chakravarti, K., Rezzolla, L., Sathyaprakash, B.S., Takami, K.: Phys. Rev. Lett. **120**, 031102 (2018). arXiv:1705.10850 [gr-qc]
Bovard, L., Martin, D., Guercilena, F., Arcones, A., Rezzolla, L., Korobkin, O.: Phys. Rev. D **96**, 124005 (2017). arXiv:1709.09630 [gr-qc]
Breu, C., Rezzolla, L.: Mon. Not. R. Astron. Soc. **459**, 646 (2016). arXiv:1601.06083 [gr-qc]
Buonanno, A., Damour, T.: Phys. Rev. D **59**, 084006 (1999). gr-qc/9811091
Buonanno, A., Damour, T.: Phys. Rev. D **62**, 064015 (2000). gr-qc/0001013
Buonanno, A., Iyer, B., Ochsner, E., Pan, Y., Sathyaprakash, B.S.: Phys. Rev. **D80**, 084043 (2009). arXiv:0907.0700 [gr-qc]
Camarda, K.D., Anninos, P., Fragile, P.C., Font, J.A.: Astrophys. J. **707**, 1610 (2009). arXiv:0911.0670 [astro-ph.SR]
Cardoso, V., Franzin, E., Maselli, A., Pani, P., Raposo, G.: Phys. Rev. **D95**, 084014 (2017) [Addendum: Phys. Rev. **D95**(8), 089901 (2017)]. arXiv:1701.01116 [gr-qc]
Carriere, J., Horowitz, C.J., Piekarewicz, J.: Astrophys. J. **593**, 463 (2003). nucl-th/0211015
Centrella, J.M., New, K.C.B., Lowe, L.L., Brown, J.D.: Astrophys. J. **550**, L193 (2001). astro-ph/0010574
Chakrabarti, S., Delsate, T., Steinhoff, J.: Phys. Rev. **D88**, 084038 (2013a). arXiv:1306.5820 [gr-qc]
Chakrabarti, S., Delsate, T., Steinhoff, J. (2013b). arXiv:1304.2228
Chakrabarti, S., Delsate, T., Gürlebeck, N., Steinhoff, J.: Phys. Rev. Lett. **112**, 201102 (2014). arXiv:1311.6509 [gr-qc]
Chan, T.K., Chan, A.P.O., Leung, P.T.: Phys. Rev. **D91**, 044017 (2015). arXiv:1411.7141 [astro-ph.SR]
Chan, T.K., Chan, A.P.O., Leung, P.T.: Phys. Rev. **D93**, 024033 (2016). arXiv:1511.08566 [gr-qc]
Chandrasekhar, S.: Hydrodynamic and Hydromagnetic Stability. Dover Edition, New York (1981)
Chatziioannou, K., Yagi, K., Klein, A., Cornish, N., Yunes, N.: Phys. Rev. **D92**, 104008 (2015). arXiv:1508.02062 [gr-qc]
Chatziioannou, K., Clark, J.A., Bauswein, A., Millhouse, M., Littenberg, T.B., Cornish, N.: Phys. Rev. D **96**, 124035 (2017). arXiv:1711.00040 [gr-qc]
Chirenti, C., de Souza, G.H., Kastaun, W.: Phys. Rev. **D91**, 044034 (2015). arXiv:1501.02970 [gr-qc]
Chirenti, C., Gold, R., Miller, M.C.: Astrophys. J. **837**, 67 (2017). arXiv:1612.07097 [astro-ph.HE]
Ciolfi, R., Siegel, D.M.: Astrophys. J. **798**, L36 (2015). arXiv:1411.2015 [astro-ph.HE]
Clark, J., Bauswein, A., Cadonati, L., Janka, H.-T., Pankow, C., Stergioulas, N.: Phys. Rev. D **90**, 062004 (2014). arXiv:1406.5444 [astro-ph.HE]
Clark, J.A., Bauswein, A., Stergioulas, N., Shoemaker, D.: Class. Quantum Grav. **33**, 085003 (2016). arXiv:1509.08522 [astro-ph.HE]
Cornish, N.J., Littenberg, T.B.: Class. Quantum Grav. **32**, 135012 (2015). arXiv:1410.3835 [gr-qc]
Corvino, G., Rezzolla, L., Bernuzzi, S., De Pietri, R., Giacomazzo, B.: Class. Quantum Grav. **27**, 114104 (2010). arXiv:1001.5281 [gr-qc]
Cutler, C., Flanagan, É.E.: Phys. Rev. D **49**, 2658 (1994). gr-qc/9402014
Cutler, C., Apostolatos, T.A., Bildsten, L., Finn, L.S., Flanagan, E.E., Kennefick, D., Markovic, D.M., Ori, A., Poisson, E., Sussman, G.J., Thorne, K.S.: Phys. Rev. Lett. **70**, 2984 (1992)
Damour, T., Lecian, O.M.: Phys. Rev. D **80**, 044017 (2009). arXiv:0906.3003 [gr-qc]
Damour, T., Nagar, A.: Phys. Rev. D **80**, 084035 (2009). arXiv:0906.0096 [gr-qc]
Damour, T., Nagar, A.: Phys. Rev. D **81**, 084016 (2010). arXiv:0911.5041 [gr-qc]
Damour, T., Soffel, M., Xu, C.: Phys. Rev. D **45**, 1017 (1992)
Damour, T., Nagar, A., Villain, L.: Phys. Rev. D **85**, 123007 (2012)
Damour, T., Jaranowski, P., Schäfer, G.: Phys. Rev. **D93**, 084014 (2016). arXiv:1601.01283 [gr-qc]
De Pietri, R., Feo, A., Maione, F., Löffler, F.: Phys. Rev. D **93**, 064047 (2016). arXiv:1509.08804 [gr-qc]

Del Pozzo, W., Li, T.G.F., Agathos, M., Van Den Broeck, C., Vitale, S.: Phys. Rev. Lett. **111**, 071101 (2013). arXiv:1307.8338 [gr-qc]
Demorest, P.B., Pennucci, T., Ransom, S.M., Roberts, M.S.E., Hessels, J.W.T.: Nature **467**, 1081 (2010). arXiv:1010.5788 [astro-ph.HE]
Dessart, L., Ott, C.D., Burrows, A., Rosswog, S., Livne, E.: Astrophys. J. **690**, 1681 (2009). arXiv:0806.4380
Detweiler, S., Lindblom, L.: Astrophys. J. **292**, 12 (1985)
Dietrich, T., Hinderer, T.: Phys. Rev. **D95**, 124006 (2017). arXiv:1702.02053 [gr-qc]
Dietrich, T., Moldenhauer, N., Johnson-McDaniel, N.K., Bernuzzi, S., Markakis, C.M., Brügmann, B., Tichy, W.: Phys. Rev. D **92**, 124007 (2015a). arXiv:1507.07100 [gr-qc]
Dietrich, T., Bernuzzi, S., Ujevic, M., Brügmann, B.: Phys. Rev. D **91**, 124041 (2015b). arXiv:1504.01266 [gr-qc]
Dietrich, T., Bernuzzi, S., Tichy, W. (2017). arXiv:1706.02969 [gr-qc]
Dietrich, T., et al. (2018). arXiv:1804.02235
Dixon, W.G.: Proc. R. Soc. Lond. **A314**, 499 (1970)
Dolan, S.R., Nolan, P., Ottewill, A.C., Warburton, N., Wardell, B.: Phys. Rev. D **91**, 023009 (2015). arXiv:1406.4890 [gr-qc]
Doneva, D.D., Yazadjiev, S.S., Stergioulas, N., Kokkotas, K.D.: Astrophys. J. Lett. **781**, L6 (2014). arXiv:1310.7436 [gr-qc]
Doneva, D.D., Kokkotas, K.D., Pnigouras, P.: Phys. Rev. D **92**, 104040 (2015). arXiv:1510.00673 [gr-qc]
East, W.E., Paschalidis, V., Pretorius, F., Shapiro, S.L.: Phys. Rev. D **93**, 024011 (2016). arXiv:1511.01093 [astro-ph.HE]
Endrizzi, A., Ciolfi, R., Giacomazzo, B., Kastaun, W., Kawamura, T. (2016). arXiv:1604.03445 [astro-ph.HE]
Essick, R., Vitale, S., Weinberg, N.N.: Phys. Rev. **D94**, 103012 (2016). arXiv:1609.06362 [astro-ph.HE]
Fairhurst, S.: J. Phys. Conf. Ser. **484**, 012007 (2014). arXiv:1205.6611 [gr-qc]
Farhi, E., Jaffe, R.L.: Phys. Rev. D **30**, 2379 (1984)
Fattoyev, F.J., Carvajal, J., Newton, W.G., Li, B.-A.: Phys. Rev. **C87**, 015806 (2013). arXiv:1210.3402 [nucl-th]
Fattoyev, F.J., Newton, W.G., Li, B.-A.: Eur. Phys. J. **A50**, 45 (2014). arXiv:1309.5153 [nucl-th]
Favata, M.: Phys. Rev. Lett. **112**, 101101 (2014). arXiv:1310.8288 [gr-qc]
Fernández, R., Foucart, F., Kasen, D., Lippuner, J., Desai, D., Roberts, L.F.: Class. Quant. Grav. **34**, 154001 (2017). arXiv:1612.04829 [astro-ph.HE]
Ferrari, V., Gualtieri, L., Pannarale, F.: Phys. Rev. D **81**, 064026 (2010). arXiv:0912.3692 [gr-qc]
Ferrari, V., Gualtieri, L., Maselli, A.: Phys. Rev. **D85**, 044045 (2012). arXiv:1111.6607 [gr-qc]
Flanagan, E.E.: Phys. Rev. D **58**, 124030 (1998)
Flanagan, É.É., Hinderer, T.: Phys. Rev. D **77**, 021502 (2008). arXiv:0709.1915
Flanagan, E.E., Racine, E.: Phys. Rev. **D75**, 044001 (2007). arXiv:gr-qc/0601029 [gr-qc]
Foucart, F., Deaton, M.B., Duez, M.D., O'Connor, E., Ott, C.D., Haas, R., Kidder, L.E., Pfeiffer, H.P., Scheel, M.A., Szilagyi, B.: Phys. Rev. D **90**, 024026 (2014). arXiv:1405.1121 [astro-ph.HE]
Foucart, F., Haas, R., Duez, M.D., O'Connor, E., Ott, C.D., Roberts, L., Kidder, L.E., Lippuner, J., Pfeiffer, H.P., Scheel, M.A.: Phys. Rev. D **93**, 044019 (2016). arXiv:1510.06398 [astro-ph.HE]
Franci, L., De Pietri, R., Dionysopoulou, K., Rezzolla, L.: Phys. Rev. D **88**, 104028 (2013). arXiv:1308.3989 [gr-qc]
Fujibayashi, S., Sekiguchi, Y., Kiuchi, K., Shibata, M.: ArXiv e-prints (2017). arXiv:1703.10191 [astro-ph.HE]
Gagnon-Bischoff, J., Green, S.R., Landry, P., Ortiz, N.: Phys. Rev. **D97**(6), 064042 (2018). arXiv:1711.05694
Giacomazzo, B., Rezzolla, L., Baiotti, L.: Phys. Rev. D **83**, 044014 (2011). arXiv:1009.2468 [gr-qc]

Gold, R., Bernuzzi, S., Thierfelder, M., Brugmann, B., Pretorius, F.: Phys. Rev. **D86**, 121501 (2012). arXiv:1109.5128 [gr-qc]
Goldberger, W.D., Rothstein, I.Z.: Phys. Rev. **D73**, 104029 (2006). arXiv:hep-th/0409156 [hep-th]
Gualtieri, L., Kantor, E.M., Gusakov, M.E., Chugunov, A.I.: Phys. Rev. **D90**, 024010 (2014). arXiv:1404.7512 [gr-qc]
Guersel, Y.: Gen. Relativ. Gravit. **15**, 737 (1983)
Gurlebeck, N.: Phys. Rev. Lett. **114**, 151102 (2015). arXiv:1503.03240 [gr-qc]
Haensel, P., Zdunik, J.L., Schaefer, R.: Astron. Astrophys. **160**, 121 (1986)
Haensel, P., Zdunik, J.L., Bejger, M., Lattimer, J.M.: Astron. Astrophys. **502**, 605 (2009). arXiv:0901.1268 [astro-ph.SR]
Hanauske, M., Takami, K., Bovard, L., Rezzolla, L., Font, J.A., Galeazzi, F., Stöcker, H.: ArXiv e-prints (2016). arXiv:1611.07152 [gr-qc]
Hansen, D.: Gen. Relativ. Gravit. **38**, 1173 (2006). arXiv:gr-qc/0511033 [gr-qc]
Harry, G.M., et al.: Class. Quantum Grav. **27**, 084006 (2010)
Hartle, J.B.: Astrophys. J. **150**, 1005 (1967)
Hartmann, T., Soffel, M.H., Kioustelidis, T.: Celest. Mech. Dyn. Astron. **60**, 139 (1994)
Haskell, B., Ciolfi, R., Pannarale, F., Rezzolla, L.: Mon. Not. R. Astron. Soc. Lett. **438**, L71 (2014). arXiv:1309.3885 [astro-ph.SR]
Hempel, M., Schaffner-Bielich, J.: Nucl. Phys. A **837**, 210 (2010). arXiv:0911.4073 [nucl-th]
Hinderer, T.: Astrophys. J. **677**, 1216 (2008). arXiv:0711.2420
Hinderer, T., Lackey, B.D., Lang, R.N., Read, J.S.: Phys. Rev. D **81**, 123016 (2010). arXiv:0911.3535 [astro-ph.HE]
Hinderer, T., Taracchini, A., Foucart, F., Buonanno, A., Steinhoff, J., Duez, M., Kidder, L.E., Pfeiffer, H.P., Scheel, M.A., Szilagyi, B., Hotokezaka, K., Kyutoku, K., Shibata, M., Carpenter, C.W. (2016). arXiv:1602.00599 [gr-qc]
Ho, W.C.G., Lai, D.: Mon. Not. R. Astron. Soc. **308**, 153 (1999). arXiv:astro-ph/9812116 [astro-ph]
Hotokezaka, K., Kyutoku, K., Okawa, H., Shibata, M., Kiuchi, K.: Phys. Rev. D **83**, 124008 (2011). arXiv:1105.4370 [astro-ph.HE]
Hotokezaka, K., Kiuchi, K., Kyutoku, K., Muranushi, T., Sekiguchi, Y.-i., Shibata, M., Taniguchi, K.: Phys. Rev. D **88**, 044026 (2013). arXiv:1307.5888 [astro-ph.HE]
Ipser, J.R., Price, R.H.: Phys. Rev. D **43**, 1768 (1991)
Ivanova, N., Justham, S., Chen, X., De Marco, O., Fryer, C.L., Gaburov, E., Ge, H., Glebbeek, E., Han, Z., Li, X.-D., Lu, G., Marsh, T., Podsiadlowski, P., Potter, A., Soker, N., Taam, R., Tauris, T.M., van den Heuvel, E.P.J., Webbink, R.F.: Astron. Astrophys. Rev. **21**, 59 (2013). arXiv:1209.4302 [astro-ph.HE]
Jimenez-Forteza, X., Abdelsalhin, T., Pani, P., Gualtieri, L. (2018). arXiv:1807.08016
Just, O., Bauswein, A., Pulpillo, R.A., Goriely, S., Janka, H.-T.: Mon. Not. R. Astron. Soc. **448**, 541 (2015). arXiv:1406.2687 [astro-ph.SR]
Kalogera, V., Psaltis, D.: Phys. Rev. **D61**, 024009 (2000). arXiv:astro-ph/9903415 [astro-ph]
Kaplan, J.D., Ott, C.D., O'Connor, E.P., Kiuchi, K., Roberts, L., Duez, M.: Astrophys. J. **790**, 19 (2014). arXiv:1306.4034 [astro-ph.HE]
Kastaun, W., Galeazzi, F.: Phys. Rev. D **91**, 064027 (2015). arXiv:1411.7975 [gr-qc]
Kastaun, W., Galeazzi, F., Alic, D., Rezzolla, L., Font, J.A.: Phys. Rev. D **88**, 021501 (2013). arXiv:1301.7348 [gr-qc]
Kawaguchi, K., Kyutoku, K., Nakano, H., Shibata, M. (2017). arXiv:1709.02754 [astro-ph.HE]
Kawaguchi, K., Kiuchi, K., Kyutoku, K., Sekiguchi, Y., Shibata, M., Taniguchi, K.: Phys. Rev. **D97**(4), 044044 (2018). arXiv:1802.06518
Khan, S., Husa, S., Hannam, M., Ohme, F., Puerrer, M., Jimenez Forteza, X., Bohe, A.: Phys. Rev. **D93**, 044007 (2016). arXiv:1508.07253 [gr-qc]
Kiuchi, K., Sekiguchi, Y., Shibata, M., Taniguchi, K.: Phys. Rev. D **80**, 064037 (2009). arXiv:0904.4551 [gr-qc]
Kiuchi, K., Sekiguchi, Y., Shibata, M., Taniguchi, K.: Phys. Rev. Lett. **104**, 141101 (2010). arXiv:1002.2689 [astro-ph.HE]

Kiuchi, K., Kyutoku, K., Shibata, M.: Phys. Rev. D **86**, 064008 (2012a). arXiv:1207.6444 [astro-ph.HE]
Kiuchi, K., Sekiguchi, Y., Kyutoku, K., Shibata, M.: Class. Quantum Grav. **29**, 124003 (2012b). arXiv:1206.0509 [astro-ph.HE]
Kiuchi, K., Sekiguchi, Y., Kyutoku, K., Shibata, M.: In: Pogorelov, N.V., Font, J.A., Audit, E., Zank, G.P. (eds.) Numerical Modeling of Space Plasma Slows (ASTRONUM 2011), Astronomical Society of the Pacific Conference Series, vol. 459, p. 85 (2012c)
Kiuchi, K., Kyutoku, K., Sekiguchi, Y., Shibata, M., Wada, T.: Phys. Rev. D **90**, 041502 (2014). arXiv:1407.2660 [astro-ph.HE]
Kiuchi, K., Kyutoku, K., Sekiguchi, Y., Shibata, M. (2017). arXiv:1710.01311 [astro-ph.HE]
Kiziltan, B., Kottas, A., De Yoreo, M., Thorsett, S.E.: Astrophys. J. **778**, 66 (2013). arXiv:1011.4291 [astro-ph.GA]
Kochanek, C.S.: Astrophys. J. **398**, 234 (1992)
Kokkotas, K.D., Schaefer, G.: Mon. Not. R. Astron. Soc. **275**, 301 (1995). arXiv:gr-qc/9502034 [gr-qc]
Kokkotas, K., Schmidt, B.: Living Rev. Relativ. **2**, 2 (1999). gr-qc/9909058
Kol, B., Smolkin, M.: J. High Energy Phys. **02**, 010 (2012). arXiv:1110.3764 [hep-th]
Kopal, Z.: Dynamics of Close Binary Systems. D. Reidel Publishing Company, Dordrecht (1978)
Kramer, M., Lyne, A., Burgay, M., Possenti, A., Manchester, R., Camilo, F., McLaughlin, M., Lorimer, D., D'Amico, N., Joshi, B., Reynolds, J., Freire, P.: In: Rasio, F.A., Stairs, I.H. (eds.) Binary Pulsars. PSAP, Chicago (2004)
Krishnendu, N.V., Arun, K.G., Mishra, C.K.: Phys. Rev. Lett. **119**, 091101 (2017). arXiv:1701.06318 [gr-qc]
Kumar, P., Pürrer, M., Pfeiffer, H.P.: Phys. Rev. **D95**, 044039 (2017). arXiv:1610.06155 [gr-qc]
Kyutoku, K., Shibata, M., Taniguchi, K.: Phys. Rev. D **82**, 044049 (2010). arXiv:1008.1460 [astro-ph.HE]
Laarakkers, W.G., Poisson, E.: Astrophys. J. **512**, 282 (1999). arXiv:gr-qc/9709033 [gr-qc]
Lackey, B.D., Wade, L.: Phys. Rev. D **91**, 043002 (2015). arXiv:1410.8866 [gr-qc]
Lackey, B.D., Kyutoku, K., Shibata, M., Brady, P.R., Friedman, J.L.: Phys. Rev. D **85**, 044061 (2012). arXiv:1109.3402 [astro-ph.HE]
Lackey, B.D., Kyutoku, K., Shibata, M., Brady, P.R., Friedman, J.L.: Phys. Rev. D **89**, 043009 (2014). arXiv:1303.6298 [gr-qc]
Lackey, B.D., Bernuzzi, S., Galley, C.R., Meidam, J., Van Den Broeck, C.: Phys. Rev. **D95**, 104036 (2017). arXiv:1610.04742 [gr-qc]
Lai, D.: Mon. Not. R. Astron. Soc. **270**, 611 (1994). arXiv:astro-ph/9404062 [astro-ph]
Lai, D., Rasio, F.A., Shapiro, S.L.: Astrophys. J. Suppl. Ser. **88**, 205 (1993)
Landry, P.: Phys. Rev. **D95**, 124058 (2017). arXiv:1703.08168 [gr-qc]
Landry, P. (2018). arXiv:1805.01882
Landry, P., Poisson, E.: Phys. Rev. **D89**, 124011 (2014). arXiv:1404.6798 [gr-qc]
Landry, P., Poisson, E.: Phys. Rev. **D91**, 104018 (2015a). arXiv:1503.07366 [gr-qc]
Landry, P., Poisson, E.: Phys. Rev. **D91**, 104026 (2015b). arXiv:1504.06606 [gr-qc]
Landry, P., Poisson, E.: Phys. Rev. **D92**, 124041 (2015c). arXiv:1510.09170 [gr-qc]
Lattimer, J.M., Lim, Y.: Astrophys. J. **771**, 51 (2013). arXiv:1203.4286 [nucl-th]
Lattimer, J.M., Prakash, M.: Astrophys. J. **550**, 426 (2001)
Lattimer, J.M., Prakash, M.: Science **304**, 536 (2004). arXiv:astro-ph/0405262
Lattimer, J.M., Schutz, B.F.: Astrophys. J. **629**, 979 (2005). astro-ph/0411470
Lattimer, J.M., Yahil, A.: Astrophys. J. **340**, 426 (1989)
Lattimer, J.M., Pethick, C.J., Prakash, M., Haensel, P.: Phys. Rev. Lett. **66**, 2701 (1991)
Lau, H.K., Leung, P.T., Lin, L.M.: Astrophys. J. **714**, 1234 (2010). arXiv:0911.0131 [gr-qc]
Lee, W.H., Ramirez-Ruiz, E., van de Ven, G.: Astrophys. J. **720**, 953 (2010). arXiv:0909.2884 [astro-ph.HE]
Lehner, L., Liebling, S.L., Palenzuela, C., Motl, P.: ArXiv e-prints (2016). arXiv:1605.02369 [gr-qc]

Lindblom, L., Indik, N.M.: Phys. Rev. **D89**, 064003 (2014) [Erratum: Phys. Rev. **D93**(12), 129903 (2016)]. arXiv:1310.0803 [astro-ph.HE]
Littenberg, T.B., Cornish, N.J.: Phys. Rev. D **91**, 084034 (2015). arXiv:1410.3852 [gr-qc]
Lombardi, J.C., Rasio, F.A., Shapiro, S.L.: Phys. Rev. D **56**, 3416 (1997)
Love, A.E.H.: Proc. R. Soc. Lond. Ser. A **82**, 73 (1909)
Luyten, P.J.: Mon. Not. R. Astron. Soc. **242**, 447 (1990)
Maione, F., De Pietri, R., Feo, A., Löffler, F. (2016). arXiv:1605.03424 [gr-qc]
Majumder, B., Yagi, K., Yunes, N.: Phys. Rev. D **92**, 024020 (2015). arXiv:1504.02506 [gr-qc]
Marchand, T., Bernard, L., Blanchet, L., Faye, G. (2017). arXiv:1707.09289 [gr-qc]
Margalit, B., Metzger, B.D.: Astrophys. J. Lett. **850**, L19 (2017). arXiv:1710.05938 [astro-ph.HE]
Markakis, C., Read, J.S., Shibata, M., Uryu, K., Creighton, J.D.E., Friedman, J.L., Lackey, B.D.: J. Phys. Conf. Ser. **189**, 012024 (2009). arXiv:1110.3759 [gr-qc]
Martin, D., Perego, A., Arcones, A., Thielemann, F.-K., Korobkin, O., Rosswog, S.: Astrophys. J. **813**, 2 (2015). arXiv:1506.05048 [astro-ph.SR]
Maselli, A., Gualtieri, L., Pannarale, F., Ferrari, V.: Phys. Rev. D **86**, 044032 (2012)
Maselli, A., Cardoso, V., Ferrari, V., Gualtieri, L., Pani, P.: Phys. Rev. D **88**, 023007 (2013a). arXiv:1304.2052 [gr-qc]
Maselli, A., Gualtieri, L., Ferrari, V.: Phys. Rev. **D88**, 104040 (2013b). arXiv:1310.5381 [gr-qc]
Maselli, A., Pani, P., Cardoso, V., Abdelsalhin, T., Gualtieri, L., Ferrari, V.: Phys. Rev. Lett. **120**, 081101 (2018). arXiv:1703.10612 [gr-qc]
McDermott, P.N., van Horn, H.M., Hansen, C.J., Buland, R.: Astrophys. J. Lett. **297**, L37 (1985)
Mendes, R.F.P., Yang, H.: Class. Quant. Grav. **34**, 185001 (2017). arXiv:1606.03035 [astro-ph.CO]
Messenger, C., Takami, K., Gossan, S., Rezzolla, L., Sathyaprakash, B.S.: Phys. Rev. X **4**, 041004 (2014)
Mora, T., Will, C.M.: Phys. Rev. D **69**, 104021 (2004). arXiv:gr-qc/0312082
Morsink, S.M., Leahy, D.A., Cadeau, C., Braga, J.: Astrophys. J. **663**, 1244 (2007). astro-ph/0703123
Muhlberger, C.D., Nouri, F.H., Duez, M.D., Foucart, F., Kidder, L.E., Ott, C.D., Scheel, M.A., Szilágyi, B., Teukolsky, S.A.: Phys. Rev. D **90**, 104014 (2014). arXiv:1405.2144 [astro-ph.HE]
Murguia-Berthier, A., Montes, G., Ramirez-Ruiz, E., De Colle, F., Lee, W.H.: Astrophys. J. **788**, L8 (2014). arXiv:1404.0383 [astro-ph.HE]
Murguia-Berthier, A., Ramirez-Ruiz, E., Montes, G., De Colle, F., Rezzolla, L., Rosswog, S., Takami, K., Perego, A., Lee, W.H.: Astrophys. J. Lett. **835**, L34 (2017). arXiv:1609.04828 [astro-ph.HE]
Nagakura, H., Hotokezaka, K., Sekiguchi, Y., Shibata, M., Ioka, K.: Astrophys. J. **784**, L28 (2014). arXiv:1403.0956 [astro-ph.HE]
Nagar, A., Riemenschneider, G., Pratten, G.: Phys. Rev. **D96**, 084045 (2017). arXiv:1703.06814 [gr-qc]
Nagar, A., et al. (2018). arXiv:1806.01772
Nakamura, T., Oohara, K.: Numerical Astrophysics 1998 (NAP98) – Proceedings (1998). gr-qc/9812054
Neilsen, D.W., Liebling, S.L., Anderson, M., Lehner, L., O'Connor, E., Palenzuela, C.: Phys. Rev. D **89**, 104029 (2014). arXiv:1403.3680 [gr-qc]
Nolan, P., Kavanagh, C., Dolan, S.R., Ottewill, A.C., Warburton, N., Wardell, B.: Phys. Rev. **D92**, 123008 (2015). arXiv:1505.04447 [gr-qc]
Oechslin, R., Janka, H.-T.: Phys. Rev. Lett. **99**, 121102 (2007). astro-ph/0702228
O'Leary, R.M., Kocsis, B., Loeb, A.: Mon. Not. R. Astron. Soc. **395**, 2127 (2009). arXiv:0807.2638
Oohara, K.-i., Nakamura, T.: Black Holes and Gravitational Waves: New Eyes in the 21st Century. Proceedings, 9th Yukawa International Seminar, Kyoto, Japan, June 28-July 2, 1999. Prog. Theor. Phys. Suppl. **136**, 270 (1999). arXiv:astro-ph/9912085 [astro-ph]
Oppenheimer, J.R., Volkoff, G.: Phys. Rev. **55**, 374 (1939)
Osłowski, S., Bulik, T., Gondek-Rosińska, D., Belczyński, K.: Mon. Not. R. Astron. Soc. **413**, 461 (2011). arXiv:0903.3538 [astro-ph.GA]

Özel, F., Freire, P.: Annu. Rev. Astron. Astrophys. **54**, 401 (2016). arXiv:1603.02698 [astro-ph.HE]
Pani, P.: Phys. Rev. D **92**, 124030 (2015). arXiv:1506.06050 [gr-qc]
Pani, P., Gualtieri, L., Maselli, A., Ferrari, V.: Phys. Rev. **D92**, 024010 (2015a). arXiv:1503.07365 [gr-qc]
Pani, P., Gualtieri, L., Ferrari, V.: Phys. Rev. **D92**, 124003 (2015b). arXiv:1509.02171 [gr-qc]
Pannarale, F., Rezzolla, L., Ohme, F., Read, J.S.: Phys. Rev. D **84**, 104017 (2011). arXiv:1103.3526 [astro-ph.HE]
Pannarale, F., Berti, E., Kyutoku, K., Lackey, B.D., Shibata, M.: Phys. Rev. **D92**, 081504 (2015). arXiv:1509.06209 [gr-qc]
Pappas, G.: Mon. Not. R. Astron. Soc. **454**, 4066 (2015). arXiv:1506.07225 [astro-ph.HE]
Pappas, G.: Mon. Not. R. Astron. Soc. **466**, 4381 (2017). arXiv:1610.05370 [gr-qc]
Pappas, G., Apostolatos, T.A.: Phys. Rev. Lett. **112**, 121101 (2014). arXiv:1311.5508 [gr-qc]
Paschalidis, V.: Class. Quantum Grav. **34**, 084002 (2017). arXiv:1611.01519 [astro-ph.HE]
Paschalidis, V., Etienne, Z.B., Shapiro, S.L.: Phys. Rev. D **86**, 064032 (2012). arXiv:1208.5487 [astro-ph.HE]
Paschalidis, V., Ruiz, M., Shapiro, S.L.: Astrophys. J. Lett. **806**, L14 (2015a). arXiv:1410.7392 [astro-ph.HE]
Paschalidis, V., East, W.E., Pretorius, F., Shapiro, S.L.: Phys. Rev. D **92**, 121502 (2015b). arXiv:1510.03432 [astro-ph.HE]
Penner, A.J., Andersson, N., Samuelsson, L., Hawke, I., Jones, D.I.: Phys. Rev. **D84**, 103006 (2011). arXiv:1107.0669 [astro-ph.SR]
Perego, A., Rosswog, S., Cabezón, R.M., Korobkin, O., Käppeli, R., Arcones, A., Liebendörfer, M.: Mon. Not. R. Astron. Soc. **443**, 3134 (2014). arXiv:1405.6730 [astro-ph.HE]
Poisson, E.: Phys. Rev. D **57**, 5287 (1998). arXiv:gr-qc/9709032
Poisson, E., Will, C.M.: Gravity. Cambridge University Press, Cambridge (2014)
Porto, R.A.: Fortsch. Phys. **64**, 723 (2016). arXiv:1606.08895 [gr-qc]
Postnikov, S., Prakash, M., Lattimer, J.M.: Phys. Rev. **D82**, 024016 (2010). arXiv:1004.5098 [astro-ph.SR]
Prakash, M., Bombaci, I., Prakash, M., Ellis, P.J., Lattimer, J.M., Knorren, R.: Phys. Rep. **280**, 1 (1997). arXiv:nucl-th/9603042
Price, D.J., Rosswog, S.: Science **312**, 719 (2006). astro-ph/0603845
Punturo, M., et al.: Class. Quantum Grav. **27**, 084007 (2010a)
Punturo, M., et al.: Class. Quantum Grav. **27**, 194002 (2010b)
Purrer, M.: Phys. Rev. **D93**, 064041 (2016). arXiv:1512.02248 [gr-qc]
Racine, E., Flanagan, E.E.: Phys. Rev. **D71**, 044010 (2005). arXiv:gr-qc/0404101 [gr-qc]
Radice, D.: Astrophys. J. Lett. **838**, L2 (2017). arXiv:1703.02046 [astro-ph.HE]
Radice, D., Rezzolla, L., Galeazzi, F.: Mon. Not. R. Astron. Soc. L. **437**, L46 (2014a). arXiv:1306.6052 [gr-qc]
Radice, D., Rezzolla, L., Galeazzi, F.: Class. Quantum Grav. **31**, 075012 (2014b). arXiv:1312.5004 [gr-qc]
Radice, D., Bernuzzi, S., Ott, C.D. (2016). arXiv:1603.05726 [gr-qc]
Radice, D., Bernuzzi, S., Del Pozzo, W., Roberts, L.F., Ott, C.D.: Astrophys. J. Lett. **842**, L10 (2017). arXiv:1612.06429 [astro-ph.HE]
Rathore, Y., Broderick, A.E., Blandford, R.: Mon. Not. R. Astron. Soc. **339**, 25 (2003). arXiv:astro-ph/0209003 [astro-ph]
Ravi, V., Lasky, P.D.: Mon. Not. R. Astron. Soc. **441**, 2433 (2014)
Read, J.S., Lackey, B.D., Owen, B.J., Friedman, J.L.: Phys. Rev. D **79**, 124032 (2009). arXiv:0812.2163
Read, J.S., Baiotti, L., Creighton, J.D.E., Friedman, J.L., Giacomazzo, B., Kyutoku, K., Markakis, C., Rezzolla, L., Shibata, M., Taniguchi, K.: Phys. Rev. D **88**, 044042 (2013). arXiv:1306.4065 [gr-qc]
Regge, T., Wheeler, J.: Phys. Rev. **108**, 1063 (1957)
Reina, B., Sanchis-Gual, N., Vera, R., Font, J.A.: Mon. Not. R. Astron. Soc. **470**, L54 (2017). arXiv:1702.04568 [gr-qc]

Reisenegger, A., Goldreich, P.: Astrophys. J. **426**, 688 (1994)
Rembiasz, T., Guilet, J., Obergaulinger, M., Cerdá -Durán, P., Aloy, M.A., Müller, E.: Mon. Not. R. Astron. Soc. **460**, 3316 (2016). arXiv:1603.00466 [astro-ph.SR]
Rezzolla, L., Kumar, P.: Astrophys. J. **802**, 95 (2015). arXiv:1410.8560 [astro-ph.HE]
Rezzolla, L., Takami, K.: Phys. Rev. D **93**, 124051 (2016). arXiv:1604.00246 [gr-qc]
Rezzolla, L., Zanotti, O.: Relativistic Hydrodynamics. Oxford University Press, Oxford (2013)
Rezzolla, L., Baiotti, L., Giacomazzo, B., Link, D., Font, J.A.: Class. Quantum Grav. **27**, 114105 (2010). arXiv:1001.3074 [gr-qc]
Rezzolla, L., Giacomazzo, B., Baiotti, L., Granot, J., Kouveliotou, C., Aloy, M.A.: Astrophys. J. Lett. **732**, L6 (2011). arXiv:1101.4298 [astro-ph.HE]
Rezzolla, L., Most, E.R., Weih, L.R.: Astrophys. J. Lett. **852**, L25 (2018). arXiv:1711.00314 [astro-ph.HE]
Rikovska-Stone, J., Guichon, P.A., Matevosyan, H.H., Thomas, A.W.: Nucl. Phys. **A792**, 341 (2007). arXiv:nucl-th/0611030 [nucl-th]
Ruiz, M., Shapiro, S.L., Tsokaros, A.: Phys. Rev. D **97**, 021501 (2018). arXiv:1711.00473 [astro-ph.HE]
Saijo, M., Baumgarte, T.W., Shapiro, S.L.: Astrophys. J. **595**, 352 (2003). astro-ph/0302436
Sathyaprakash, B.S., Schutz, B.F.: Living Rev. Relativ. **12**, 2 (2009). arXiv:0903.0338 [gr-qc]
Schmidt, P., Ohme, F., Hannam, M.: Phys. Rev. **D91**, 024043 (2015). arXiv:1408.1810 [gr-qc]
Schnittman, J.D., Dal Canton, T., Camp, J., Tsang, D., Kelly, B.J.: Astrophys. J. **853**, 123 (2018). arXiv:1704.07886 [astro-ph.HE]
Sekiguchi, Y., Kiuchi, K., Kyutoku, K., Shibata, M.: Phys. Rev. Lett. **107**, 211101 (2011a). arXiv:1110.4442 [astro-ph.HE]
Sekiguchi, Y., Kiuchi, K., Kyutoku, K., Shibata, M.: Phys. Rev. Lett. **107**, 051102 (2011b). arXiv:1105.2125 [gr-qc]
Sekiguchi, Y., Kiuchi, K., Kyutoku, K., Shibata, M.: Prog. Theor. Exp. Phys. **2012**, 01A304 (2012). arXiv:1206.5927 [astro-ph.HE]
Sekiguchi, Y., Kiuchi, K., Kyutoku, K., Shibata, M.: Phys. Rev. D **91**, 064059 (2015). arXiv:1502.06660 [astro-ph.HE]
Sennett, N., Hinderer, T., Steinhoff, J., Buonanno, A., Ossokine, S.: Phys. Rev. **D96**, 024002 (2017). arXiv:1704.08651 [gr-qc]
Shah, A.G., Pound, A.: Phys. Rev. **D91**, 124022 (2015). arXiv:1503.02414 [gr-qc]
Shibata, M.: Prog. Theor. Phys. **91**, 871 (1994)
Shibata, M.: Phys. Rev. D **60**, 104052 (1999). gr-qc/9908027
Shibata, M., Kiuchi, K.: Phys. Rev. D **95**, 123003 (2017). arXiv:1705.06142 [astro-ph.HE]
Shibata, M., Taniguchi, K.: Phys. Rev. D **73**, 064027 (2006). astro-ph/0603145
Shibata, M., Taniguchi, K.: Living Rev. Rel. **14**, 6 (2011)
Shibata, M., Uryū, K.: Phys. Rev. D **61**, 064001 (2000). gr-qc/9911058
Shibata, M., Uryū, K.: Prog. Theor. Phys. **107**, 265 (2002). gr-qc/0203037
Shibata, M., Taniguchi, K., Uryū, K.: Phys. Rev. D **71**, 084021 (2005). gr-qc/0503119
Shibata, M., Suwa, Y., Kiuchi, K., Ioka, K.: Astrophys. J. Lett. **734**, L36 (2011). arXiv:1105.3302 [astro-ph.HE]
Shibata, M., Taniguchi, K., Okawa, H., Buonanno, A.: Phys. Rev. D **89**, 084005 (2014). arXiv:1310.0627 [gr-qc]
Shibata, M., Fujibayashi, S., Hotokezaka, K., Kiuchi, K., Kyutoku, K.: Sekiguchi, Y., Tanaka, M.: Phys. Rev. D **96**, 123012 (2017). arXiv:1710.07579 [astro-ph.HE]
Siegel, D.M., Ciolfi, R., Rezzolla, L.: Astrophys. J. **785**, L6 (2014). arXiv:1401.4544 [astro-ph.HE]
Silva, H.O., Sotani, H., Berti, E.: Mon. Not. R. Astron. Soc. **459**, 4378 (2016). arXiv:1601.03407 [astro-ph.HE]
Steiner, A.W., Gandolfi, S., Fattoyev, F.J., Newton, W.G.: Phys. Rev. **C91**, 015804 (2015). arXiv:1403.7546 [nucl-th]
Steiner, A.W., Lattimer, J.M., Brown, E.F.: Eur. Phys. J. A **52**, 18 (2016). arXiv:1510.07515 [astro-ph.HE]

Steinhoff, J., Hinderer, T., Buonanno, A., Taracchini, A.: Phys. Rev. **D94**, 104028 (2016). arXiv:1608.01907 [gr-qc]
Stergioulas, N., Apostolatos, T.A., Font, J.A.: Mon. Not. R. Astron. Soc. **352**, 1089 (2004). arXiv:astro-ph/0312648
Stergioulas, N., Bauswein, A., Zagkouris, K., Janka, H.-T.: Mon. Not. R. Astron. Soc. **418**, 427 (2011). arXiv:1105.0368 [gr-qc]
Takami, K., Rezzolla, L., Baiotti, L.: Phys. Rev. Lett. **113**, 091104 (2014). arXiv:1403.5672 [gr-qc]
Takami, K., Rezzolla, L., Baiotti, L.: Phys. Rev. D **91**, 064001 (2015). arXiv:1412.3240 [gr-qc]
Taranto, G., Baldo, M., Burgio, G.F.: Phys. Rev. C **87**, 045803 (2013). arXiv:1302.6882 [nucl-th]
The LIGO Scientific Collaboration and the Virgo Collaboration: Phys. Rev. Lett. **116**, 061102 (2016). arXiv:1602.03837 [gr-qc]
Thompson, T.A.: Astrophys. J. **741**, 82 (2011). arXiv:1011.4322 [astro-ph.HE]
Thorne, K.: Rev. Mod. Phys. **52**, 299 (1980)
Thorne, K.S.: Phys. Rev. D **58**, 124031 (1998). gr-qc/9706057
Thorne, K.S., Campolattaro, A.: Astrophys. J. **149**, 591 (1967)
Thorne, K.S., Hartle, J.B.: Phys. Rev. **D31**, 1815 (1984)
Tolman, R.C.: Phys. Rev. **55**, 364 (1939)
Tsang, D.: Astrophys. J. **777**, 103 (2013). arXiv:1307.3554 [astro-ph.HE]
Tsang, D., Read, J.S., Hinderer, T., Piro, A.L., Bondarescu, R.: Phys. Rev. Lett. **108**, 011102 (2012). arXiv:1110.0467 [astro-ph.HE]
Tsui, L.K., Leung, P.T.: Mon. Not. R. Astron. Soc. **357**, 1029 (2005). gr-qc/0412024
Uchikata, N., Yoshida, S.: Class. Quant. Grav. **33**, 025005 (2016). arXiv:1506.06485 [gr-qc]
Urbanec, M., Miller, J.C., Stuchlík, Z.: Mon. Not. R. Astron. Soc. **433**, 1903 (2013). arXiv:1301.5925 [astro-ph.SR]
Vallisneri, M.: Phys. Rev. Lett. **84**, 3519 (2000). arXiv:gr-qc/9912026
Van Oeveren, E.D., Friedman, J.L.: Phys. Rev. **D95**, 083014 (2017). arXiv:1701.03797 [gr-qc]
Vines, J., Flanagan, E.E., Hinderer, T.: Phys. Rev. D **83**, 084051 (2011a). arXiv:1101.1673 [gr-qc]
Vines, J., Hinderer, T., Flanagan, É.É. (2011b). arXiv:1101.1673 [gr-qc]
Wade, L., Creighton, J.D.E., Ochsner, E., Lackey, B.D., Farr, B.F., Littenberg, T.B., Raymond, V.: Phys. Rev. D **89**, 103012 (2014). arXiv:1402.5156 [gr-qc]
Watts, A.L., Andersson, N., Jones, D.I.: Astrophys. J. **618**, L37 (2005). astro-ph/0309554
Weissenborn, S., Sagert, I., Pagliara, G., Hempel, M., Schaffner-Bielich, J.: Astrophys. J. **740**, L14 (2011). arXiv:1102.2869 [astro-ph.HE]
Wilson, J.R., Mathews, G.J.: Phys. Rev. Lett. **75**, 4161 (1995)
Witten, E.: Phys. Rev. D **30**, 272 (1984)
Xu, W., Lai, D.: Phys. Rev. **D96**, 083005 (2017). arXiv:1708.01839 [astro-ph.HE]
Yagi, K.: Phys. Rev. **D89**, 043011 (2014). arXiv:1311.0872 [gr-qc]
Yagi, K., Yunes, N.: Science **341**, 365 (2013a). arXiv:1302.4499 [gr-qc]
Yagi, K., Yunes, N.: Phys. Rev. D **88**, 023009 (2013b). arXiv:1303.1528 [gr-qc]
Yagi, K., Yunes, N.: Phys. Rev. **D89**, 021303 (2014). arXiv:1310.8358 [gr-qc]
Yagi, K., Yunes, N.: Class. Quant. Grav. **33**, 13LT01 (2016). arXiv:1512.02639 [gr-qc]
Yagi, K., Yunes, N.: Phys. Rep. **681**, 1 (2017a). arXiv:1608.02582 [gr-qc]
Yagi, K., Yunes, N.: Class. Quant. Grav. **34**, 015006 (2017b). arXiv:1608.06187 [gr-qc]
Yagi, K., Kyutoku, K., Pappas, G., Yunes, N., Apostolatos, T.A.: Phys. Rev. D **89**, 124013 (2014a). arXiv:1403.6243 [gr-qc]
Yagi, K., Stein, L.C., Pappas, G., Yunes, N., Apostolatos, T.A.: Phys. Rev. D **90**, 063010 (2014b)
Yamamoto, T., Shibata, M., Taniguchi, K.: Phys. Rev. D **78**, 064054 (2008). arXiv:0806.4007 [gr-qc]
Yang, H., Paschalidis, V., Yagi, K., Lehner, L., Pretorius, F., Yunes, N.: Phys. Rev. D **97**, 024049 (2018). arXiv:1707.00207 [gr-qc]
Yu, H., Weinberg, N.N.: Mon. Not. R. Astron. Soc. **464**, 2622 (2017). arXiv:1610.00745 [astro-ph.HE]
Zahn, J.-P.: Astron. Astrophys. **4**, 452 (1970)
Zahn, J.-P.: Astron. Astrophys. **57**, 383 (1977)